University of Technology Sydney

Faculty of Engineering and Information Technology

Design and Control of a Novel Uninterrupted Dual Input Powertrain System for Electric Vehicles

A thesis submitted for degree of

Doctor of Philosophy

Jiejunyi LIANG

2018

Certificate of Original Authorship

I certify that the work in this thesis has not previously been submitted for a degree nor has it been submitted as part of requirements for a degree except as fully acknowledged within the text.

I also certify that the thesis has been written by me. Any help that I have received in my research work and the preparation of the thesis itself has been acknowledged. In addition, I certify that all information sources and literature used are indicated in the thesis.

This research is supported by an Australian Government Research Training Program Scholarship

Signature of Student: Production Note:
Signature removed prior to publication.

Date: Feb. 2019

Acknowledgments

I would like to take this opportunity to thank many people for their assistance, encouragement and support throughout my candidature.

First and foremost, I would like to thank my supervisor Prof. Nong Zhang and my co-supervisor Dr. Paul Walker. They guided me both in research direction and academic writing and supported me both in my study and my life. Their valuable knowledge and research attitude reshaped me and made it possible for me to continue my research career.

I would also like to show my thankfulness to my colleagues Jinglai Wu, Jiageng Ruan, Haitao Yang, Wenwei Mo, Weiwei Yang, Hanfei Wu, Shilei Zhou, Yang Tian and Ying Zhang. They helped me overcome all the difficulties in my study and life.

Financial support for my study is provided by the University of Technology Sydney (UTS) and Australian Research Council (ARC) Discovery Projects (DP).

At last, I would take this opportunity to thank my family, they are my source of strength and my cornerstone, without them, I could not achieve so much. Thank you.

Jiejunyi Liang

Sydney, 2018

Publications

International journals

[1] **J. Liang**, H. Yang, J. Wu, N. Zhang, P.D. Walker, Shifting and power sharing control of a novel dual input clutchless transmission for electric vehicles, Mech. Syst. Signal Process. 104 (2018) 725–743. (Chapter 2, 4, 5)

[2] **J. Liang**, H. Yang, J. Wu, N. Zhang, P.D. Walker, Power-on shifting in dual input clutchless power-shifting transmission for electric vehicles, Mech. Mach. Theory. 121 (2018) 487–501. (Chapter 2, 3, 4)

[3] **J. Liang**, J.-H.J.-H. Zhong, Z.-X.Z.-X. Yang, Correlated EEMD and Effective Feature Extraction for Both Periodic and Irregular Faults Diagnosis in Rotating Machinery, Energies. 10 (2017) 1652. doi:10.3390/en10101652.

[4] **J. Liang**, J. Wu, N. Zhang, Z. Luo, S. Zhu, Interval uncertain analysis of active hydraulically interconnected suspension system, Adv. Mech. Eng. 8 (2016). doi:10.1177/1687814016646331.

[5] W. Yang, **J. Liang***, J. Yang, N. Zhang, Investigation of a novel coaxial power-split hybrid powertrain for mining trucks, Energies. 11 (2018). doi:10.3390/en11010172. (Chapter 2, 7)

[6] J. Wu, **J. Liang**, J. Ruan, N. Zhang, P.D. Walker, Efficiency comparison of electric vehicles powertrains with dual motor and single motor input, Mech.

Mach. Theory. 128 (2018) 569–585.
doi:https://doi.org/10.1016/j.mechmachtheory.2018.07.003. (Chapter 5)

[7] J. Wu, **J. Liang**, J. Ruan, N. Zhang, P.D. Walker, A robust energy management strategy for EVs with dual input power-split transmission, Mech. Syst. Signal Process. 111 (2018) 442–455. doi:10.1016/j.ymssp.2018.04.007. (Chapter 5)

[8] H. Yang, Y. Zhang, **J. Liang**, J. Gao, P.D. Walker, N. Zhang, Sliding-Mode Observer Based Voltage-Sensorless Model Predictive Power Control of PWM Rectifier Under Unbalanced Grid Conditions, IEEE Trans. Ind. Electron. 65 (2018) 5550–5560. doi:10.1109/TIE.2017.2774730.

[9] H. Yang, Y. Zhang, **J. Liang**, J. Liu, N. Zhang, P. Walker, Robust Deadbeat Predictive Power Control with a Discrete-time Disturbance Observer for PWM Rectifiers under Unbalanced Grid Conditions, IEEE Trans. Power Electron. (2018). doi:10.1109/TPEL.2018.2816742.

[10] H. Yang, Y. Zhang, **J. Liang**, B. Xia, P.D. Walker, N. Zhang, Deadbeat control based on a multipurpose disturbance observer for permanent magnet synchronous motors, IET Electr. Power Appl. 12 (2018) 708–716.

[11] H. Yang, Y. Zhang, P.D. Walker, **J. Liang**, N. Zhang, B. Xia, Speed sensorless model predictive current control with ability to start a free running induction motor, IET Electr. Power Appl. 11 (2017). doi:10.1049/iet-epa.2016.0481.

[12] J.-H. Zhong, **J. Liang**, Z.-X. Yang, P.K. Wong, X.-B. Wang, An Effective Fault Feature Extraction Method for Gas Turbine Generator System Diagnosis, Shock Vib. 2016 (2016). doi:10.1155/2016/9359426.

International conferences

[1] H. Yang, Y. Zhang, **J. Liang**, N. Zhang, W. Paul, A robust deadbeat predictive power control with sliding mode disturbance observer for PWM rectifiers, in: Energy Convers. Congr. Expo. (ECCE), 2017 IEEE, 2017: pp. 4595–4600.

[2] **J. Liang**, H. Yang, W. Mo, N. Zhang, and P. D. Walker, Modelling and Control of Dual Input Clutchless Transmission for Electric Vehicles, in: Intern. Conf. on Adv. Veh. Powert. (ICAVP), 2017 (best paper award)

Contents

List of Figures

List of Tables

Abbreviations

HEV - Hybrid Electric Vehicle

PHEV - Plug-in Hybrids Electric Vehicles

EV - Electric Vehicle

FCV - Fuel Cell Vehicles

CVT - Continuously Variable Transmission

DCT - Dual Clutch Transmission

EMS - Energy Management Strategies

ICE - Internal Combustion Engine

AMT - Automated Manual Transmission

DP - Dynamic Programming

SA - Simulated Annealing

GA - Genetic Algorithms

PMP - Pontryagin's Minimum Principle

PSC - Power Sharing Control

THS - Toyota Hybrid System

ECVT - Electronic Continuously Variable Transmission

CHS - China Hybrid System

IVT - Infinitely Variable Transmission

FHS - Ford Hybrid System

UMST - Uninterrupted Multi-Speed Transmission

RTCS - Real-Time Control Stragety

SOC - State of Charge

FOC - Field Oriented Control

DTC - Direct Torque Control

MPTC - Model Predictive Torque Control

MPFC - Model Predictive Flux Control

MT - Manual Transmission

AT - Automatic Transmission

CLAMT - Clutchless Automated Manual Transmission

LA-92 - Los Angeles 92 / Unified Cycle Driving Schedule

HWFET- Highway Fuel Economic Test

Abstract

The automotive powertrain is one of the most important subsystems of any vehicle whose major function is to convert the stored energy to kinetic energy and deliver it as tractive load to the road. In order to reduce the harmful emissions and the dependence on fossil fuels, the development. The new technology will improve the overall efficiency, the drivability and the driving comfort, and reduce the tailpipe emissions. However, the inclusion of electric machines alone does not guarantee these improvements, proper transmission structure design and adequate control strategy should be designed to fully exploit the potential of the whole system, thereby maximizing the benefits to end users.

In order to achieve the aforesaid benefits of electric vehicle, a novel dual input clutchless transmission configuration is proposed which consists of an automated manual transmission (AMT) and a fixed gear pair. It has the merits of low manufacturing cost, robustness and easy implementation. With the proposed gear shift control strategy, the novel configuration could eliminate the torque interruption of conventional AMT systems, improving the drivability and driving comfort.

To fully exploit the efficiency improvements of the proposed system, a real time power sharing control strategy is proposed to balance the load distribution between the two motors. By adequately choosing the gear position and distributing the power demand, the overall efficiency could be improved by more than 10%.

The proposed power sharing strategy has the disadvantage encountered by many other energy-oriented energy management strategies which is high gear shifting frequency. To keep a high overall efficiency and at the same time significantly reduce the shift frequency, a shifting stabilizer is proposed and embedded in to the control strategy.

At last, a modified hybrid configuration based on the proposed concept is developed for mining trucks. The hybrid system could satisfy the specific requirements of mining trucks and present high overall efficiency and drivability.

To evaluate the effectiveness of the proposed approaches, various detail mathematical models have been built and tested in sets of driving conditions which could reflect the practical implementations.

CHAPTER 1 : Introduction

1.1 Current developments

Vehicle electrification and hybridisation is viewed as one of the primary methods for directly reducing emissions and improving vehicle economy in passenger vehicles. Due to the inclusion of electric motors, the diversity of the powertrain structure has been significantly expanded from micro-scale hybrids to pure electric vehicles and there are many successful implementations such as the hybrids electric vehicles (HEV) plug-in hybrids electric vehicles (PHEV), electric vehicles (EV), and fuel cell vehicles (FCV). In the market, there are also many successful models include the prevailing Toyota Prius, Tesla, BMW I-series, the emerging brands such as DENZA and BYD, and many subclasses in the traditional model series. These vehicles are designed to be more efficient and more eco-friendly by combining improved engine, on-board stored electricity, regenerative system and superior overall configuration. As a result, the synergistic development of powertrain configuration, the corresponding control strategies and adequate fault diagnosis method are crucial to guarantee the performance of the green energy techniques.

The powertrain architectures and the corresponding control strategies are the subject of much research in the wider automotive engineering field. Novel configurations are constantly sought to achieve the maximum efficiency without compromising the performance. In practice, the continuously variable transmission (CVT) based Toyota Prius has attracted the most attention due to its high overall efficiency under various

driving conditions. Other competitors such as the Chevrolet Volt and Ford Hybrid are based on a dual clutch transmission (DCT) system. Pure electric vehicles like early models of Tesla are based on a fixed ratio transmission system. However, most of the aforesaid structures are heavily dependent on complex and expensive clutches which require for complicated clutch control strategies and corresponding actuation system which are detrimental to powertrain efficiency and vehicle performance. Energy management strategy is another important issue in exploiting the potential of each system. Due to the development of computer technology, many optimization based strategies such as dynamic programming (DP) and fussy algorithm based strategies like neural networks have been developed to replace the traditional rule-based strategies which require the experience of engineers.

1.2 Significance and Innovations

The successful commercialisation of green energy vehicles will significantly reduce the dependence of the transportation sector on fossil fuels, thereby lessening carbon emissions and pollution resulting from the transportation industry. Current trends demonstrate that only moderate improvements are now realised as new green energy systems are brought to the market. The proposed strategy will expand knowledge on how to minimise the use of transmission components that contribute most to the losses in the system, providing a leap forward in the development of very efficient hybrid and electric vehicle technologies. Ultimately such technologies will further reduce demand on carbon based fuels (e.g. diesel, petrol. gas, and ethanol blended fuels), and provide cost effective alternatives for current power splitting transmissions.

The key innovations of this thesis include:

1. The development of a series of novel transmission architecture for hybrid electric and electric vehicles that provides power shifting capabilities without the use of friction based clutch elements. This is specifically achieved through the integral control of two motors during gear change. Such innovation will significantly improve the efficiency of hybrid and electric vehicle transmissions.
2. The model-based control of transient dynamics of the transmission during gear and mode change between power sources, verified through simulations under various drive cycles. This will provide first-hand information for the assessment of the noise and vibration characteristics of the powertrain.
3. The development of optimal energy management strategies and alternative methods that best suit the powertrain operation, independent of chosen driving cycle and evaluated through simulations.
4. The design of a shifting stabilizer which could significantly reduce the shift times during a certain period without compromise the overall efficiency. This method could considerably improve the driving comfort and elongate the durability of the transmission system.
5. As the driving conditions of mining trucks are quite different from those of passenger vehicles, the design concept and requirements are also very different. A novel coaxial transmission for mining trucks is designed with corresponding control strategies and has been verified by simulations.

1.3 Presentation of this thesis

Chapter 1. The main aims and contributions of the thesis are introduced.

Chapter 2. In-depth background introduction and literature review are given in this chapter.

Chapter 3. The proposed dual input clutchless transmission system structure with possible working conditions are introduced together with the variations based on the same idea.

Chapter 4. Advanced shifting control strategy for the proposed transmission structure is proposed. The modified bump function based shifting control strategy could adequately compensate the torque hole during shifting, achieving non-interrupted gear changing which could both improve the driving comfort and drivability.

Chapter 5. An effective power sharing strategy is proposed for the proposed transmission system to coordinate the power of the two employed electric motors. The designed power sharing strategy could be implemented online and has sub-optimized performance.

Chapter 6. As many other energy management strategies, the proposed power sharing control strategy also suffers from excessive gear shifts. To solve this problem, a novel shift stabilizer is designed and embedded into the strategy which could significantly reduce the shift times while keeping desirable overall efficiency.

Chapter 7. A novel uninterrupted multi-speed transmission for hybrid electric mining trucks is proposed with corresponding control strategies. The simulation

results demonstrate the efficiency and drivability improvements of the proposed structure.

Chapter 8. Conclusions are made in the last chapter and further development recommendation is also given.

CHAPTER 2 : Background and literature review

2.1 Dual input clutchless transmission system

Transportation systems are experiencing considerable changes in terms of electrification [1] because of the mounting demand for reduction of fossil fuel consumption and green-gas emissions and the improvements of vehicle overall efficiency [2]. In the past decades, groundbreaking achievements have been made in the realms of researches and industries to build more intelligent and more eco-friendly new energy vehicles, such as electric vehicles [3], hybrid electric vehicles [4] and fuel cell electric vehicles [5]. All of these approaches have to some certain extent helped alleviate the aforesaid problems, but there are still challenges to further improve the energy consumption performance while maintaining satisfactory vehicle drivability as drivability generally goes against the optimization of energy consumption [6].

In order to achieve a desirable balance between efficiency and drivability, two aspects can be focused on which are powertrain architecture [7] including advanced vehicle dynamic control [8–10], and energy management strategies (EMS) [11]. Many successful commercial pure electric vehicles, which could achieve good acceleration performance and relatively low energy consumption, have been promoted to customers such as Nissan Leaf [12,13], Mitsubishi iMIEV [14,15] and Tesla [16,17]. For most on sale pure electric vehicles, single fixed ratio transmission system serves as a core component of their powertrains, the merits of this kind of architecture are lower manufacturing cost, relatively smaller volumes and less drive train mass [18]. Besides

the advantages, the drawbacks of this kind of transmission system are also obvious which are compromised drivability performance comes from compromises between speed and torque range and lower overall efficiency because of the non-adjustable transmission ratios [19,20].

Multi-speed transmission system is an effective solution to further improve the overall efficiency and guarantee the drivability for electric vehicles [21]. However, most existing investigations of multi-speed transmission systems are focused on internal combustion engine (ICE) related vehicles such as conventional ICE vehicles and HEV [22]. As a result, conventional multi-speed transmission architectures and the related control strategies cannot be directly adopted in pure electric vehicles. Moreover, the differences between electric motor and ICE give electric vehicles more advantages to make the most of these transmission systems [23,24]. As maximizing the overall efficiency is one of the priorities in designing electric vehicle transmission, automated manual transmission stands out as it provides the highest efficiency, meanwhile, has low manufacture cost and is light in weight, among all alternative options [25]. But its popularization is hindered due to two drawbacks which are jerks caused by torque interruption in shifting process and excessive wear of friction components [26–28]. Extensive studies [29] have proved that the major parasitic losses in transmission system come from friction clutch elements and electro-hydraulic actuators and these two account for 4% to 6% losses of overall efficiency. In [30], it is proved possible to minimize the reduction in efficiency by using clutchless variants.

To solve the torque interruption problem, many feasible solutions have been proposed such as adding a servo-assisted clutch to replace the fifth synchronizer in [31], the

additional clutch could provide certain power when the ICE is disconnected from the transmission during gear shifting. This method could only alleviate the torque hole problem as it doesn't have its own power source. In [32], a modification is made to the original AMT which puts the gearbox before the friction clutch and to some extent, solves the problem of torque interruption. As to the problem of excessive wear of friction components and parasitic losses, the adoption of electric motors provides a desirable solution which is to avoid using friction clutches [33–35]. For conventional ICE vehicles, the adoption of friction clutches is inevitable as the inertia of the engine is too high to perform prompt speed and torque adjustment, and it also entails long speed synchronization duration and exacerbates the wear of the friction plates. Due to three advantages of electric motors [36] which are small inertia, excellent low speed control capabilities and torque/speed operation modes, a clutchless AMT could be designed for electric vehicles. Aiming at maximizing overall efficiency and solving the aforesaid problems, a series of dual input clutchless transmission systems is proposed.

To achieve a non-interruption power-on shifting, suitable shifting control strategy should be designed and implemented [37]. Through precisely control the torque and speed profiles of the motors, the final shaft torque would stay steady during gear shifting with which a smooth and power-on shifting process could be achieved.

2.2 Power sharing control of the dual input system

Solving the problem of architecture design and its shifting control strategy alone can only partly guarantee the efficiency and drivability, the performance of the proposed dual input clutchless transmission system also depends on how to distribute the power

demand among the two motors [38]. Only by controlling the two motors work in their higher efficiency region can the system provide satisfying dynamic and efficient performance [39].

Many profound researches have been conducted in the field of energy management which roughly divide the methods into two categories: rule-based control and optimization based control [40]. Rule-based control is famous for its simplicity which comes from the avoidance of explicit optimization algorithm [41]. Compared with optimization-based approaches, rule-based methods are more effective in real-time implementation because the time-consuming calibration and tuning work for various parameters are conducted off-line before implementation. The fundamentals of the rules are usually heuristic, intuitive, and experiential [42] which make them generate suboptimal results under different driving conditions. According to the way the rules are designed, rule-based control can be further divided into deterministic rule-based and fuzzy rule-based methods [43]. In [44], a successful rule-based strategy is designed for fuel cell hybrid system. In this strategy, the parameters are tuned according to the knowledge of each element used in the feeding system which makes it a deterministic approach.

For optimization-based strategy, current or future driving information is necessary to generate noncausal minimum value of certain cost functions. Classic optimization methods based on dynamic programming [45], simulated annealing (SA) [46] and genetic algorithms (GA) [47] are adopted as numerical approaches which entails complete information of the driving cycle to generate global optimal solutions. Pontryagin's minimum principle (PMP) has also been brought out as an optimization-

based method and its performance is verified in [48]. Another method called equivalent consumption minimization strategy [49] is designed for hybrid electric vehicles and this method is proved to have similar performance compared with PMP. Both of these methods could minimize the instantaneous cost to generate optimized results [50]. In [51], neural networks are adopted to achieve real-time optimization with the assistance of particle swarm optimization, although the solution is suboptimal, the computational cost is greatly reduced and the controller could promptly respond to the driving condition which is important in controlling a vehicle.

The problem arising from the proposed structure is different from the aforesaid problems and the mentioned strategies cannot be directly applied here. In the aforesaid problems, the driving power comes from different power sources such as battery, supercapacitor and engine and there could be losses when energy flows from one source to another, as a result, balancing the power distribution while taking the energy transfer efficiency into account is the feature [52–54]. Another difference is that in the aforesaid problems, efficiency performance at different timings depends on each other. If one of the power sources is depleted in order to achieve the highest overall efficiency at an early time, the whole system may work in low efficiency area later because there is only one power source left to provide all the demanded power [55,56]. This is also the reason why prior knowledge of the trip should be given for the optimization-based approaches in order to achieve global optimization. For vehicles that only have one power source like conventional electric vehicle, the efficiency is only decided by the driving pattern or the driving demand and has nothing to do with power distribution because there is only one motor which should meet the power demand. In the proposed system, although

there is only one power source which is the battery, there are two motors which could provide the demanded power together and a suitable power sharing control (PSC) strategy should be designed to both guarantee the power provision and maximize the overall efficiency. As there is only one power source, the energy transfer problem could be ignored and the efficiency at different timings is relatively independent. As a result, prior knowledge of the whole trip is not necessary and real-time implementations and high efficiency could be possibly achieved at the same time.

2.3 Shifting stability control

As minimizing the overall energy consumption is the primary objective for most energy management strategies, drivability constrains are always neglected resulting in many problems [57–59]. Aspects of drivability such as the acceleration performance [60], the controllability [61], the driving comfort [62] and smoothness [63] also have great influence on the driving experience and are important for a customer to decide whether to buy a car or not. However, as the absence of drivability consideration, a detrimental phenomenon, excessive gear shifting happens in most existing energy-oriented strategies [9,64]. By investigating a specific shifting process, it can be found that there would be two types of undesirable shifting [65]. The first scenario is the energy consumptions for each gear position are very close and the lowest consumption position is frequently changing between different gears. In this situation, the change of gear positions would not bring much efficiency improvement. However, the excessive shifting times will downgrade the driving comfort and cause extra energy consumption due the process of gear shifting. Eliminating this kind of shifts could not compromise

the overall efficiency much while greatly reducing the gear shift frequent [66]. Another problem is the short gear shifting interval [67]. Basically, except for the aggressive driving pattern which requires for frequent gear shifting to satisfy the acceleration and braking demand, the interval between two gear shifts should not be too short [68]. In other words, if not conflicts with the acceleration demand, the interval between two shifts should be as long as possible [69]. By solving this problem, the driving comfort will be significantly improved that there would not be gear shifts in rapid succession. In order to overcome the problems in the proposed power sharing strategy and other similar energy management strategies, a shifting stabilizer is designed and embedded into the system to make a restriction on gear shifting events.

Another problem in achieving a desirable shifting performance is to optimize the weighting factors of the designed shifting stabilizer. If the parameter is too large, the shift frequent will be greatly reduced, together with the overall efficiency. If the value is too small, the drivability improvement would be unnoticeable [70]. To solve this problem, multi-objective optimization methods should be adopted to keep the balance between the drivability and the overall efficiency [71]. In recent years, applying evolutionary algorithms into multi-objective optimization problems is a popular research topic [72,73]. Non-inferior solution is the most important concept in conducting multi-objective optimization. It refers to an improvement in one objective does not cause degradation in other objectives, and all the non-inferior solutions form the non-inferior set, which is also called the Pareto optima [74]. By adopting the multi-objective optimization method, the parameters of the stabilizer could be adjusted co-ordinately and an improved drivability could be achieved.

2.4 A novel uninterrupted multi-speed transmission for hybrid electric mining trucks

Mining trucks are widely used as a main transportation for mining and water conservancy projects [75]. However, the operations of the mining trucks have the following characteristics [76]. The daily operational time is usually over 20h, the trucks travel to and fro between the loading point and the unloading point with a relatively fixed route, the road slope and truck load change greatly, and the trucks frequently drive uphill and downhill, which will cause serious pollution emissions, harsh noises, and poor economical performances [77]. Therefore, it is important to reduce the fuel consumption and emissions of mining trucks by developing more efficient drivetrain system [78].

Moreover, the special performance requirements for mining trucks are quite different from those of normal passenger vehicles [79], making the design of a hybrid transmission system for mining trucks of great importance.

Currently, series, parallel, and series-parallel or power-split hybrid system are well known [80]. Among them, power-split hybrid system possesses the advantages of the first two types [81–84], and it has been widely applied to passenger cars and transit buses, as a result, it is adopted here as the basic structure. The merits and demerits of several well-known power-split systems are illustrated. The Toyota Prius hybrid system (THS) has been popular for its high fuel efficiency since 1997 [85,86], and it is a single-mode configuration [87,88]. Many studies have proved that THS is comparatively simple and it is suitable for regular passenger cars [89]. However, due to the limitation

of the single-mode [90], THS may cause excessive fuel consumption if the vehicle drives in diversified conditions, such as variations of slope and payload [91]. Therefore, dual-mode hybrid systems are proposed. In [92], 12 configurations are evaluated by adding clutches in THS, and the results demonstrate that Prius+ has better fuel economy and drivability. In [93], The structure of the electronic continuously variable transmission of Timken (ECVT) is shown. Two clutches and two brakes are added to achieve higher efficiency at mid-high speed compared to THS. However, ECVT makes the system much more complex and difficult to control. Therefore, in [94] and [82], GM and Allison hybrid system (AHS) is introduced. Compared to ECVT, only two clutches and one brake are adopted, and one of the two clutches is used to eliminate the engine impact during all-electric driving mode. Compared to AHS, China hybrid system (CHS) only use a one-way clutch and one brake, which makes system more simple and easy to control [95]. Due to the high cost of wet or dry clutch, two dog-tooth clutch are used in infinitely variable transmission of Renault (IVT) [96]. Ford hybrid system (FHS) replace the planetary gear with spur gear to reduce manufacturing cost. Modelling and experimental validation has been carried out and prove that FHS still possesses excellent fuel economy and dynamic performance [97]. Zhang proposed a novel multi-mode hybrid system, which is composed of a planetary set and corresponding lay-shaft gears [98]. The merit of the structure is that only one motor is used which serves both as a generator and a motor. It overcomes the disadvantage of THS that the engine cannot directly drive the vehicle at high-speed. However, the system cannot satisfy the torque requirement when the vehicle operates in low speed and steep slope situation, unless

increasing the gear ratios of lay-shaft gearbox, which will significantly increase the manufacturing cost.

From the aforesaid solutions, the planetary gear set interacted with spur gears seem to be a good way to design a novel hybrid configuration. Therefore, a novel uninterrupted multi-speed transmission is proposed, which consists of a planetary gear set and a lay-shaft transmission. Although single-speed transmission makes system simple [99,100], it is still not considered because the motor torque has to be large to meet the climbing requirements of mining trucks. Meanwhile, the motor cannot always operate in high-efficiency area [101,102]. Many researchers have proved that multi-speed transmission can adjust the engine or motor working points to improve the fuel efficiency by gear-shifting. Two-speed transmission is widely equipped with the electric cars at present [29,103]. However, it may be not feasible for mining trucks. The performance indexes of mining trucks include: 1) maximum speed of full-load truck is not less than 56km/h; 2) maximum grade-ability of full-load truck is more than 30%; 3) the engine output shaft must be coaxial with the driving shaft. To meet the demands, assuming the gear ratios are 1 and 3.46, the large gear-ratio gap would cause shifting difficult or large shifting jerks during shifting process [104,105]. Unfortunately, overmuch gear ratios will also make the control system too complex and unreliable [106]. Moreover, the overall efficiency of dual clutches transmission is relatively lower compared with automatic manual transmission [107]. By comprehensive consideration, three-ratio AMT (3-AMT) is more applicative and proposed.

The torque interruption of AMT severely affects drivability, and it cannot be ignored. Given this, many optimized system configurations and shift control strategies are

proposed to enhance driving comfort. Some approaches and testing criterion have been introduced in the authors' previous studies [108,109].

To evaluate overall performance of the proposed uninterrupted multi-speed transmission (UMST), drivability is not the only criterion, as fuel economy must also be considered [110]. Two types of energy control strategy including rule-based control strategies and optimal control strategies are usually used [111]. The merit of rule-based energy management strategy is the easy and robust implementation [112–115]. However, it mostly depends on the experiences of the researcher. As a result, the ability to obtain the optimal solution is compromised [116]. The optimal strategies could solve the problem encountered with rule-based strategy [117–119]. Therefore, dynamic programming is adopted to calculate the optimal solution for evaluating a novel design, which is usually regarded as a benchmark [120,121]. However, it is well-known that DP requires much time of calculation and is hard to be applied in real time. Therefore, a real-time control strategy (RTCS) is also proposed.

According to the characteristics of mining trucks, a novel non-interrupted multi-speed transmission with energy and shift control strategy is proposed. More specially, the key novel contributions include:

1. An uninterrupted configuration consisting of a planetary gear set integrated with 3-AMT is proposed;
2. Shift control strategy with an adjunct function is proposed to compensate or alleviate the torque hole smoothly;

3. DP and RTCS are applied to evaluate the fuel economy of the proposed UMST, respectively.

CHAPTER 3 : Investigation of dual input powertrain configurations for electric vehicles

3.1 Introduction

As the regulation for vehicle exhaust emission becomes stricter and the price of fossil fuel keeps rising all the time, the development of electric vehicle and hybrid electric vehicle has attracted worldwide attention [122]. Due to the different characters between conventional inter combustion engine and electric motor, the development of adequate transmission system for electric motor which can both achieve drivability and comfort is imperative [123]. Taking advantage of the electric motor, this chapter investigates a novel dual input power-shifting system, and possible variations, which are efficient, robust and cost effective and could achieve torque hole compensation with the assistance of the second motor. With different configurations, the proposed system could serve both electric vehicle and hybrid vehicle.

3.2 Configuration investigations

To achieve the goal of making cleaner and more efficient vehicles without losing drivability and comfort, many innovative designs have been brought out and proved to be successful [124]. Prius earned its reputation by greatly reducing its fuel consumption in the meantime maintaining the smoothness in driving, but the ECVT transmission system in Prius is only for hybrid electric vehicle. There are also some successful pure electric vehicles such as Nissan Leaf, Mitsubishi iMIEV and early stage Tesla. They all

adopt single fixed ratio transmission system which has the advantages of lower manufacturing cost, relatively smaller powertrain volumes and less drive-train mass [86]. The limitations of this kind of transmission are also obvious. Firstly, the dynamic performance is poor because the speed and torque range are compromised; secondly, overall operating energy efficiencies are lower as the motor has its own efficiency curve that varies with torque and speed.

To overcome the problems that single fixed ratio transmissions have encountered, the development of multi-speed transmission attracts considerable attention. It entitles electric vehicles to higher efficiency [101] and better longitudinal behaviour [125]. For multi-speed transmission [126], manual transmission (MT) has the highest efficiency which is around 96%, the efficiency of automatic transmission (AT) is about 86% but it can transmit large torque as MT. Continuously variable transmission is famous for its smoothness but the overall efficiency is 85%. Based on the fundamentals of these transmissions, many novel configurations have been designed. In [36], detailed shifting mechanisms and control strategy for clutchless automated manual transmission (CLAMT) has been carried out, and the experiment results prove it is possible to remove the friction clutch of an AMT in the electric vehicle without compromising the dynamic performance. A planetary transmission is adopted in [127] to construct a seamless two-speed power split system. Walker et al. [128] introduce the dual clutch transmission to a pure electric vehicle and evaluate its detailed transient dynamic performance by both simulation and experiment. Fang et al. [129] bring out a new concept of uninterrupted mechanical transmission by modifying traditional planetary gearbox. In [130], a novel 4-wheel-drive two-speed electric vehicle layout is proposed.

Two sets of electric drivetrains are designed for the axles and by controlling the behaviours of both drivetrains, torque hole compensation is achieved which both improves the drivability and the driving comfort. Besides the novelty in transmission configuration, many researchers improve the drivability and the comfort by adding a various numbers of motors [131]. In [132], an on-board configuration is brought and in [133], the motors are mounted on the wheels which will directly provide the required speed and torque.

Among the aforesaid configurations, automated manual transmission is a promising solution to meet both requirements of dynamic performance and riding comfort, it has the advantages of high efficiency, low manufacture cost, and light in weight as a manual transmission and auto shifting ability as an automatic transmission [134,135]. But AMT also has its own drawbacks, which are the jerks during gear shifting, the excessive wear of the friction components and the torque interruption in the shifting process. To improve the drivability, Galvagno et al. proposed torque assisted AMT in [31], it uses a servo-assisted clutch to replace the fifth gear synchronizer which will provide certain power while the engine is disconnected from the powertrain, but the assisted clutch doesn’t have its own power source which means it can’t eliminate the torque hole but alleviate it. In [32], a modified AMT called Inverse-AMT is proposed, it puts the friction clutch after the gears instead before them. Experiment results prove it to some extent solves the torque interruption problem.

Extensive study has proved that the two major parasitic loss sources in transmission system are friction clutch elements and electro-hydraulic actuators [136]. The overall efficiency is compromised by 4% to 6% because of clutch drag and oil pumping. By

comparison in [29,30], it is feasible to greatly minimize the reduction in overall efficiency for the transmission using clutchless variants. For a conventional vehicle which adopts internal combustion engine, the clutch in the AMT is inevitable because of the speed and torque adjustment delay caused by the poor controllability of the engine, which also entails long speed synchronization duration and exacerbates the wear of the friction plates. But it is not the case for electric vehicles [137], there are three reasons [36]. First, the inertia of a motor is much smaller than that of an ICE which makes it capable of changing speed swiftly. Second, due to the excellent low-speed control capability, by controlling the motor, the vehicles can be launched smoothly. Third, it's easy to change the motor from torque mode to speed mode and vise versa. Therefore, after the synchronizer disengages the gears, the motor could change into speed mode which outputs little torque but reaches target speed immediately and then changes back to torque mode. Thus, the friction clutch is removed. Furthermore, because of the wide high-efficiency range, excellent speed regulation capability and fast torque response characteristics, transmission systems for EV need fewer gear ratios [138]. Zeroshift [139] is an example to remove friction clutch by re-designing the dog clutches to engage different gears without the need for speed synchronization. In [140], a series of controllable one-way clutches are employed to realize gear selection. In terms of the control strategy, [141] not only removes the friction clutch but also the synchronizer by refining the control algorithm. And in [8], the speeds and torques of the engine and motor are coordinately controlled to make it not necessary to have a clutch.

Aiming at designing a transmission system which could maximize energy efficiency, minimize emissions, and has certain drivability and comfort, this chapter brings out a

novel clutchless two motor power-shifting transmission where a single fixed ratio motor is utilized in parallel with a multi-speed transmission and second motor to balance the needs for improved motor efficiency in conjunction with power-on shifting capabilities. The structure of the system is presented below in Fig. 3-1.

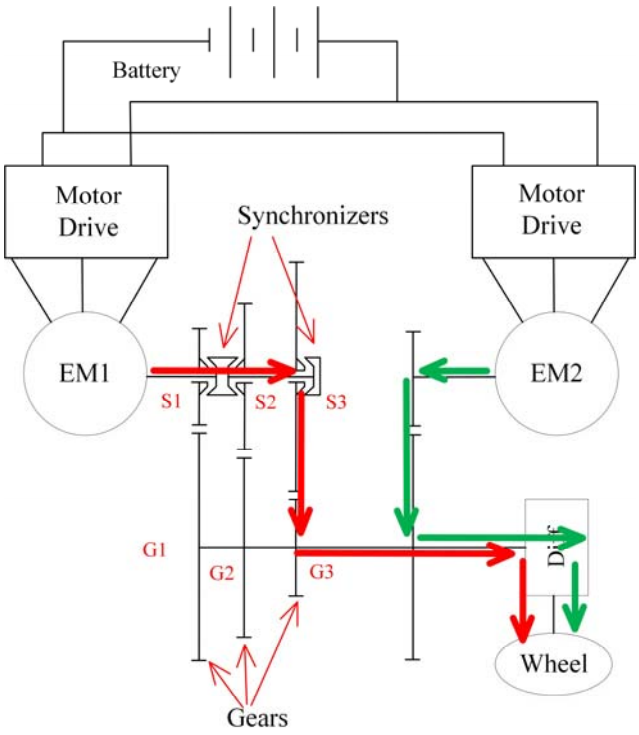

Figure. 3-1 Fixed-Multispeed transmission with synchronizer configuration.

The first motor drives the wheels through a multispeed transmission, with gear actuation achieved through a combination of motor speed control and synchronizer actuation [37]. This is a cost-effective and efficient method for achieving multispeed functionality without power-on shifting functionality. The second motor drives the transmission output shaft using a fixed reduction ratio and must be designed to achieve torque hole compensation through all of the gear shifts and also act as a driving motor under specified driving conditions. Such configurations have applications for both pure

electric and hybrid electric vehicle powertrains. This would include HEV variants with a conventional engine upstream of EM1 would allow for both series and parallel operation of the vehicle.

The possible working conditions are shown in Fig. 3-2.

	S1	S2	S3	EM1	EM2
idle	0	0	0	0	0
G1	1	0	0	1	1
					0
G2	0	1	0	1	1
					0
G3	0	0	1	1	1
					0

Figure. 3-2 Working conditions for the Fixed-Multispeed transmission with synchronizers.

It can be seen that for each gear, motor 1 could word alone as it is connected to the multispeed structure which will have a high efficiency. Moreover, it could work together will motor 2 when the torque demand exceeds its capacity or the overall efficiency will be higher if motor 2 is included.

3.3 Possible variations of the transmission configuration

Based on the ideas of choosing the most efficient fundamental transmission structure and achieving torque hole compensation to both improve the drivability and driving comfort, the proposed structure can be further improved through various variations.

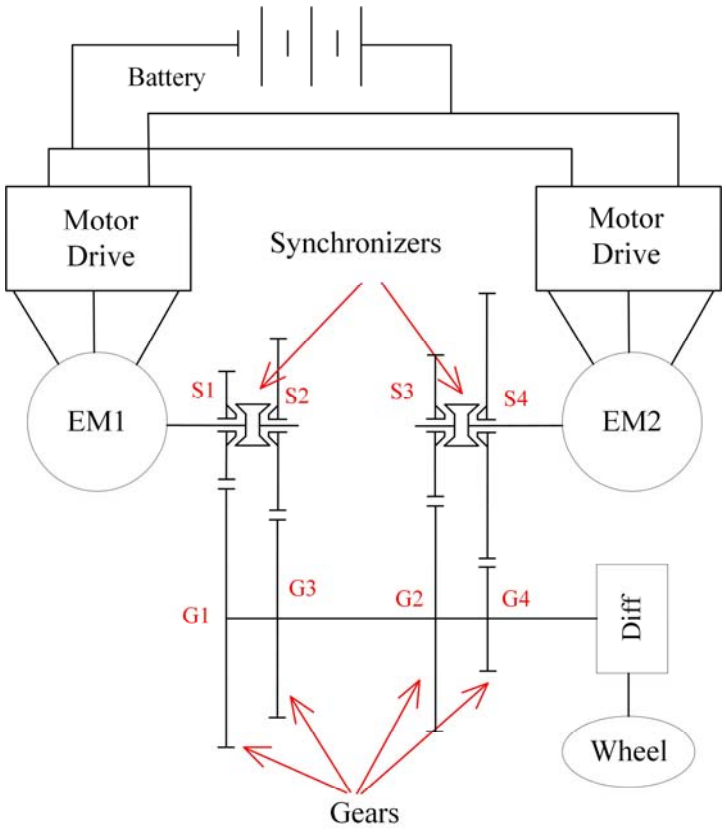

Figure. 3-3 Multispeed-Multispeed transmission with synchronizer configuration.

From the perspective of improving the overall efficiency of motor 2, the Multispeed-Multispeed transmission with synchronizer configuration is proposed and shown in Fig. 3-3.

The difference between the basic configuration and this structure is that a synchronizer and an additional gear pair is added to assist motor 2, and motor 1 is only connected with the odd gears and motor 2 is connected with even gears. Actually, this is pretty like the structure of a dual clutch transmission. The idea of a dual clutch transmission is to improve the drivability by connecting the odd gears and the even gears to different clutches that during the disengagement of one clutch, the other clutch can be energised at the same time. As a result, the torque hole during gear shifting can be compensated and the drivability will be improved. However, due to the different basic structures, the proposed system has more advantages. The first one is that clutch, with could cause considerable energy loss, is not necessary in the proposed system due to the dual input idea. The second one is that the proposed system could eliminate the torque hole completely with relatively simple control strategy while dual clutch transmission can only alleviate the torque hole problem by implementing complicated control algorithm which has to be optimized. The possible working conditions are listed in Fig. 3-4.

	S1	S2	S3	S4	EM1	EM2
idel	0	0	0	0	0	0
G1	1	0	0	0	1	0
G2	0	0	1	0	0	1
G3	0	1	0	0	1	0
G4	0	0	0	1	0	1

Figure. 3-4 Working conditions for the Multispeed-Multispeed transmission with synchronizers.

It can be seen that with the engagement of one synchronizer, the corresponding motor is activated to provide certain driving torque. It should be noted that beside the listed working conditions, the two motors could actually work together to assist each other in high demand scenario. To achieve this, a proper power sharing strategy should be developed to distribute the total power demand between the two motors and choose the proper gear position for each motor. The power sharing strategy is discussed in Chapter 5.

Fig. 3-5 shows a modified structure replacing the synchronizer with dog clutches.

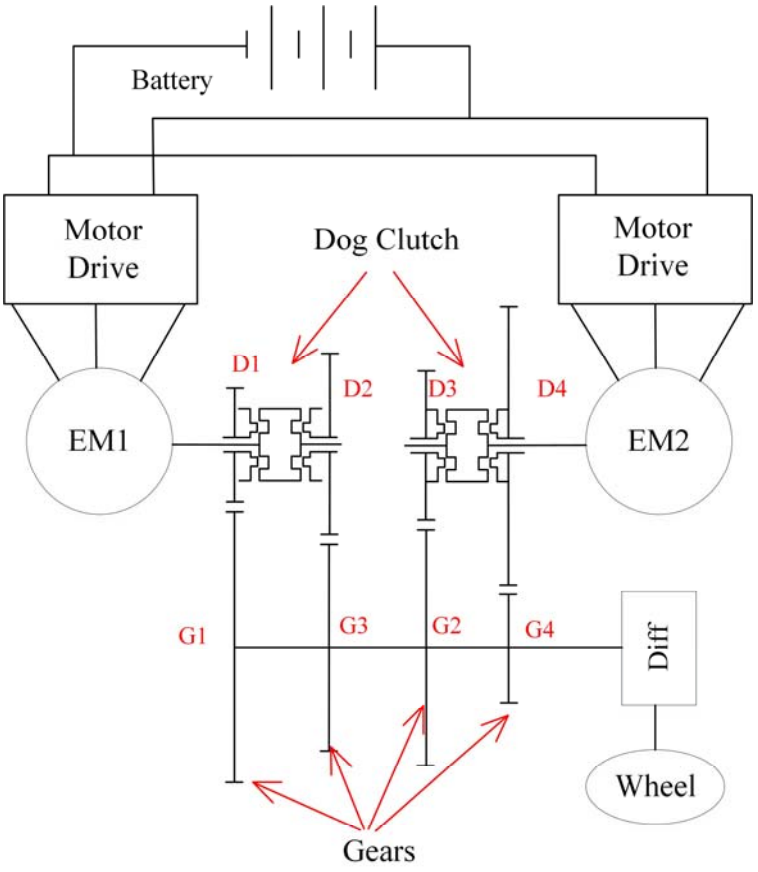

Figure. 3-5 Multispeed-Multispeed transmission with dog clutch configuration.

The purpose of this design is to completely remove the friction components which is the synchronizer in the aforesaid configuration. This configuration could avoid the wear of the friction components, improving the robustness, and improve the overall efficiency slightly. However, it requires advanced motor control strategies, as the engaging speeds of the two motors should be as accurate as possible to avoid undesirable vehicle jerks. The design of the dog clutch is also very important as an advanced design could help a lot to achieve the smoothness of clutch engagement [108].

The operating conditions for this configuration are shown in Fig. 3-6 and are very similar to the aforesaid configuration.

	D1	D2	D3	D4	EM1	EM2
idle	0	0	0	0	0	0
G1	1	0	0	0	1	0
G2	0	0	1	0	0	1
G3	0	1	0	0	1	0
G4	0	0	0	1	0	1

Figure. 3-6 Working conditions for the Multispeed-Multispeed transmission with dog clutches.

The further improved configuration is shown in Fig. 3-7. It can be seen that one more dog clutch is adopted between the output shafts of the two motors. This design gives both motor the ability to operate in all gear positions. For example, the torque demand is relatively high which requires the activation of both motors. However, for the aforesaid configuration, it is only possible for the two motors to work in different gear positions, which may compromise the overall efficiency as one of them may work in low efficiency area. For the proposed structure, the output torque of the two motors can be combined and work in any single gear position which could possibly provide the best fuel economy.

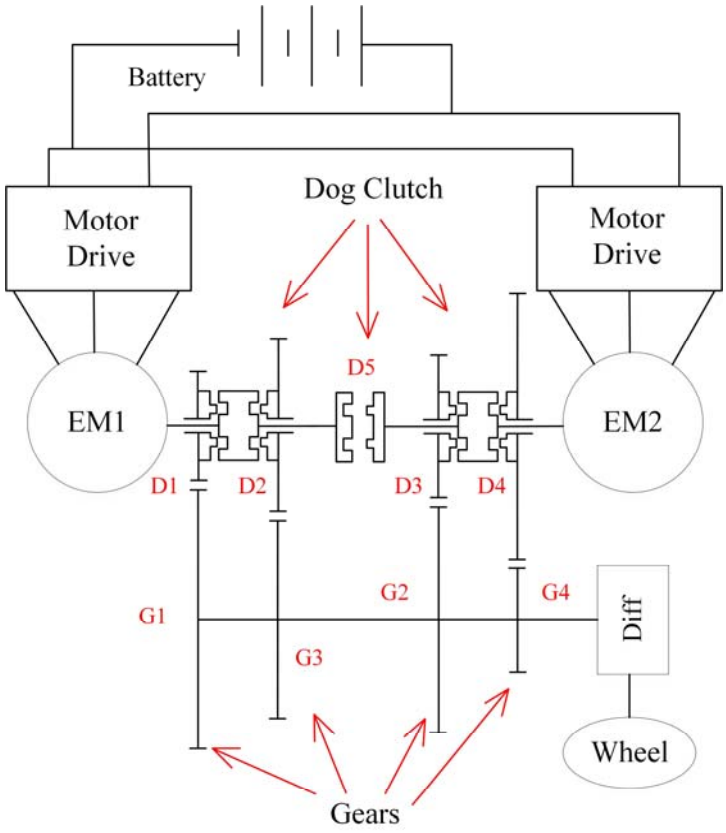

Figure. 3-7 Multispeed-Multispeed and combined motor transmission with dog clutch configuration.

Due to the changes of the structure, the possible working conditions are also more complicated and are shown in Fig. 3-8. It can be seen that for each gear position, there is a subclass depends on the condition of the fifth dog clutch. Take the first gear as an example, when D5 is not engaged, only motor 1 will be activated and motor 2 will stay idle. However, if D5 is engaged, motor 2 will also be activated to provide the required torque. For gear 2 and gear 4, it is the opposite, the activation of motor 1 depends on the condition of D5.

	D1	D2	D3	D4	D5	EM1	EM2
idle	0	0	0	0	0	0	0
G1	1	0	0	0	0	1	0
					1	1	1
G2	0	0	1	0	0	0	1
					1	1	1
G3	0	1	0	0	0	1	0
					1	1	1
G4	0	0	0	1	0	0	1
					1	1	1

Figure. 3-8 Working conditions for the Multispeed-Multispeed and combined motor transmission with dog clutches

3.4 Conclusions

This chapter introduces the possible variations based on the basic configuration. Actually, there are more variations and it is even possible to add a third power input. Motor 1 could be replaced with a more complex structure which consists of an engine, a motor and a planetary gear box. One of the planetary component could be connected to the input shaft of the proposed system and the other two can be connected to the power sources. This idea will converter the pure electric powertrain system into a hybrid electric system which makes the configuration more adaptive.

CHAPTER 4 : Gear shifting control strategy for the dual input system

4.1 Introduction

The purpose of this chapter is to study the practical application of a two-motor electric vehicle powertrain utilizing a combination of fixed and multiple speed gear ratios. To realize power-on shifting without torque hole and maximize overall efficiency [140], a high-speed motor is adopted as the primary motor connecting to the multiple speed clutchless automated manual transmission and a low-speed high torque electric motor is employed as the assisting motor connected to the final shaft with fixed gear ratio [142]. Motor torque and speed are controlled using improved model predictive flux control method [143] in conjunction with synchronizer mechanism actuation to best fill the torque hole to improve both drivability and driving comfort. To evaluate the proposed system, a complete mathematical model is built and compared with a conventional single motor transmission system. The detailed transient dynamic results in terms of final shaft torque, acceleration and vehicle jerk demonstrate the effectiveness of the proposed powertrain. Fig. 4-1 shows the structure of the proposed system.

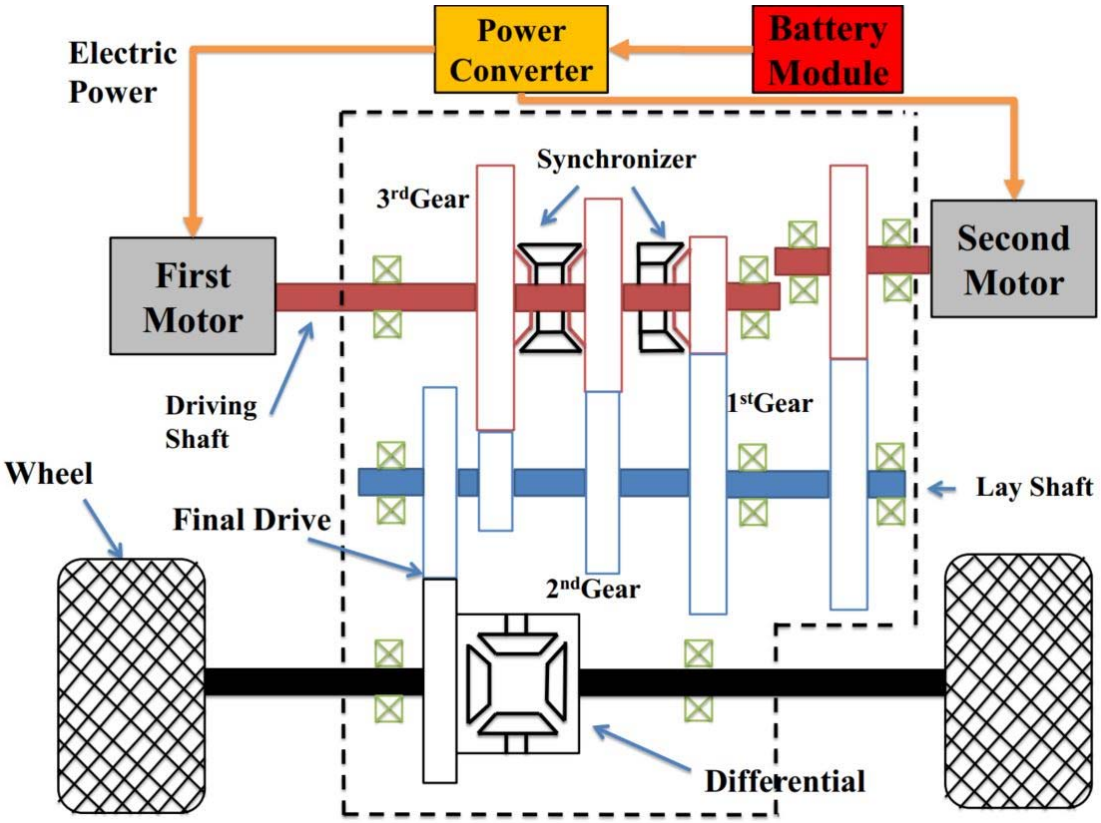

Figure. 4-1 Proposed dual input clutchless transmission system.

4.2 System modeling and control methodology

To fully study and verify the dynamic performance of the proposed architecture and its shifting control strategy, a detailed powertrain model is built in this section as follows:

1. Electric motor with improved model-predictive flux control
2. Simplified synchronizer mechanism, that assumes once speed synchronization is complete the engagement process is successful
3. Multibody powertrain model using lumped torsional elements
4. Vehicle model

4.2.1 Electric motor model and control

In order to maximize the drivability and driving comfort, the electric motor should be precisely controlled to follow torque and speed profile to accomplish a seamless gear shifting process. There are many existing high-performance control methods [144] such as field oriented control (FOC), direct torque control (DTC) and model predictive torque control (MPTC). FOC decomposes the stator currents into torque and flux components, which will be regulated by proportional integral controllers separately, in synchronous frame and uses a modulation block to generate the final gating pulses. It would achieve high torque and flux control performance but also requires fine-tuning work. DTC is an effective way to give quick dynamic responses with a simple structure, but it generates high steady-state torque ripples. MPTC takes credits for an intuitive concept, high flexibility and easy incorporation of constraints but the tedious stator flux weighting factor tuning work limits its application.

To overcome the aforesaid drawbacks in motor control methods, an improved model predictive flux control (MPFC) method is adopted. Not as conventional MPTC which needs to generate a proper weighting factor between control variables of torque and stator flux, MPFC converts these two components into a stator flux vector in which they have the same unit, eliminating the use of weighting factor.

The electric motor can be expressed as:

$$\dot{\boldsymbol{x}} = \boldsymbol{A}\boldsymbol{x} + \boldsymbol{B}\boldsymbol{u} \qquad (1)$$

where $\boldsymbol{x}=\left[\boldsymbol{i}_s \boldsymbol{\psi}_s\right]^T$ are state variables, ψ_s stator flux and $\boldsymbol{i}_s$ is stator current, $\boldsymbol{u}=\boldsymbol{u}_s$ is the stator voltage. Matrix $\boldsymbol{A}$ and $\boldsymbol{B}$ are defined as:

The electric motor can be expressed as:

$$\boldsymbol{A}=\begin{bmatrix} -\lambda(R_s L_r + R_r L_s) + j\omega_r & \lambda(R_r - jL_r\omega_r) \\ -R_s & 0 \end{bmatrix} \quad (2)$$

$$\boldsymbol{B}=\begin{bmatrix} \lambda L_r \\ 1 \end{bmatrix} \quad (3)$$

where R and L are stator resistance and inductance and subscripts s, r, and m are stator, rotor and mutual, respectively, and ω_r is electrical rotor speed, $\lambda=\frac{1}{(L_s L_l - L_m^2)}$.

In order to predict $\boldsymbol{x}$ at the next control instant, second-order Euler discretization is adopted instead of the first-order one to improve accuracy:

$$\begin{cases} \boldsymbol{x}_p^{k+1} &= \boldsymbol{x}^k + T_{sc}(\boldsymbol{A}\boldsymbol{x}^k + \boldsymbol{B}\boldsymbol{u}_s^k) \\ \boldsymbol{x}^{k+1} &= \boldsymbol{x}_p^{k+1} + \frac{T_{sc}}{2}\boldsymbol{A}(\boldsymbol{x}_p^{k+1} - \boldsymbol{x}^k) \end{cases} \quad (4)$$

where T_{sc} is the control period and $\boldsymbol{x}^{k+1}=\left[\boldsymbol{i}_s^{k+1} \boldsymbol{\psi}_s^{k+1}\right]$ is the predicted state vector.

The accuracy of state estimation will directly affect the performance of MPFC, here a full order observer is adopted:

$$\frac{d\hat{\boldsymbol{x}}}{dt} = \boldsymbol{A}\hat{\boldsymbol{x}} + \boldsymbol{B}\boldsymbol{u} + \boldsymbol{G}(\boldsymbol{i}_s - \hat{\boldsymbol{i}}_s) \tag{5}$$

where $\hat{\boldsymbol{x}}$ is the estimated state and $\mathbf{G} = -\begin{bmatrix} 2b \\ b/(\lambda L_r) \end{bmatrix}$ is a constant gain matrix used to improve the stability and b is a negative constant gain.

Because of the delay compensation, not only reference $\boldsymbol{\psi}_s^{ref}$ at (k+1)th instant should be calculated but also reference $\boldsymbol{\psi}_s^{ref}$ at (k+2)th instant. The procedure can be summarized as:

$$\boldsymbol{\psi}_r^{k+1} = \frac{L_r}{L_m}\boldsymbol{\psi}_s^{k+1} - \frac{1}{\lambda L_m}\boldsymbol{i}_s^{k+1} \tag{6}$$

$$\boldsymbol{\psi}_r^{k+2} = \boldsymbol{\psi}_r^{k+1} + T_{sc}(R_r\frac{L_m}{L_r}\boldsymbol{i}_s^{k+1} - (\frac{R_r}{L_r} - j\omega_r)\boldsymbol{\psi}_r^{k+1}) \tag{7}$$

After acquiring $\boldsymbol{\psi}_r^{k+2}$, the phase angle of $\boldsymbol{\psi}_s^{ref}$ at (k+2)th instant could be expressed as:

$$\angle\boldsymbol{\psi}_s^{ref} = \boldsymbol{\psi}_r^{k+2} + \arcsin(\frac{T_e^{ref}}{\frac{3}{2}pL_m\left|\boldsymbol{\psi}_r^{k+2}\right|\left|\boldsymbol{\psi}_s\right|^{ref}}) \tag{8}$$

where T_e^{ref} is the torque reference. The final stator flux vector reference can be obtained as:

$$\boldsymbol{\psi}_s^{ref} = \left|\boldsymbol{\psi}_s^{ref}\right| \bullet \exp(j \angle \boldsymbol{\psi}_s^{ref}) \tag{9}$$

Although eliminating the weighting factor saves much offline time, torque ripples and current harmonics still exist if selected voltage vector is applied during the whole control period. In order to further improve the electric motor performance, it is imperative to optimize the switching instant of the selected vector during $[0, T_{sc}]$ which can be expressed as:

$$t_{opt} = \frac{(\boldsymbol{\psi}_s^{ref} - \boldsymbol{\psi}_r^{k+1} - f_i^{k+1} T_{sc}) \odot (\boldsymbol{f}_{old} - \boldsymbol{f}_i^{k+1})}{\left|\boldsymbol{f}_{old} - \boldsymbol{f}_i^{k+1}\right|^2} \tag{10}$$

where $\boldsymbol{f}_{old}$ is the stator flux slope for voltage vector, subscript old means it is applied at the end of the previous control period, $\boldsymbol{f}_i^{k+1}$ is for the selected voltage vector in this control period and $\odot$ is the dot product.

For a given voltage vector $\boldsymbol{u}_{si}^{k+1}$, stator flux at ($k$+2)th instant can be obtained after getting the optimal switching time t_{opt} as:

$$\boldsymbol{\psi}_{si}^{k+2} = \boldsymbol{\psi}_s^{k+1} + (\boldsymbol{u}_{old} - \boldsymbol{u}_{si}^{k+1}) t_{opt} + (\boldsymbol{u}_{si}^{k+1} - R_r \boldsymbol{i}_s) T_{sc} \tag{11}$$

In order to force stator flux to track its reference and prevent high deviation of stator flux, a cost function can be built as:

$$J = \left|\boldsymbol{\psi}_s^{ref} - \boldsymbol{\psi}_s^{k+2}\right| + \left|\psi_s^{ref} - \left|\boldsymbol{\psi}_s^{t}\right|\right| \tag{12}$$

where $\psi_s^t = \psi_s^{k+1} + u_{old} t_i$ is the stator flux vector at the optimal switching instant.

The whole control strategy is summarized in Fig. 4-2.

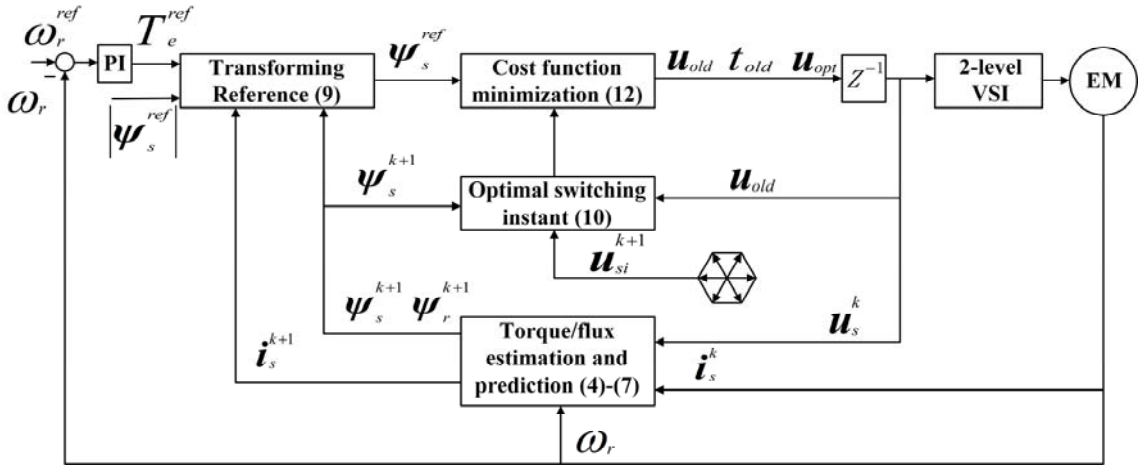

Figure. 4-2 Proposed switching instant optimized electric motor control diagram.

A simulation comparison has been made in Fig. 4-3 which shows torque response performance between DTC, FOC and MPFC, to demonstrate the effectiveness of the proposed MPFC.

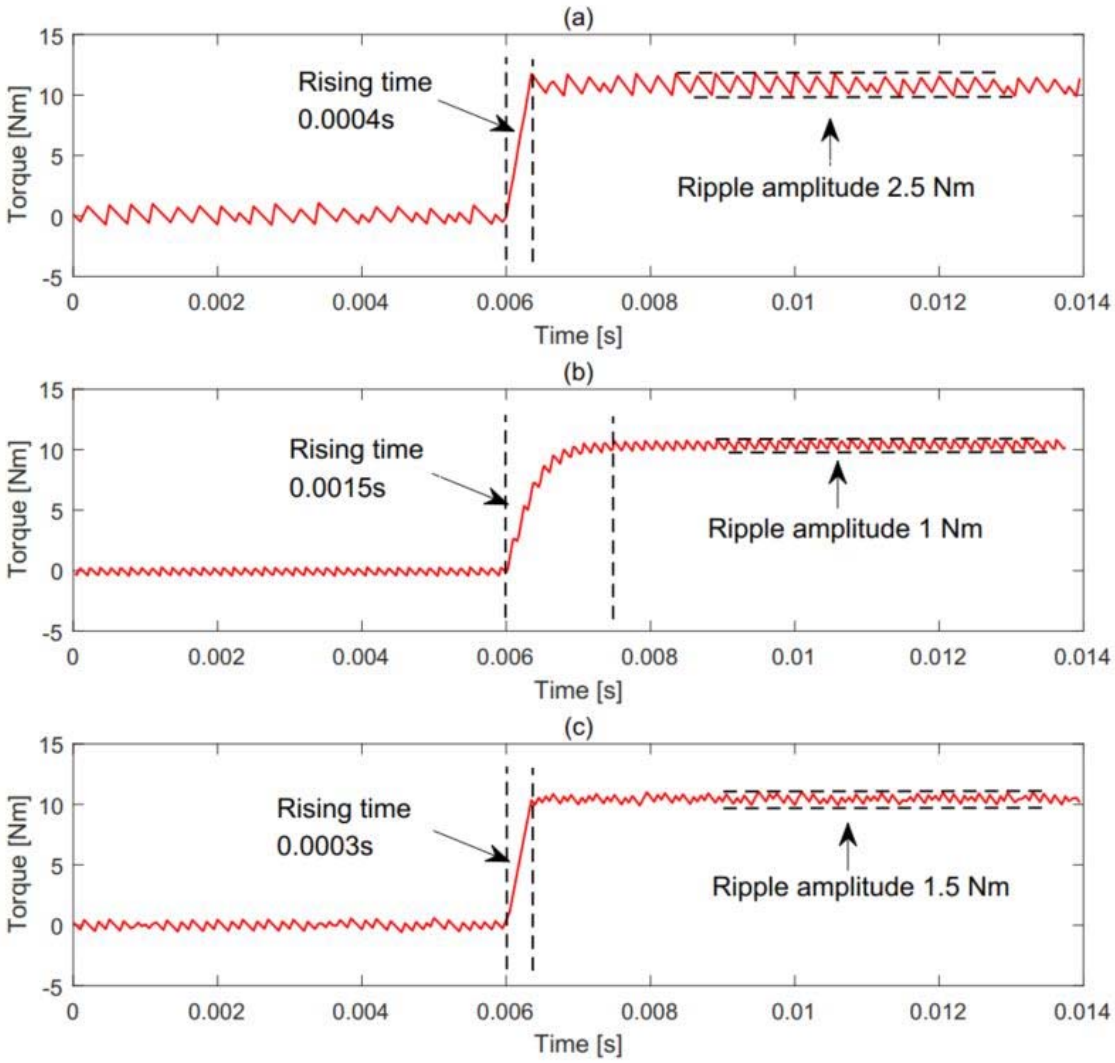

Figure. 4-3 Torque response performance of (a) DTC, (b) FOC, (c) MPFC.

It can be seen in Fig. 4-3 that DTC and MPFC take only about 0.0003s to reach 10Nm while FOC takes about 0.0015s which means that DTC and MPFC are better in terms of dynamic performance. As to static performance, FOC is better with a ripple amplitude around 1 Nm while DTC has the largest amplitude of 2.5 Nm. MPFC has an acceptable ripple amplitude which is 1.5 Nm.

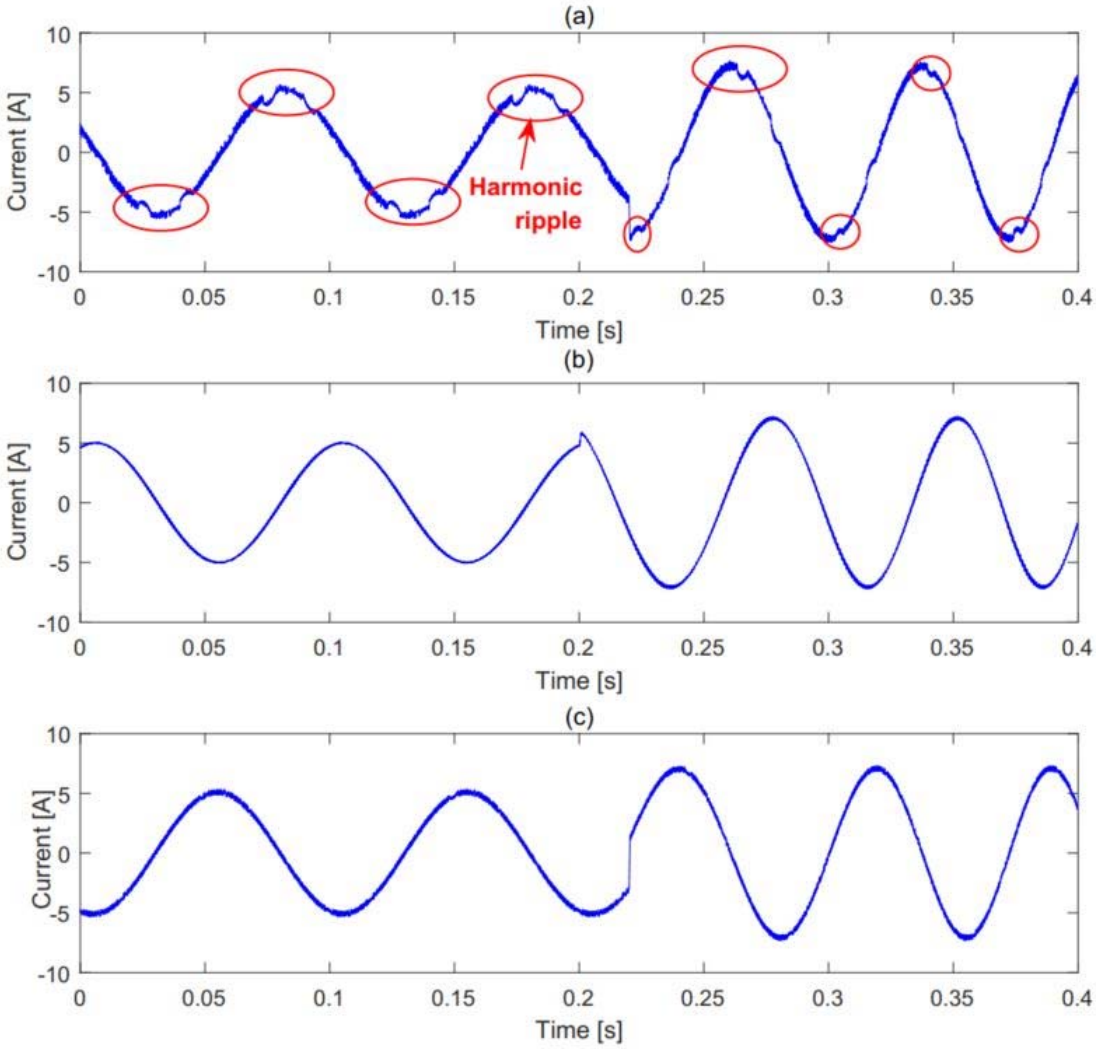

Figure. 4-4 Current response performance of (a) DTC, (b) FOC, (c) MPFC.

In the current response performance in Fig. 4-4, FOC and MPTC have similar performance with no obvious harmonic ripple in 0.4s while DTC has significant distortions, which will cause more losses.

4.2.2 Synchronizer model

For the purpose of this study the synchronizer mechanism is simplified to capture the main actuation characteristics. It includes only the speed synchronization stage of engagement, and post-synchronization is considered to be completely locked, with the other states of engagement ignored. This is a consequence of the speed synchronization component being critical to ensure actuation, whilst other stages, such as dog clutch engagement, are not critical to the duration of shifting [37].

Thus the synchronizer model is reduced to a cone clutch. The cone clutch torque is described as follows:

$$T_{SYN} = \frac{u_D R_C F_S}{\sin \alpha} \tag{13}$$

where T_{SYN} is the cone torque, u_D is the dynamic friction coefficient, R_C is the mean cone radius and α is the cone angle.

An ideal actuation process is considered for the synchronizer mechanism. The energized and neutral states of the synchronizer mechanism results in two possible engagement states, these are simulated as follows:

$$F_S = \begin{cases} P & Energised \\ 0 & Neutral \end{cases} \tag{14}$$

where F_S is the synchronizer load and P is the magnitude of the applied load. Values for P are set based on the duration of actuating the simplified mechanism and are

consistent with typical values. To compensate the time required to release or engage the synchronizer after an actuation request, a small-time delay will be employed to maintain these characteristics.

4.2.3 Powertrain dynamics model

The proposed transmission system is shown in Fig. 4-5.

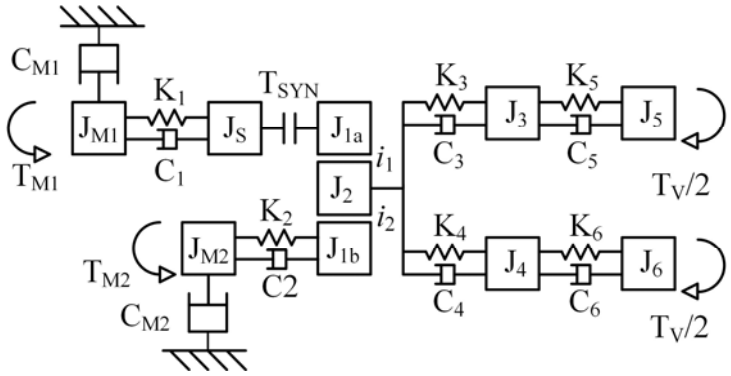

Figure. 4-5 Clutchless AMT multi-body model.

In Fig. 4-5, J represents the inertia of each component and $M1$ and $M2$ are for the first motor and the second motor, respectively. K is the stiffness of each shaft and C is its damping coefficient. i_1 and i_2 are the chosen gear ratio for motor 1 and the fixed gear ratio for motor 2, respectively. Subscripts S, $1a$, $1b$ and 2 are for the synchronizer, the chosen gear for motor 1, the fixed gear for motor 2 and the driven gear, respectively, and subscripts 3 and 4 represent the half shafts. Finally, the tires are represented by subscript 5 and 6. The first motor is directly connected to a multi-speed transmission through an input shaft by pairs of synchronizers without using flywheel, clutch or torsional dampers due to the merits of electric motor. This simplification cannot be

achieved in conventional ICE transmission system because the inertia of ICE is much larger and the speed and torque control cannot be as precise as electric motor. The second motor uses another power path directly connect the differential with a fixed gear.

Based on free body diagram and assuming there is no eccentricity existed in the transmission system, the equations of system inputs are expressed as follows

$$J_{M1}\ddot{\theta}_{M1} = T_{M1} - C_{M1}\dot{\theta}_{M1} - K_1(\theta_{M1} - \theta_S) - C_1(\dot{\theta}_{M1} - \dot{\theta}_S) \quad (15)$$

$$J_{M2}\ddot{\theta}_{M2} = T_{M2} - C_{M2}\dot{\theta}_{M2} - K_2(\theta_{M2} - i_2\theta_2) - C_2(\dot{\theta}_{M2} - i_2\dot{\theta}_2) \quad (16)$$

where θ is the angular displacement and the first and second derivative of θ are angular velocity and angular acceleration.

If the synchronizer is not completely closed, the dynamic equation for the synchronizer should be like

$$J_S\ddot{\theta}_S = K_1(\theta_{M1} - \theta_S) + C_1(\dot{\theta}_{M1} - \dot{\theta}_S) - T_{SYN} \quad (17)$$

where T_{SYN} is the torsional force from the cone of the synchronizer. As the chosen driving gear 1a and motor 2 output driving gear 1b are engaged with output driven gear noted as 2, the lumped dynamic equation for these three parts can be summarized as

$$\begin{aligned}(J_2 + i_1^2 J_{1a} + i_2^2 J_{1b})\ddot{\theta}_2 &= i_1 T_{SYN} + [K_2(\theta_{M2} - i_2\theta_2) + C_2(\dot{\theta}_{M2} - i_2\dot{\theta}_2)]i_2 \\ &- K_3(\theta_2 - \theta_3) - C_3(\dot{\theta}_2 - \dot{\theta}_3) - K_4(\theta_2 - \theta_4) - C_4(\dot{\theta}_2 - \dot{\theta}_4)\end{aligned} \quad (18)$$

For the half shaft and vehicle tires, as they are symmetrical and the equations are the same for both sides, only one side will be illustrated as

$$J_3 \ddot{\theta}_3 = K_3(\theta_2 - \theta_3) - C_3(\dot{\theta}_2 - \dot{\theta}_3) - K_5(\theta_3 - \theta_5) - C_5(\dot{\theta}_3 - \dot{\theta}_5) \quad (19)$$

$$J_5 \ddot{\theta}_5 = K_5(\theta_3 - \theta_5) + C_5(\dot{\theta}_3 - \dot{\theta}_5) - T_V / 2 \quad (20)$$

where T_V is the driving resistance. When the synchronizer is completely engaged, the transmission is closed and the lumped inertia of the synchronizer and the driving gear 1a are rigidly connected, Eq. (17) and Eq. (18) can be reduced as

$$\begin{aligned}\left[J_2 + i_1^2(J_{1a} + J_S) + i_2^2 J_{1b}\right]\ddot{\theta}_2 &= \left[K_1(\theta_{M1} - i_1\theta_2) + C_1(\dot{\theta}_{M1} - i_1\dot{\theta}_2)\right] i_1 \\ &+ \left[K_2(\theta_{M2} - i_2\theta_2) + C_2(\dot{\theta}_{M2} - i_2\dot{\theta}_2)\right] i_2 - K_3(\theta_2 - \theta_3) - C_3(\dot{\theta}_2 - \dot{\theta}_3) \\ &- K_4(\theta_2 - \theta_4) - C_4(\dot{\theta}_2 - \dot{\theta}_4)\end{aligned} \quad (21)$$

4.2.4 Vehicle model

For a driving vehicle, there are generally three main sources of resistance which are the incline of the road, aerodynamic drag, and tire rolling resistance. These resistances can be expressed as

$$T_V = \left(m_V g \sin\varphi + \frac{1}{2}\rho A_V C_d v^2 + m_v g C_t\right) R_w \quad (22)$$

where m_V is the mass of the vehicle and φ is the degree of the road incline, ρ is the air density, A_V is the area of the vehicle front side and C_d is the drag coefficient, v is the current vehicle speed, C_t is the tire rolling friction coefficient and R_w is the tire radius. The speed of the vehicle v can be calculated as

$$v = 3.6 R_w \dot{\theta}_2 / \gamma_f \tag{23}$$

where the coefficient 3.6 makes the speed unit as km/h and γ_f is the ratio of the final differential.

The key parameters of the transmission and the vehicle are listed in Table 4-1.

Table 4-1 Key parameters for the proposed system

Symbol	Name	Value	Unit
J_{M1}	Motor 1	0.045	$kg \bullet m^2$
J_{M2}	Motor 2	0.065	$kg \bullet m^2$
J_S	Synchronizer	0.025	$kg \bullet m^2$
J_{1a}	Driving gear	0.02	$kg \bullet m^2$
J_{1b}	Driving gear	0.02	$kg \bullet m^2$
J_2	Driven gear	0.2	$kg \bullet m^2$
J_3	Half shaft	1	$kg \bullet m^2$
C_1	Damping	50	$Nm \bullet s$ / rad
C_4	Tire damping	100	$Nm \bullet s$ / rad
K_1	Motor output	50000	Nm / rad
K_3	Half shaft	50000	Nm / rad
K_4	Tire stiffness	10000	Nm / rad
m_V	vehicle mass	1200	kg
R_w	tire radius	0.3	m

ρ	Air density	1.127	$kg \bullet m^3$
φ	Road incline	0	°
u_D	Dynamic friction coefficient	0.3	
u_S	Static friction coefficient	0.35	

4.2.5 Electric motor selection

The purposes of the two motors are slightly different, for the first motor, it will be working as the primary power source in relatively low speed conditions where frequent starts and stops are required like urban traffic because it is connected to a multispeed transmission which will greatly improve the driving efficiency under a wider speed range. For the second motor, it would help compensate the torque hole, which happens in conventional AMT transmission system, during shifting process to improve the dynamic performance of the vehicle and the driving comfort. The second motor would also help provide certain torque when the power demand from the driver exceeds the capability of the first motor in prompt acceleration either in low or high speed, or under certain driving condition that the second motor could work in its high efficiency area. The combination output from both motors will together provide the system with demand power.

As the second motor should achieve torque hole compensation during gear shifting, the peak torque and speed for the second motor should meet some constraints which are expressed as

$$T_{M2} = \frac{i_{M1}}{i_{M2}} T_{M1} \tag{24}$$

$$\dot{\theta}_{M2} = \frac{i_{M2}}{i_{M1}} \dot{\theta}_{M1} \tag{25}$$

where i_{M1} is the current gear ratio for motor 1 and i_{M2} is the direct gear ratio for motor 2.

It is worth pointing out that Eq. (24) and Eq. (25) are not strict constraints choosing the motor because gear shifting is a process within 2 seconds or less, for most motors, it is allowed to work beyond their preference working area for a very short time. As a result, a balance can be achieved to choose a motor that both can work together with the first motor in its high efficiency region and provide enough power during gear shifting. Fig. 4-6 shows the efficiency map of the first and the second motor.

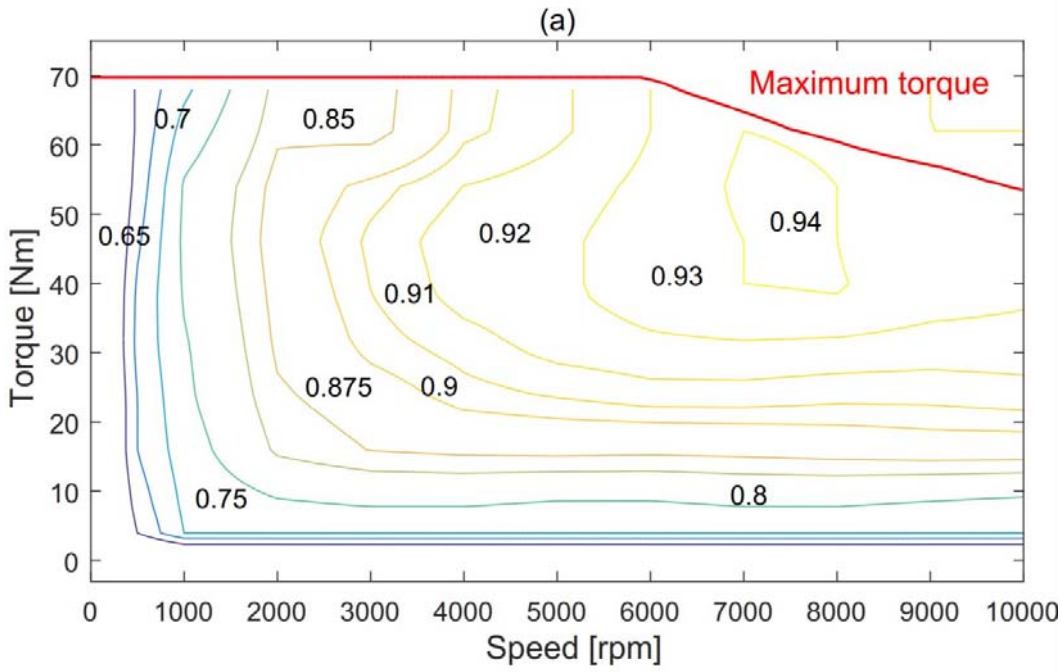

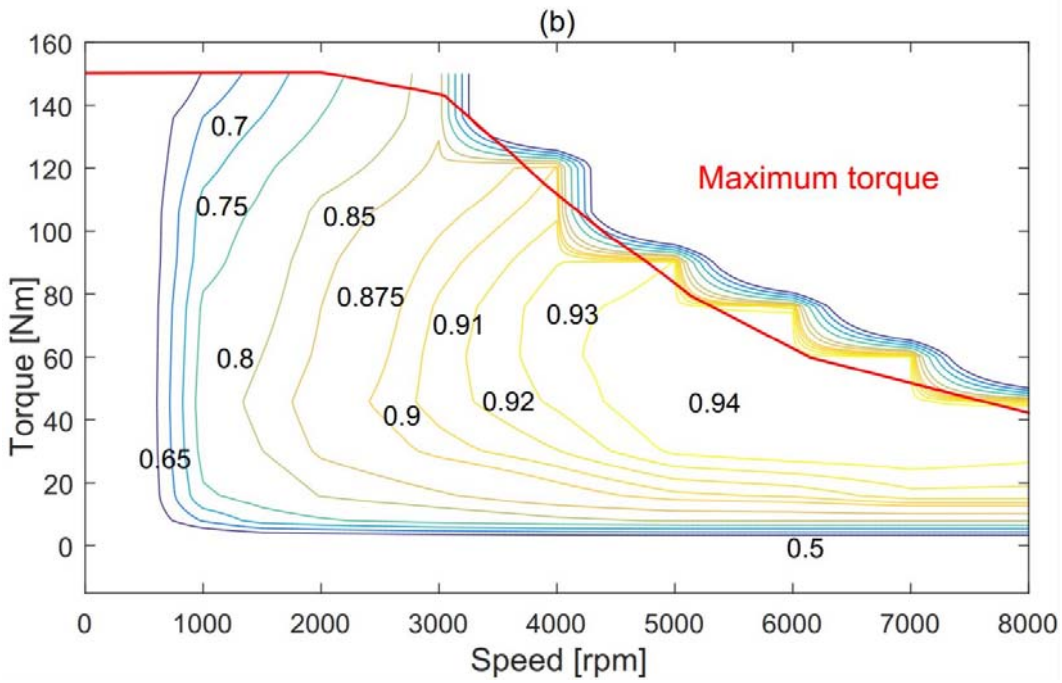

Figure. 4-6 Motor efficiency maps, (a) first motor, (b) second motor.

It can be seen that the power of both motors are very similar about 42 kW which is designed to maximize the usage and efficiency of both motors and reduce the overall cost and the volume. It should be noted that the power of two motors should be similar in order to achieve torque hole compensation. In order to meet the requirements from Eq. (24) and Eq. (25), the peak torque of motor two should be larger than that of motor one as the gear ratio range for the first motor is larger which is the advantage of multispeed transmission. The first and second gear ratio for the first motor are designed for low speed situation which happens in city driving condition and the third gear ratio is meant to meet high speed cruising requirements. The gap between the second and third gear are filled with the gear ratio of the second motor, which means motor 2 will provide most of the power demand in medium-high speed condition like the speed profile in HWFET driving cycle. In acceleration condition which demands a lot of

power, both motors will work together, decidied by the PSC, helping guarantee the drivability and efficiency. For this system, the corresponding gear ratios are listed in Table 4-2.

Table 4-2 Designed gear ratios

Symbol	Name	Value
i_{c1}	Counter gear for Motor 1	4.62
i_{c2}	Counter gear for Motor 2	2.16
i_{g1}	First gear for Motor 1	3.46
i_{g2}	Second gear for Motor 1	2.08
i_{g3}	Third gear for Motor 1	1.32
i_2	Gear for Motor 2	3.46

4.3 Gear shifting control

Compared with conventional AMT, the proposed system could achieve torque hole compensation during gear shifting process under appropriate shifting control strategy which is shown in Fig. 4-7.

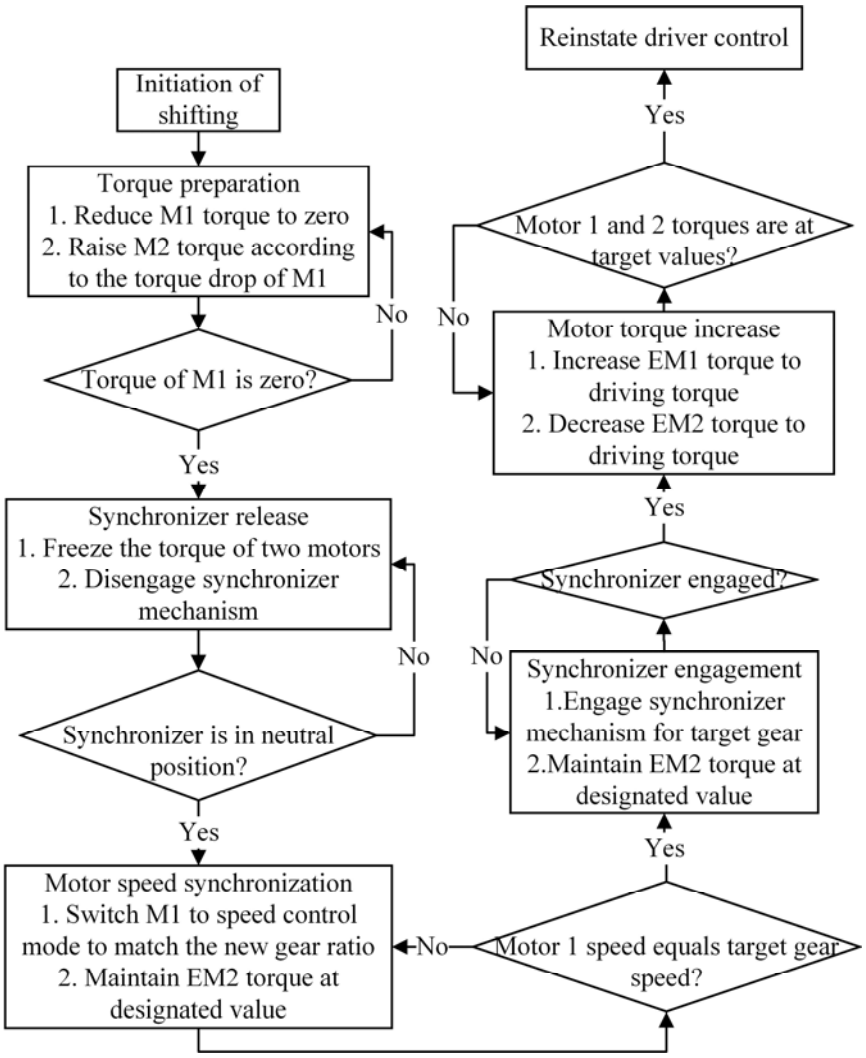

Figure. 4-7 Shifting control strategy.

The proposed strategy can be roughly divided into 7 steps including shift initiation and torque reinstatement. Before the initiation of gear shifting, the torque demands for both motors and activated gears are decided by the PSC strategy, if the PSC gives an order to change gear ratio, the gear shifting control unit will take over the control of motor speeds and torques and the actuation of synchronizers. The five main control phases are listed as follows:

1. Motor torque preparation. In this stage, the torque of the first motor should drop to zero as the situation of conventional AMT to prepare for synchronizer disengagement. The final driving shaft torque will plunge evidently which would cause perceivable vehicle jerks. To compensate the torque hole, the torque of motor 2 should rise simultaneously according to the torque drop of motor 1, maintaining adequate torque output during shifting, to improve the drivability and driving comfort.
2. Synchronizer release. After the torque of motor 1 drops to zero, the synchronizer would move to neutral position preparing for the following engagement. The whole power of the powertrain is provided by motor 2 alone which guarantee the vehicle could accelerate as desired.
3. Motor speed synchronization. Motor 1 should switch into speed control mode after the synchronizer is released. As motor 1 is not connected to the powertrain in this stage, the torque pulse here to match the motor speed with the target gear speed will not affect the final shaft torque.
4. Synchronizer engagement. After the speed of the first motor is the same with target gear speed, the actuator of the synchronizer will push the sleeve towards the new gear hub. The cone clutch in the synchronizer will help eliminate the speed difference within tolerance.
5. Motor torque reinstatement. Motor 1 would switch back to torque control mode if the synchronizer is completely locked and then increase its torque to target level which is decided by PSC strategy while motor 2 would reduce its torque to guarantee there is not torque overshot in the final shaft.

The proposed gear shifting steps alone cannot guarantee a smooth power-on gear shifting, a more specific torque and speed change profile for torque preparation, speed synchronization and torque reinstatement should be proposed. To avoid sudden torque change in the final shaft, a modified bump function is used as

$$T_M = Ae^{\frac{-1}{1-x^2}} \tag{26}$$

where A is the coefficient for the bump amplitude to fit the input torque, and x is a variable to control the duration of torque change which is defined as $x = \frac{t_0 - t}{t_D}$. Here, t_0 is the time when the torque phase begins and t_D is the designed duration for the phase. At the beginning of the stage, the profile will change slowly making it easier for the final shaft torque to maintain as steady as possible. Then, the torque profile will drop quickly to the target value which shortens the duration of whole gear shifting process. Finally, the profile reaches the target value slowly to end torque preparation phase. During the same phase, the torque of the second motor will rise to exactly make up for the equivalent torque loss in the final shaft because of the first motor.

For the torque reinstate phase, the bump function should be

$$T_M = B - Ae^{\frac{-1}{1-x^2}} \tag{27}$$

where B is the target torque for the first motor. To demonstrate how the torque control strategy works to guarantee a smooth power-on shifting, a simulation has been conducted and shown in Fig. 4-8.

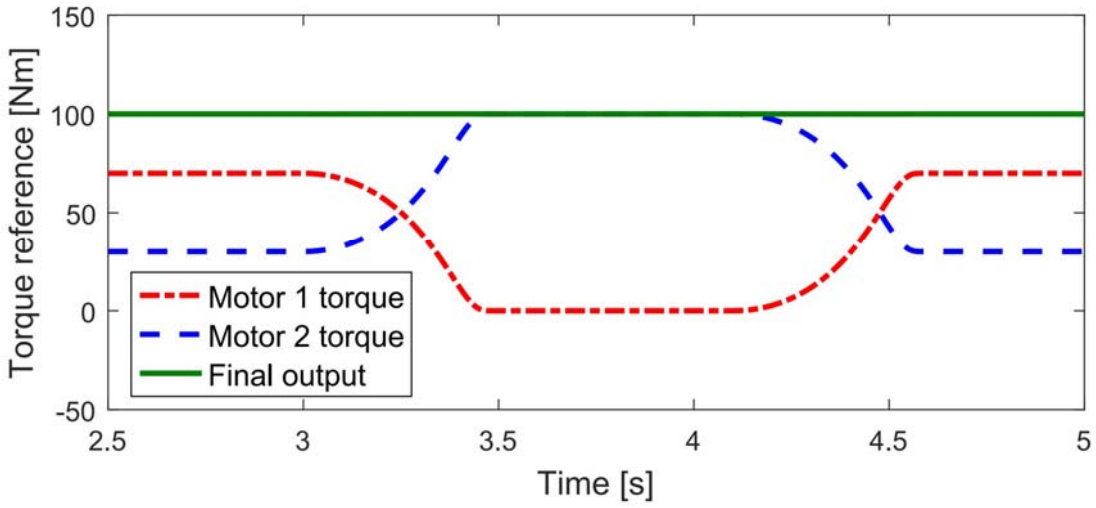

Figure. 4-8 Torque reference controlled by bump function.

It can be seen that although the torque from the first motor reduces to zero, the torque in the final shaft doesn't change, a smooth power-on shifting can be realized.

The speed synchronization phase is also controlled by a modified bump function as

$$\dot{\theta}_M = i_T i_2 \dot{\theta}_{2b} \pm i_A i_2 \dot{\theta}_{2b,0} e^{\frac{-1}{1-x^2}} \quad (28)$$

where T and A are for target and actual gear, respectively, and subscript 0 is for the initial value at the beginning of this phase. This control profile is only for the first motor because the second motor is directly connected to the final shaft through a pair of fixed ratio gears.

4.4 Driving comfort and drivability improvement

In this section, the proposed dual input clutchless transmission system with its shifting control strategy is verified in terms driving comfort and drivability, which are improved by torque hole compensation and measured in vehicle accelerations and jerks.

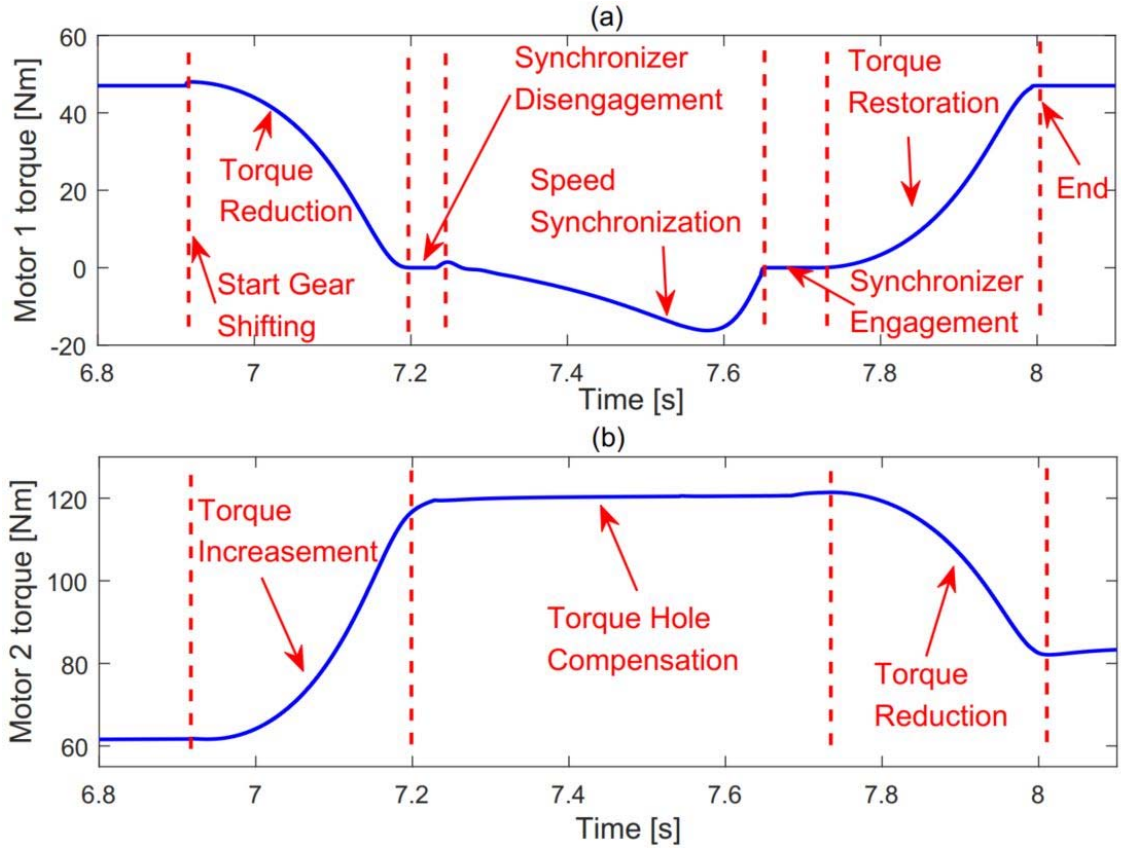

Figure. 4-9 Shifting control for both motors.

To demonstrate the torque hole compensation performance, an acceleration from 0 to 70 km/h in 8 seconds has been conducted, and it experiences gear shifts from idle state to the third gear during the linear acceleration. In order to see the detailed shifting process clearly, a segment is taken out and shown is Fig. 4-9.

For the first motor, the seven stages mentioned before can be easily seen. The torque reduction phase takes about 300 ms to bring down the torque from 48 Nm to 0, meanwhile, the torque of motor 2 rises up by around 60 Nm. The difference between the reduction and rise is caused by the gear ratios for both motors. After the completion of synchronizer disengagement which takes about 70 ms, the first motor switches into speed control mode. Because it is an up shift from 2nd gear to 3rd gear, the speed of motor 1 should be reduced and the torque for speed synchronization goes negative. It will be the opposite for down shift. The slight torque rise for the second motor during torque hole compensation is caused by the vehicle acceleration demand given by the driver according to the speed reference, because from this stage, motor 2 is designed to provide all the required power. The speed synchronization phase takes about 450 ms to match the speed of motor 1 with the speed of target gear, then the actuator pushes the synchronizer towards the hub of the new gear to accomplish re-engagement. At the final stage, the first motor switches back to torque control mode and restores its output according to the torque profile decided by the proposed bump function.

In terms of driving comfort criteria, vehicle acceleration changes and jerks from this segment are shown in Fig. 4-10. It can be seen that there are four main fluctuations which come from motor 1 torque reduction, synchronizer disengagement, synchronizer engagement and motor 1 torque restoration, respectively. The maximum acceleration change amplitude is around 0.18 m/s^2 which is very small and the change is very smooth due to the advantages of the modified bump function. The peak of the vehicle jerks is around 4 m/s^3 which is greatly lower than 10 m/s^3 which is recommended in [145]. It should be pointed out that the reason why synchronizer engagement generates

the peak jerk is the actual rotation speed of the target gear can just be approximately measured in real situation and there could be fluctuations in the motor output speed, here, the engagement launching tolerance is set to simulate real driving condition.

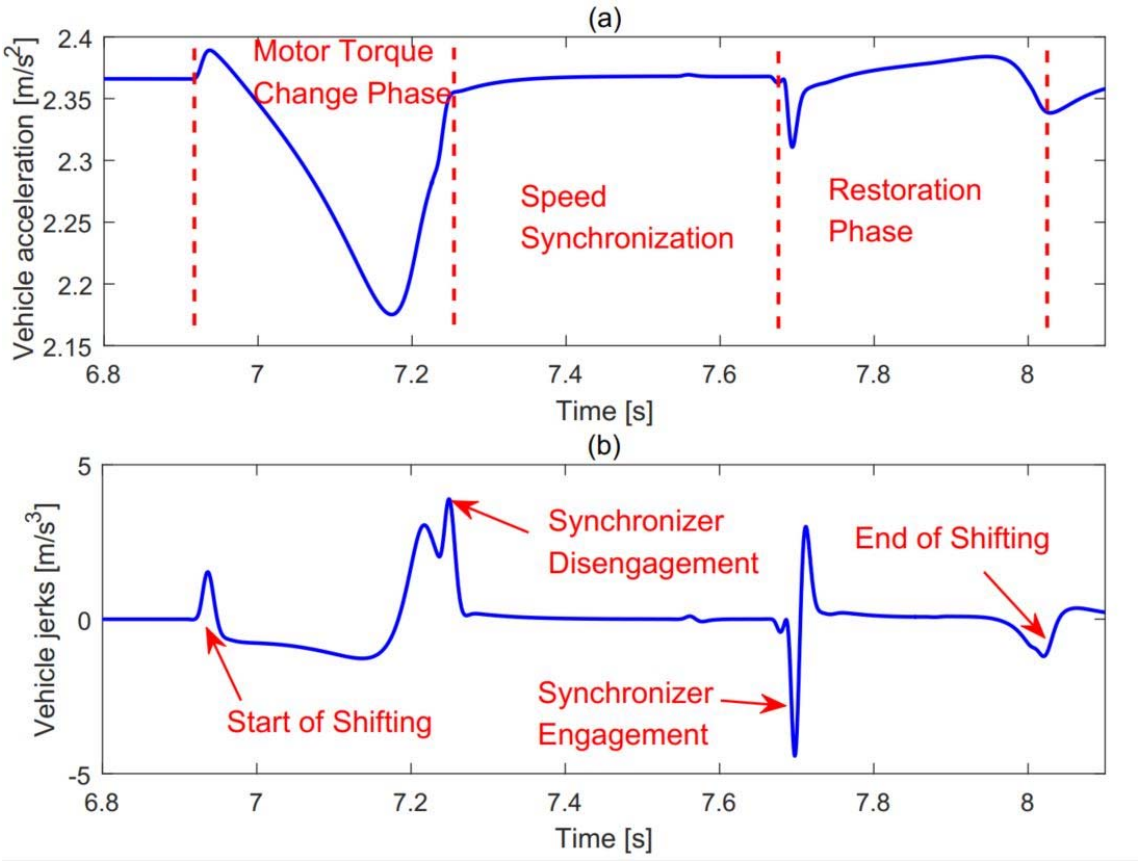

Figure. 4-10 Vehicle acceleration and jerks for the proposed system.

In order to demonstrate the improvements of our proposed system, comparisons are conducted with a conventional one input AMT system with same acceleration demand and torque adjusting profile. In the first comparison, two systems work in exactly the same situation and conduct the shifting process in same duration.

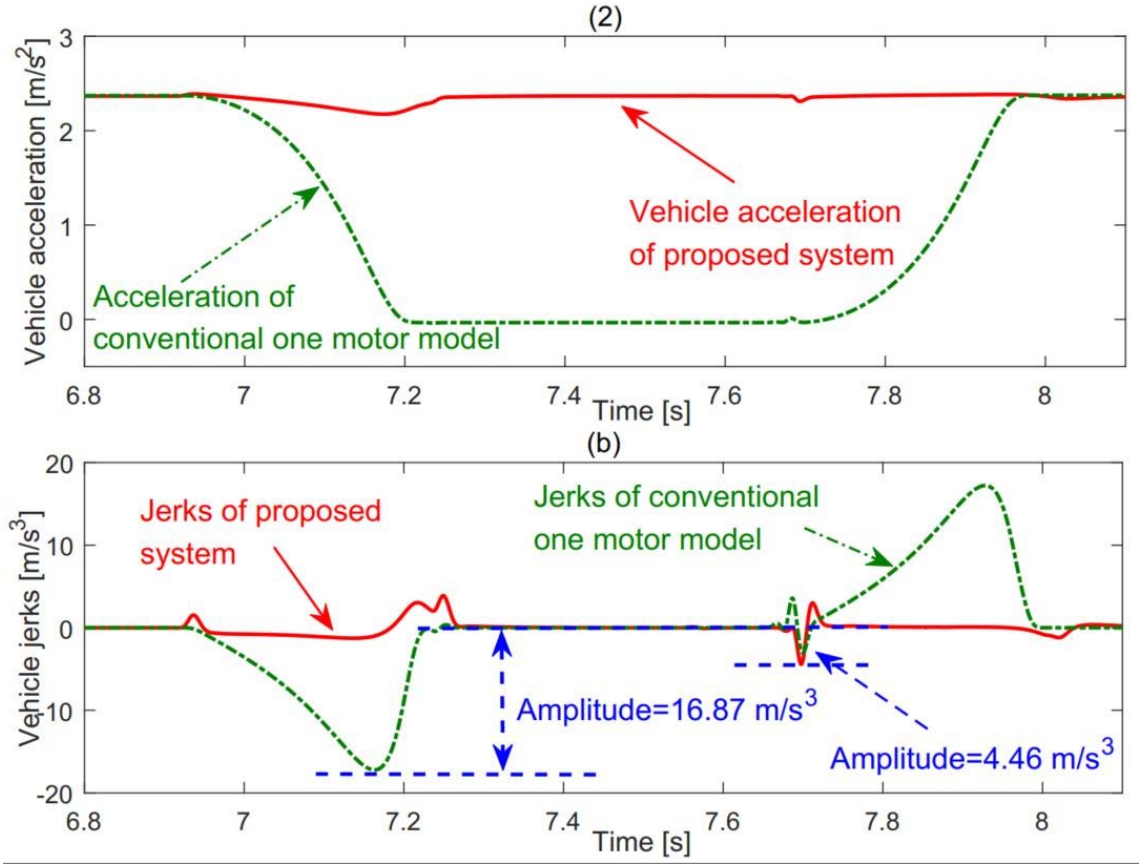

Figure. 4-11 Acceleration and jerk comparisons in same shifting duration.

It is demonstrated that the acceleration change in Fig. 4-10 (a) is very small and smooth compared to that of conventional one motor model in the same shifting process. The acceleration for the conventional model drops to zero as the driving motor is disconnected from the powertrain while the proposed system keeps its acceleration nearly constant. Fig. 4-10 (b) shows the vehicle jerk performance of both systems, in the same shifting duration, the jerk amplitude of conventional method is about 16.87 m/s^3 which is much larger than the proposed 4.46 m/s^3.

The shifting control strategy doesn't only solve the problem of driving comfort but also greatly improves the vehicle drivability. In conventional one input model, the vehicle

completely lost traction force as the motor is disconnected from powertrain for gear shifting. In the proposed model, motor 2 will continuously drive the vehicle to keep desired acceleration.

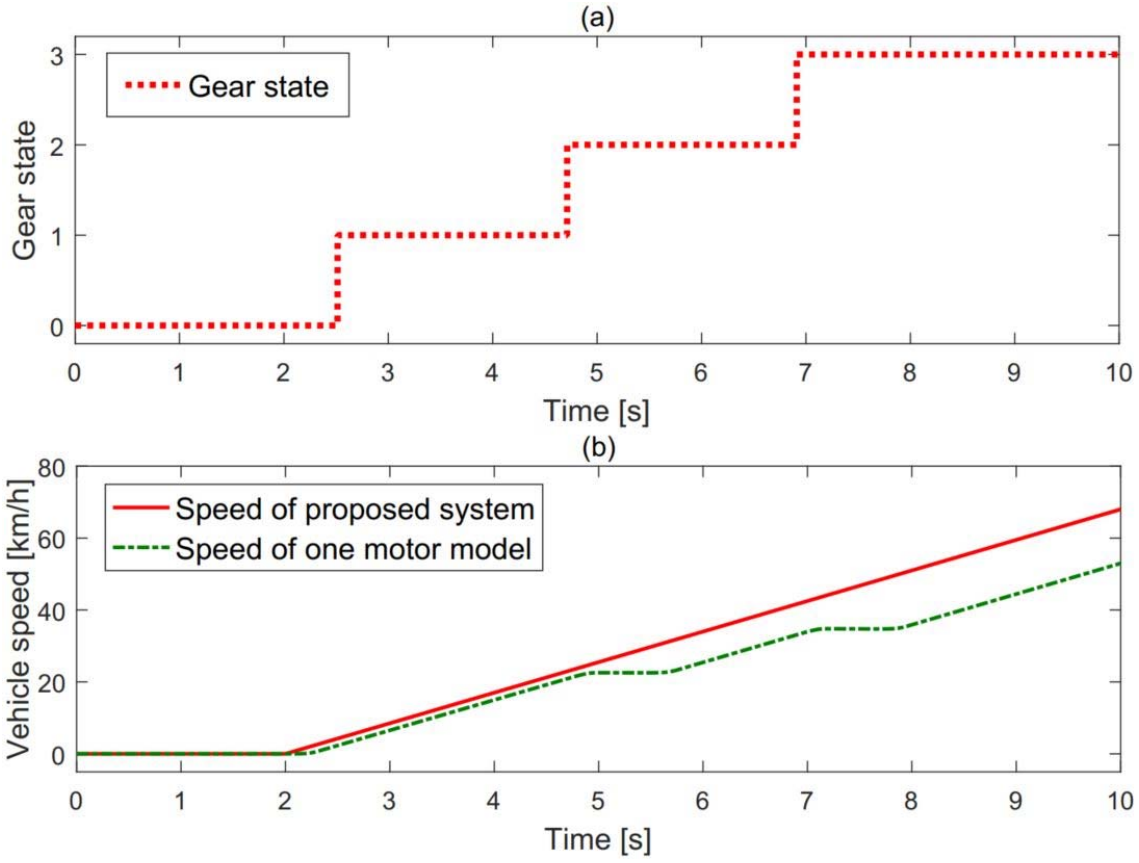

Figure. 4-12 Speed comparison in same shifting duration.

Fig. 4-12 (a) shows the shifting schedule for both models and Fig. 4-12 (b) shows the speed comparisons. It can easily be seen that there are pauses of acceleration in every gear shift for the conventional model while the proposed model could accelerate linearly. The difference between the final speed demonstrates the superior accelerate capability of the proposed system. For the conventional model, in order to achieve same final

speed as the proposed one, the acceleration should be greater which will further amplify the torque change during shifting causing uncomfortable feelings.

As to the second comparison, the shifting duration of the comparison model is lengthened to make the vehicle jerk as small as the proposed system. The results are shown in Fig. 4-13.

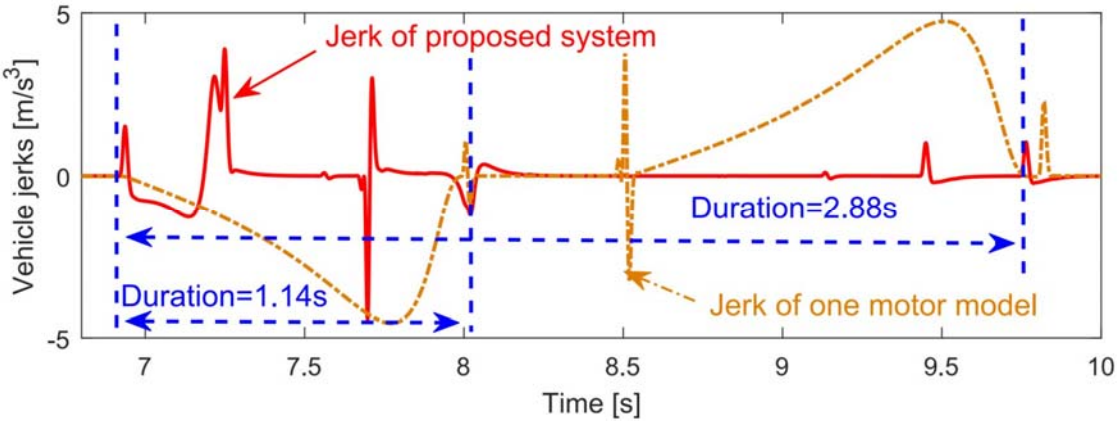

Figure. 4-13 Shifting duration comparisons with similar amplitude.

In Fig. 4-13, the peak of the conventional method is reduced similar to that of the proposed method but the shifting duration has been largely lengthened to 2.88 s. This again verifies the effectiveness of the proposed model.

4.5 Conclusions

The objective of this chapter is to propose a high efficient transmission system which has the merits of efficient, robust, low manufacture cost and could achieve torque hole compensation and improve drivability and driving comfort. In order to maximize the overall efficiency and the robustness, a modified clutchless AMT is adopted as the basis

of the multi-speed transmission part for the primary motor. To guarantee the quality of gear shifting without traditional friction clutch, an advanced motor control strategy is designed to follow its torque and speed references more accurately and swiftly. As to achieving torque hole compensation to improve the drivability and driving comfort, an assisting motor is designed to provide the required torque during shifting with a control strategy that maintains constant torque. It also provides torque when the torque demand exceeds the capacity of the primary motor. To verify its effectiveness, a detailed mathematical model has been built. The transient shifting dynamics has been studied and the outcomes are compared with those of a traditional single motor CLAMT transmission in terms of torque, acceleration and vehicle jerk. It is demonstrated that the proposed system could adequately achieve the goal to compensate the torque hole during gear changing to realize power-on shifting with cost-effective and low mass CLAMT system.

CHAPTER 5 : Energy management strategy for the dual input system

5.1 Introduction

Although the proposed dual input cltuchless transmission system and the corresponding shifting control strategy, which could achieve torque hole compensation, could improve the overall efficiency from the structure perspective and achieve better drivability and driving comfort, the real energy efficiency depends on the performance during normal driving condition other than the shifting process [146]. The most important difference between a single input system and a multi-input system is the energy management strategy [147]. However, the energy management strategies discussed by most researchers cannot be directly adopted here as the power usually comes from different power sources, while the power in the proposed system only originates from the onboard battery. This means that the overall efficiency only depends on the instant energy consumption rate other than the optimal solution of the whole trip [148].

To solve this problem, the power demand distribution between the two motors becomes important [149]. Only an adequate power sharing strategy which can achieve the highest efficiency at the same time under certain power demand can help guarantee the overall efficiency of the whole trip [150] .

5.2 Proposed power sharing control strategy

Solving the problem of shifting control only guarantee the driving comfort and the continuity of power flow during shifting, to maximize the overall efficiency and meet acceleration demand, a proper power sharing control strategy should be designed to distribute power between the two motors. Both motors can work alone and if needed, they can cooperate with each other to provide the demand power with desirable efficiency. For example, when the speed of the vehicle is relatively low and the acceleration demand is not large, the first motor will work alone to provide all the power in the first gear and the second motor will be idle because it is in the low efficiency area. If the acceleration demand is huge at low speed which exceeds the capacity of the first motor, the second motor could jointly provide the power. If the vehicle speed is already very high, the second motor may work alone to provide all the power.

There are two design variables of the PSC strategy in this system, one of which is the desired gear state and the other is the torque of the first motor because once the gear ratio and the torque of motor 1 are decided, the torque of motor 2 is settled. For a certain speed and throttle demand where the acceleration is decided, the speeds of the motors can be expressed as

$$\dot{\theta}_{M1} = \frac{\overline{v}}{3.6R_w} i_1, \dot{\theta}_{M2} = \frac{\overline{v}}{3.6R_w} i_2 \qquad (29)$$

As to the torque, there is only one independent design variable which is the first motor torque in this study, once it is decided, the torque of the second motor can described as

$$T_{M2} = \frac{J_{eq3}\overline{\alpha_{Final}} + T_v - i_1\left(T_{M1} - J_{eq1}\overline{\alpha_{M1}}\right)}{i_2} + J_{eq2}\overline{\alpha_{M2}} \quad (30)$$

where J_{eq1} is the equivalent inertia connected to the first motor and J_{eq2} is for motor 2 driveline and J_{eq3} is for the following transmission components including the vehicle body. The equivalent inertia and the demanded angular acceleration $\overline{\alpha_{M1}}$ and $\overline{\alpha_{M2}}$ for motor 1, motor 2 and final shaft can be calculated according to the given information.

Once the equations of speeds and torques for both motors are decided, the sum of power consumption for both motors can be expressed as

$$P_{out} = T_{M1}\dot{\theta}_{M1}/\eta_{M1} + T_{M2}\dot{\theta}_{M2}/\eta_{M2} (T_{M1}\dot{\theta}_{M1} > 0 \,\&\, T_{M1}\dot{\theta}_{M1} > 0) \quad (31)$$

where η_{M1} and η_{M2} are the specific efficiencies under the demanded speed and torque for motor 1 and motor 2, respectively.

The charging power under the situation of braking or one motor charges the other one is as follows

$$P_{in} = T_{M1}\dot{\theta}_{M1}\eta_{M1} + T_{M2}\dot{\theta}_{M2}/\eta (T_{M1}\dot{\theta}_{M1} < 0 \,\&\, T_{M1}\dot{\theta}_{M1} < 0) \quad (32)$$

The total energy consumption is

$$P_e = P_{out} + P_{in} \quad (33)$$

For any driving cycles where the target speed $\bar{v}$ and acceleration $\bar{\alpha}$ are given, the optimization model is expressed as

$$\begin{aligned}
&\min_{T_{M1}} P_e\left(\bar{v},\bar{\alpha},T_{M1},i_1\right) \\
&s.t.-\dot{\theta}_{M1,max}\leqslant-\dot{\theta}_{M1}\leqslant\dot{\theta}_{M1,max}; \\
&-T_{M1,max}\left(\dot{\theta}_{M1}\right)\leqslant T_{M1,max}\leqslant T_{M1,max}\left(\dot{\theta}_{M1}\right); \\
&-\dot{\theta}_{M2,max}\leqslant-\dot{\theta}_{M2}\leqslant\dot{\theta}_{M2,max}; \\
&-T_{M2,max}\left(\dot{\theta}_{M2}\right)\leqslant T_{M2,max}\leqslant T_{M2,max}\left(\dot{\theta}_{M2}\right).
\end{aligned} \tag{34}$$

Since there are several local optimal points contained in the design space, it is hard to seek the global optimal point by using traditional derivative based optimization algorithm. Here enumerating method is adopted to search the approximately global optimal point, which also does not need much computational cost. In the enumerating method, the design variable T_{M1} is discretized by a regular dense grid with 2 Nm interval in its design space. Then compute the objective function value P_e and constraints values at these discretized points. After getting rid of the points located in the unfeasible region, the final optimal design point will be chosen as the remaining discretized point which has the minimum objective value. The plot of objective function under different driving demands in the feasible region is shown in Fig. 5-1. It shows that the shapes of the objective function and the feasible solution spaces would be adjusted adaptively according to the driving condition.

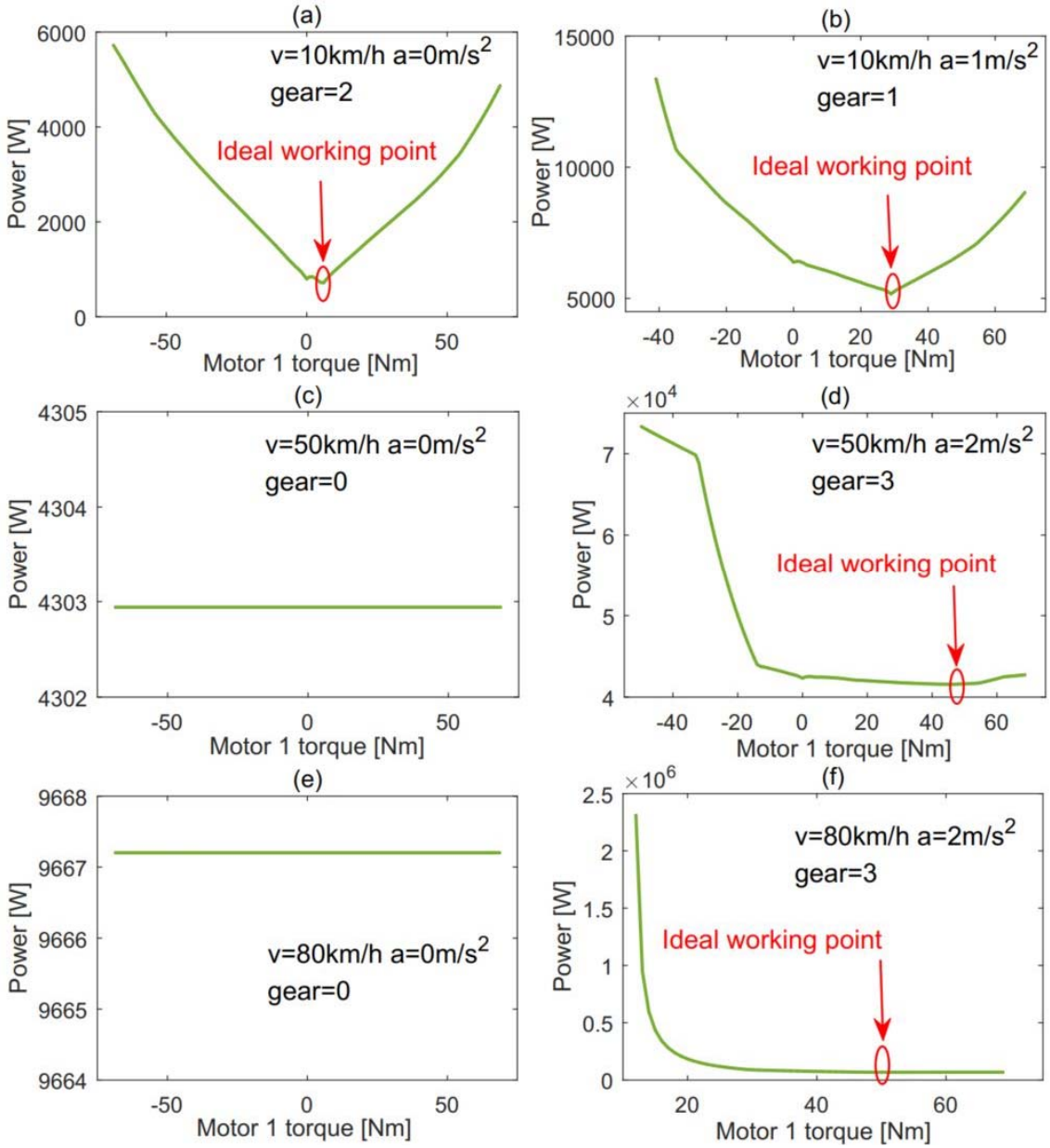

Figure. 5-1 The PSC objective function under different driving demands.

It can be seen that the shapes of the objective function change according to different driving conditions and the ideal driving point varies too. The vehicle speed and acceleration are given by the driver and the suitable gear state is decided by the proposed PSC strategy. In Fig. 5-1 (a), as the speed is very slow and acceleration

demand is small, the possible working torque for motor 1 is from -70 Nm to 70Nm and the ideal working point, which renders the minimum energy consumption, is very close to zero. If the acceleration is set to 1 m/s^2, Fig. 5-1 (b) can be generated and it can be seen the possible working space is narrowed down only starts from -40 Nm. The power in Fig. 5-1 (c) and Fig. 5-1 (e) is constant because motor 1 is disconnected from the powertrain according to the PSC strategy. In Fig. 5-1 (f), the torque of motor 1 can only be positive because the speed and acceleration are already very high. The overall energy consumption would rise dramatically if the torque of motor 1 drops below 10 Nm, the reason is that the corresponding torque of motor 2 has reached its limit and the efficiency changes fiercely in that area.

The proposed PSC strategy is summarized in Fig. 5-2. In order to make the shifting frequency more reasonable, a delay function is added into the system to avoid undesirable frequent gear changing.

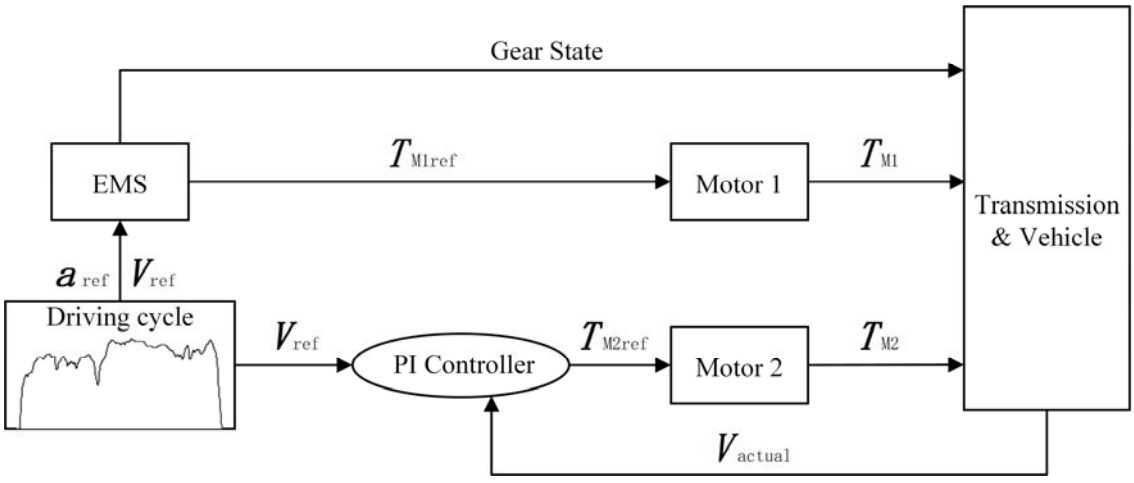

Figure. 5-2 Proposed power sharing control strategy.

5.3 Power distribution analysis

Although the proposed transmission structure and shifting control strategy could considerably improve driving comfort and drivability, it encounters the problem of how to distribute the whole demanded power among the two motors. If not properly solved, the overall efficiency could be compromised and the drivability could also be affected as the assigned power for one motor may exceed its rated power in certain acceleration conditions.

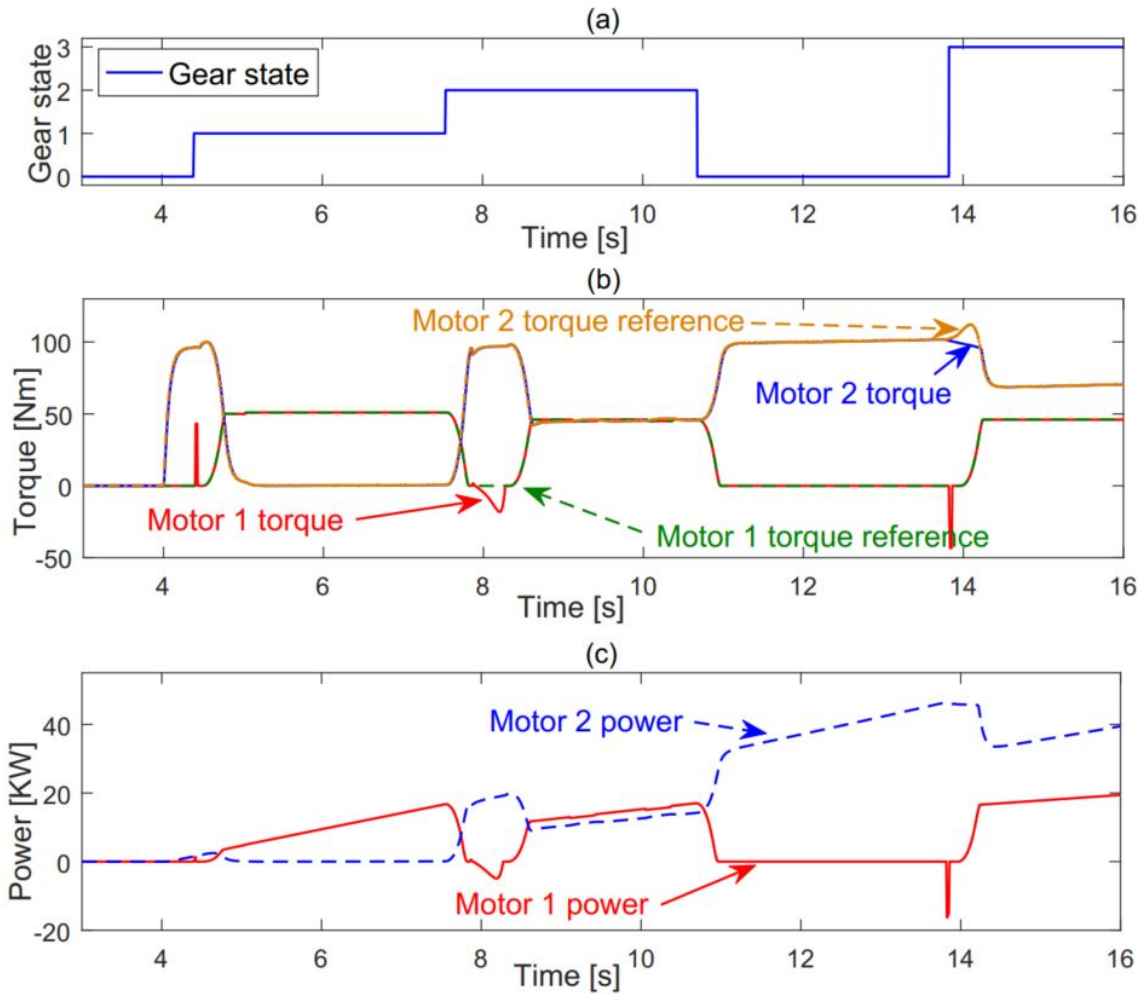

Figure. 5-3 Acceleration performance, (a) gear states, (b) torques, (c) power.

In this section, a typical rapid acceleration test is conducted to reveal how the proposed PSC strategy works to meet the power demand while keeping the energy consumption as low as possible. The acceleration is linear, takes 12 s and ends up with a final speed of 80 km/h. The gear state, torque and power are shown in Fig. 5-3.

It can be seen in Fig. 5-3 (a) that gear stays idle before 4.4 s and then starts shifting, the shifts could cover most of daily driving shift situations and the shifting pattern can be explained by the illustrations the aforesaid section that the gear ratios for the first and second gear are designed for low speed city driving condition and the third gear ratio is for high speed cruising, the gear ratio for the second motor is for mid-high speed cruising.

Fig. 5-3 (b) shows the torque distribution for both motors during this acceleration. The second motor starts first to launch the vehicle at 4 s while the first motor stays idle before 4.4 s as the speed during launching is very slow and both motors will be working in low efficiency area and according to the proposed PSC, which will minimize the overall energy consumption, the second motor should provide all demanded power. At 4.4 s the torque of motor 1 rises quickly and drops to zero again to adjust to the engaging speed and prepare for the synchronizer engagement. After the completion of engagement, the torque of motor 1 rises, according to the torque change profile, to the target value to provide all the power alone for the next 3 seconds, which is decided by the proposed real-time PSC. Since the vehicle speed rises, in order to maintain the lowest energy consumption, PSC strategy gives the order to switch to the second gear and re-distribute the power demand for both motors at around 7.5 s. After a standard shifting process demonstrated in the previous section, motor 1 and motor 2 work

together to drive the vehicle. It should be pointed out that at 13.7 s motor 2 has reached its torque limit so the PSC strategy decides to activate motor 1 to compensate the torque demand, because it takes around 0.5 s for motor 1 to accomplish gear shifting, motor 2 couldn't follow its torque reference during that time. The torque drop for motor 1 is to slow down to match the target engagement speed because the damping coefficient for the motor is relatively small which couldn't slow it down in around 3 seconds.

Fig. 5-3 (c) shows the output power for both motors, as power is the product of motor torque and speed, the pattern of output power is similar with that of the torque. Although the distribution of power for the two motors, which is decided by the real-time PSC strategy, is varying, the total output power rises linearly with the vehicle speed.

In order to further investigate the performance of the proposed real-time PSC strategy, Fig. 5-4 shows the efficiency maps for both motors during the acceleration. It can be seen motor 2 launches the vehicle when the speed is very slow and as soon as motor 1 could work above the efficiency of 65%, the real-time PSC shuts down motor 2 and shifts to the first gear to improve the efficiency performance. Due to the changeable gear ratios, motor 1 could work along around its highest efficiency line, providing all the power alone while motor 2 stays idle. Then, as a best distribution scheme that can be achieved, motor 1 switches to the second gear and motor 2 restores its output torque.

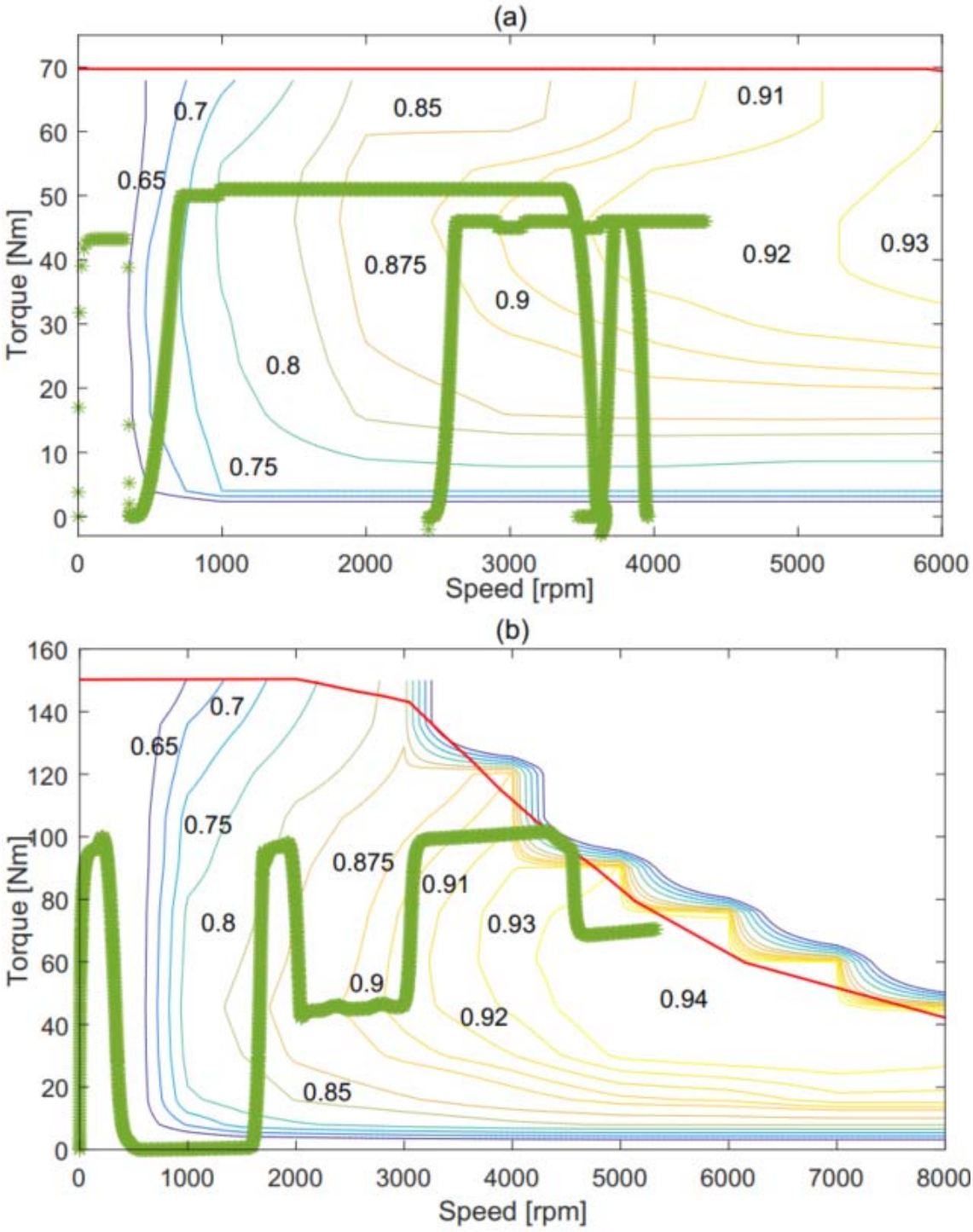

Figure. 5-4 Actual efficiencies for both motors.

It can be seen in this period, motor 1 could work exactly alone its highest efficiency line between 2500 rpm and 3800 rpm while motor 2 could also work alone its highest efficiency line between 2000 rpm and 3000 rpm. Because the efficiency of motor 1 is very sensitive to its torque change when its torque and speed are relatively high, which can be seen from the efficiency map, while motor 2 is less sensitive, motor 2 provides all the power alone between 11 s and 14 s with an efficiency above 90%. When motor 2 reaches its torque limit at 4200 rpm, motor 1 is activated to share the power load. Again, both motors could work alone their highest efficiency line.

This acceleration test adequately demonstrates the effectiveness of the proposed real-time PSC strategy to guarantee the drivability while keeping the whole system at a relatively high efficiency level.

5.4 Energy consumption

In order to further demonstrate the effectiveness of the proposed PSC strategy in terms of efficiency improvement, two driving cycles which are LA92 and HWFET are adopted and various fixed distribution ratios are used for the same system as comparisons. As overall efficiency and power distribution are mainly focused on how to control the power flow and would not be affected by the detailed gear shifting process which is demonstrated in the previous section, the detailed shifting dynamic responses are ignored here to make the simulations under different driving cycles possible. Because the model with detailed shifting dynamic responses is much more complicated than the energy verification model and runs very slowly in steps of 0.001 s, only by removing this part will it be possible to accomplish a driving cycle over 1000 seconds.

5.4.1 LA92

LA92 is used as a standard testing driving cycle for light-duty vehicles as it covers most driving situations in daily life. It runs about 1435 s and the total distance is 15.8 km with an average speed of 39.6 km/h. Fig. 5-5 (a) shows the profile of the driving cycle and how the proposed system could follow the reference speed.

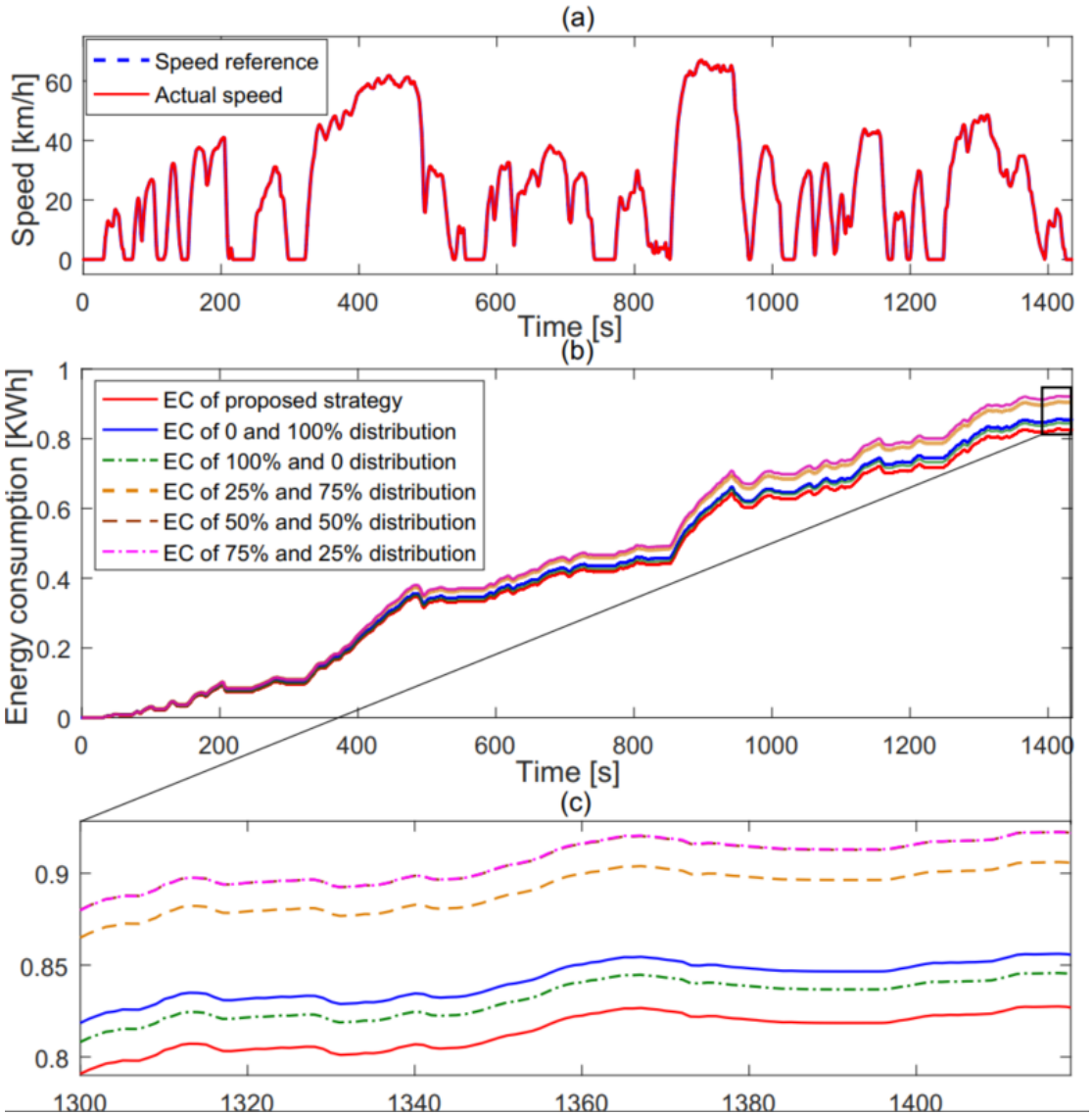

Figure. 5-5 Energy consumption of LA92.

It can be seen that the speed profile contains many starts and stops which simulate the signals from traffic lights and has adequate cruising stage over 300 seconds. The proposed system could exactly follow the speed reference.

Fig. 5-5 (b) shows the overall energy consumption by the proposed system and various fixed distribution system. It can be seen that the total energy consumption is not monotonically increasing because when the vehicle decelerates, the motor will switch into generator mode and recover this part of energy. In Fig. 5-5 (c), the proposed system generates the best performance followed by the performance of 100% and 0 distribution. This is due to the wide high efficiency speed range from the multispeed transmission of motor 1. The performance of 0 and 100% distribution comes third as a considerable part of speed in this driving cycle is around 40 km/h or above which just meets the design of gear ratio for motor 2. Other distributions relatively have lower overall efficiencies because the accelerations and decelerations in this driving cycle are not rapid, if both motors share the power demand equally or similarly in light duty condition, none of them could work in high efficiency area. In high speed rapid acceleration situations, the result would be different as two motors must work together to drive the vehicle as demonstrated before.

The power distributions for both motors of the proposed system and 100% and 0 distribution system are shown in Fig. 5-6 (a). In order to show the details clearly, a part of Fig. 5-6 (a) is amplified in Fig. 5-6 (b). It can be seen that the power demand of LA92 is not large, one motor alone can cover that and stay in its high efficiency area. For the proposed system, motor 1 and motor 2 work alternately, which can be clearly revealed by the seemingly vertical blue dash line in Fig. 5-6 (b), and for the 100% and 0

distribution system, motor 1 is working according to fixed ratio. It should be noted that higher power load ratio for the first motor doesn't always guarantee higher overall efficiency, it depends on the driving pattern and the driving load.

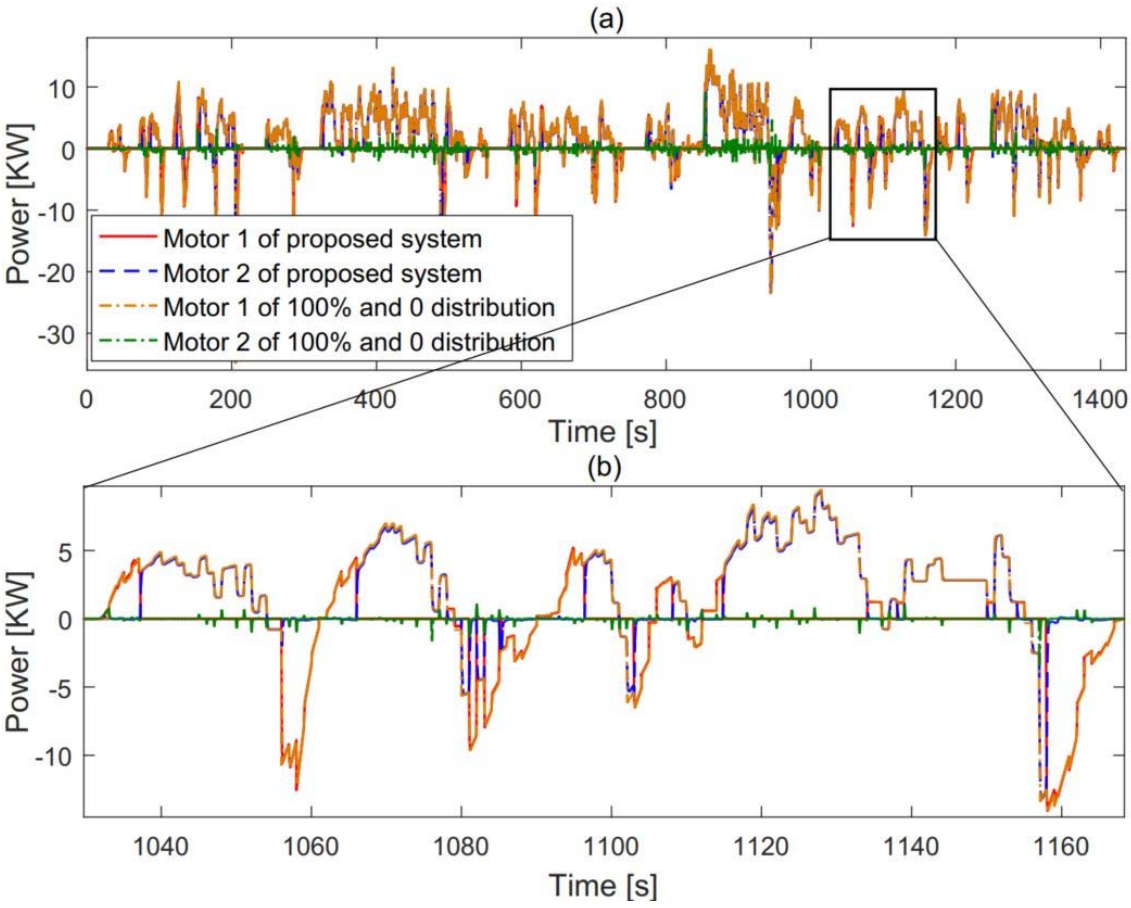

Figure. 5-6 Power sharing comparisons for LA92.

5.4.2 HWFET

To further demonstrate how the proposed real-time PSC strategy works, HWFET driving cycle is adopted as a mid-high speed cruising comparison. Fig. 5-7 shows the speed profile and energy consumption comparisons.

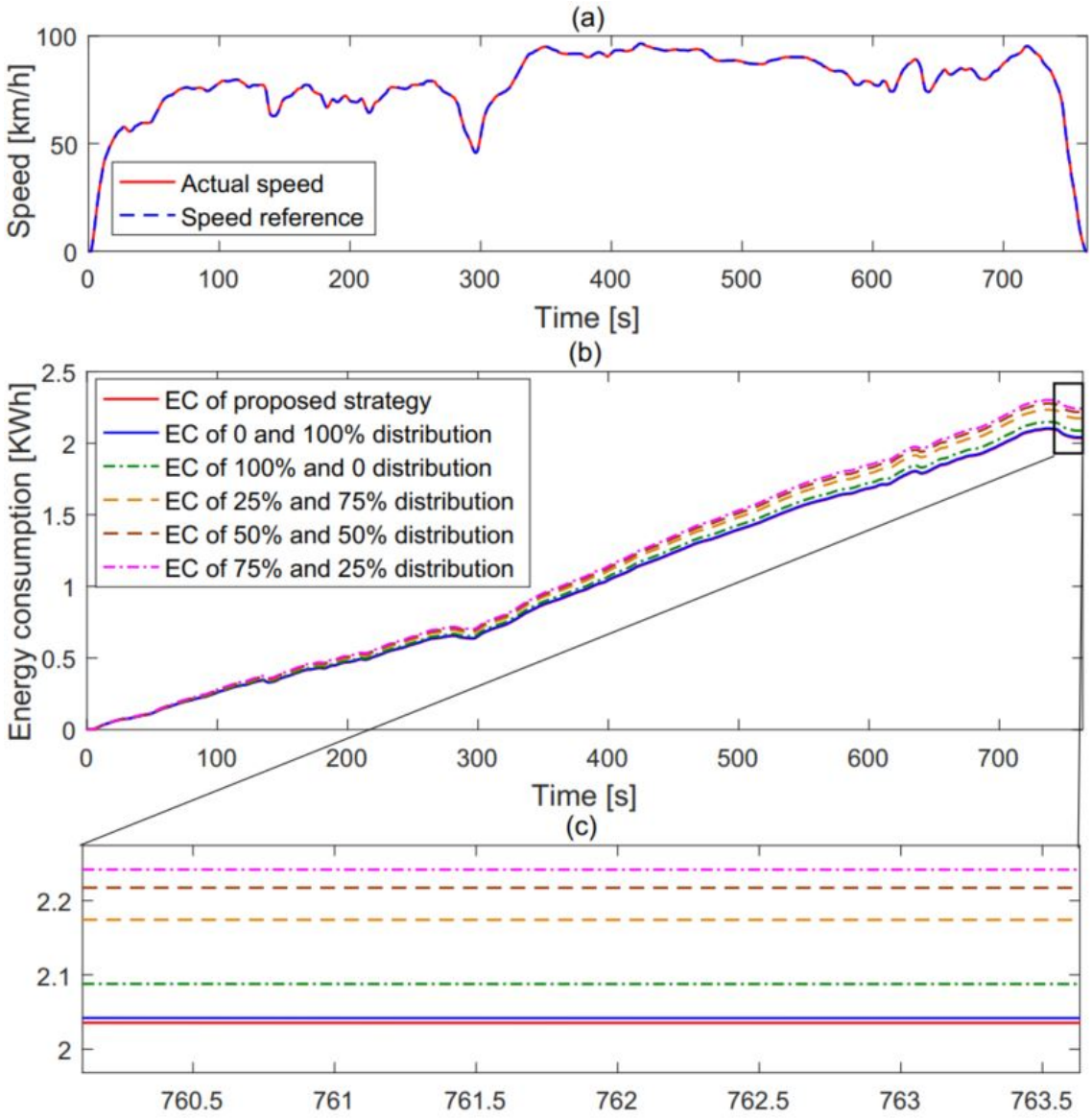

Figure. 5-7 Energy consumption of HWFET.

As the driving pattern switches to mid-high speed cruising, the performance of each fixed ratio distribution system changes a lot. Motor 1 alone and motor 2 alone exchange their positions because the gear ratio for motor 2 is exactly designed for this kind of situation where speed is relatively high, and in the mean time, the acceleration demand is very small that only motor 2 could cover. This feature can also be seen in other

distributions that the overall efficiency drops with the rises of the load allocation for motor 1. It can be seen motor 2 alone strategy renders similar results as the proposed real-time PSC strategy because in the proposed system, motor 2 also covers most of the power demand as it is the best scheme.

5.5 Conclusions

This chapter proposed a detailed real-time PSC strategy for a novel dual input clutchless transmission system which could achieve desirable overall efficiency, at the meantime, provide adequate drivability and driving comfort.

To improve the efficiency and drivability of the proposed system, a real-time PSC strategy is designed and verified under different driving conditions including different driving cycles and a typical linear acceleration. The proposed PSC strategy doesn't require complicated tuning work by experienced engineers which makes it easier to be implemented and the results proved that it could deal with various driving conditions with high overall efficiency.

CHAPTER 6 : Shifting stability control strategy

6.1 Introduction

Excessive gear shifting is a very common phenomenon residing in most existing energy-oriented energy management strategies as improving the overall efficiency is to some extent contradict to the shift frequent. To solve this problem, this chapter proposed a shifting stabilizer which can significantly reduce the shift frequency while compromising little overall efficiency. As a balance between the shift frequency and the efficiency should be achieved, the stabilizer parameters are optimized using a multi-objective optimization method. In order to verify the effectiveness of the proposed stabilizer, two typical driving cycles revealing daily driving scenarios are adopted and the results demonstrate that considering the gear shift energy losses, the stabilizer could even improve the overall efficiency while reducing the gear shift frequency.

6.2 The design of shifting stabilizer

Since the proposed PSC as well as most energy management strategies focusing on the minimization of power consumption, attributes such as vehicle acceleration responsiveness and smoothness are often overlooked. However, these strategies impact the quality of gear shifting, particularly for real-time strategy where decisions are made instantly as the global minimization problems are divided into instantaneous minimization steps. As a result, optimal gear ratio will change frequently with the driving conditions, which leads to excessive gear shifting. Moreover, excessive gear

shifting not only influences drivability but also increase energy consumption because the shifting actuator consumes energy as well.

In order to reduce excessive gear shifting encountered by the proposed energy management strategy, drivability constraints should be considered. A shifting stabilizer is built to make a trade-off between the energy consumption and the gear shifting frequency, which can significantly reduce the gear shifting events with insignificant extra energy consumption. It is written as the following

$$f_{cost} = \alpha P + Ae^{-\frac{1}{1-x^2}} \quad (35)$$

subject to

$$\begin{cases} (0 < x < 1) \\ g\_ratio \neq OldG \end{cases}$$

The first part of the shifting stabilizer is designed to avoid unnecessary gear events by improving the shifting margin. Initially, to improve energy efficiency, the gear change schedule is set to follow the trajectory of minimum power consumption. However, the disadvantage is that sometimes the power consumption between the current gear and the next gear is quite close, which means that the saved energy consumption from gear shifting is insignificant. To solve this issue, a shifting margin controller is designed to increase the threshold required for shifting, which only allows for gear changes when energy saving is obvious.

The shifting margin controller can be expressed as the following

$$f_1 = \alpha P \quad (36)$$

where α is the weight factor and P is the corresponding consumed power of each gear state.

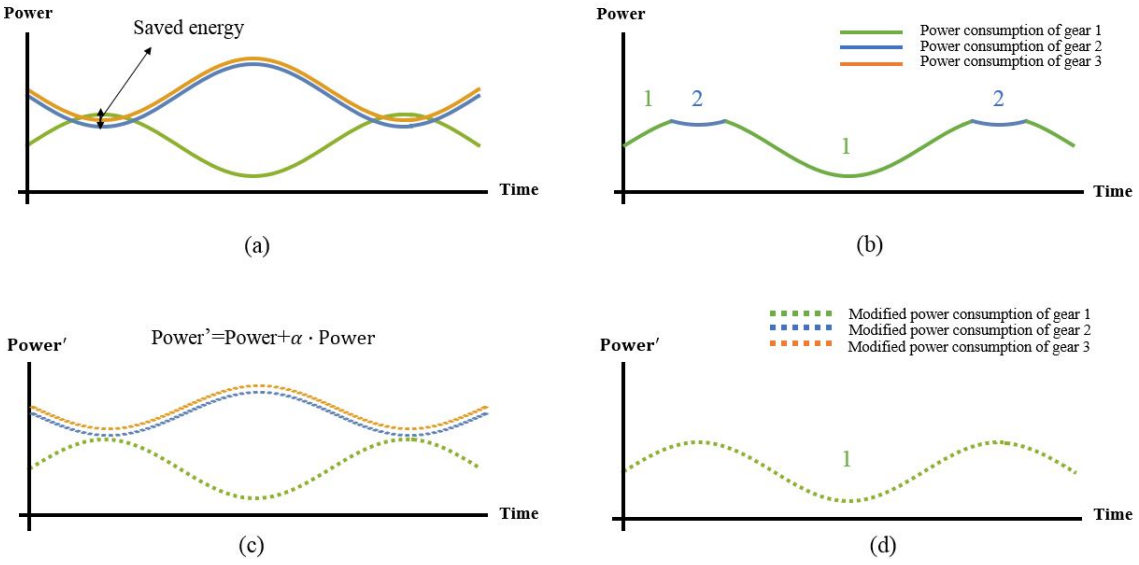

Figure. 6-1 The schematic diagram of the designed shifting margin controller.

Fig. 6-1 illustrates the conceptual principle of the shifting margin controller, in which Fig. 6-1 (a) represents the instant power consumption of each gear directed by PSC. Based on the minimum power consumption principle, the intersections of the lowest curve are the points where gear shifting occurs. Accordingly, the determined gear shifting schedule is showed in Fig. 6-1 (b). However, it is worth noting that the saved energy from changing gear 1 to gear 2 is insignificant but this causes unnecessary gear shifting. To avoid this condition, the shifting margin controller will impose a penalty to all other non-working gears, which causes overall elevation in their power consumption. As shown in Fig. 6-1 (c), gear 1 (green line) is the working gear in the initial stage, so that the power consumption of gear 2 (blue line) and gear 3 (orange line) is modified to

a higher level by the shifting margin controller. In consequent, the unnecessary gear shifting is reduced and there is no gear change, as shown in Fig. 6-1 (d).

The second part of the shifting stabilizer is designed to avoid undesired gear events by extending the shifting interval. This means to avoid successive and frequent gear shifting in a short period, which is not desired even though it could save much energy. Furthermore, a modified bump function is introduced to prevent too short shifting interval.

The shifting interval controller can be expressed as the following

$$f_2 = Ae^{-\frac{1}{1-x^2}} \quad (37)$$

where A is for the designed amplitude coefficient of the bump function, and x is to control the duration of gear shifting which is defined as $x = \frac{Time-t_1}{t_d}$, where *Time* is the system time, t_1 is the last gear shifting time, t_d is the designed duration coefficient of the bump function.

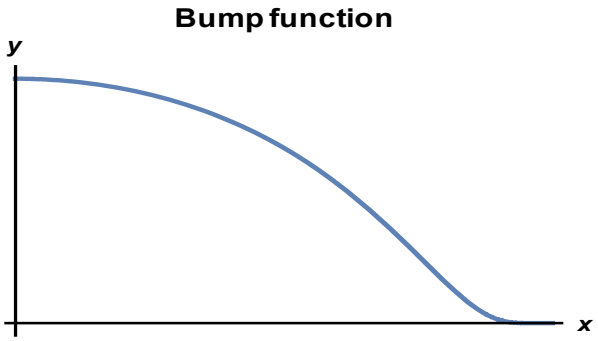

Figure. 6-2 Diagram of the bump function

As shown in Fig. 6-2, the bump function declines slowly in the early stage but fast at the late stage. According to this, the shifting interval controller will impose a large penalty to the non-working gears when gear shifting is just completed. As a result, the system prefers to maintain the working gear when searching for the minimum power consumption of each gear. Moreover, the penalty value will decline fast to zero to reduce the continuous influence.

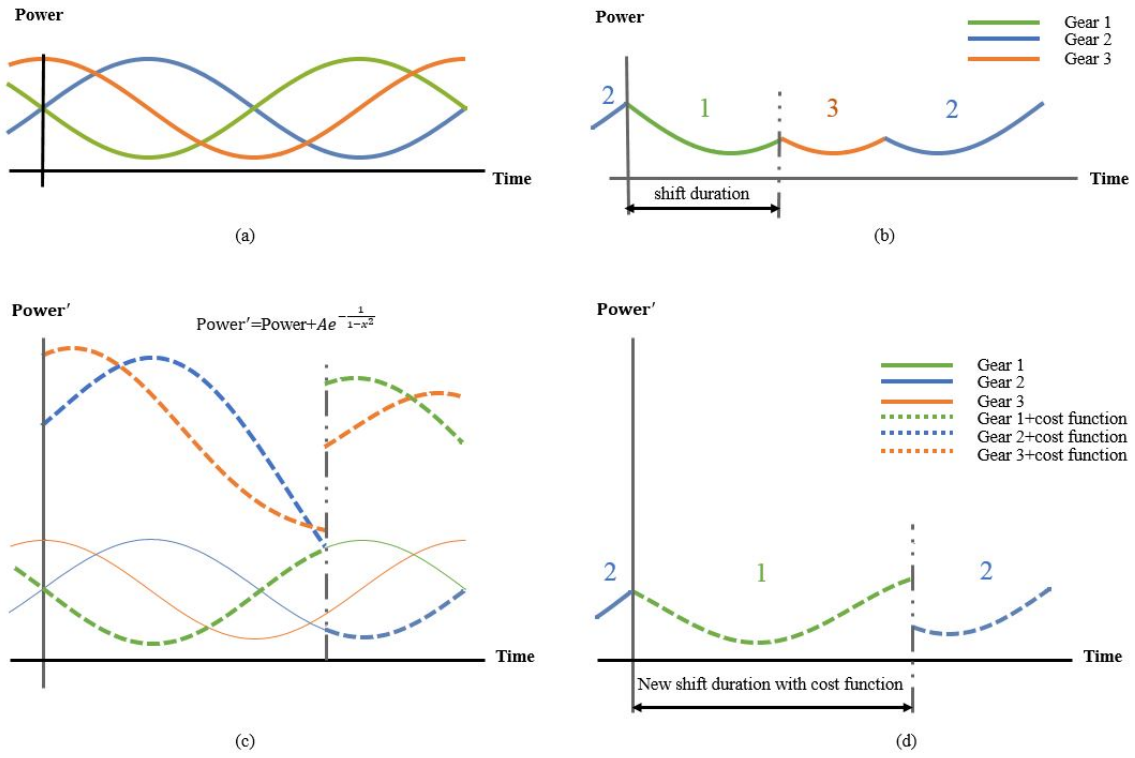

Figure. 6-3 The schematic diagram of the designed shifting interval controller

Fig. 6-3 illustrates the conceptual principle of the shifting interval controller, in which Fig. 6-3 (a) represents the instant power consumption of each gear directed by PSC, in which three curves cross frequently in a short period. Based on the minimum power consumption principle of PSC, the intersections of the lowest curve are the points where

gear shifting occurs. Accordingly, the working gear changes frequently in a short shifting duration, as shown in Fig. 6-3 (b). To avoid this condition, the shifting interval controller is designed to impose a large penalty to all other non-working gears right after gear shifting occurs. As shown in Fig. 6-3 (c), gear 2 (blue line) is the working gear in the initial stage, then the working gear changes to gear 1 at the intersection. After this gear shifting, a penalty is imposed to the non-working gears immediately, causing a large elevation in their power consumption from the solid lines to the dotted ones. Then, the proposed PSC will search for the minimum power consumption through the modified power consumption (dotted lines). As a result, in Fig. 6-3 (d), the shift duration of gear 1 is longer than that in Fig. 6-3 (b). Moreover, every time gear shifting occurs, the shifting interval controller will intervene to avoid successive and frequent gear shifting.

With the two points elaborated above, the original objective function focusing on minimum energy consumption in the energy management strategy is developed to take shifting stability into consideration. The final objective function can be written as the following:

$$\begin{aligned} P_{sub_{opt}} &= P + f_{cost} \\ &= P + \alpha P + A e^{-\frac{1}{1-x^2}} \end{aligned} \quad (38)$$

6.3 Multi-objective optimization

From Eq. (38), in order to filter out undesired gear shifting while minimizing the extra energy consumption, the weight factor α, amplitude (A) and the duration (t_d) play

important roles. To compromise between energy consumption and gear shifting, a multi-objective genetic algorithm is introduced to optimize these coefficients.

In a 3-dimensional domain, the multi-objective functions and constraints are expressed as

$$min\ (f_1) = (1+\alpha)\int_0^{\infty} T_{EM1}\frac{\dot{\theta}_{EM1}}{\eta_{EM1}} + T_{EM2}\frac{\dot{\theta}_{EM2}}{\eta_{EM2}} + Ae^{-\frac{1}{1-t_d{}^2}} \quad (39)$$

$$min\ (f_2) = \sum Gear_{num} \quad (40)$$

subject to

$$0 \leqslant \alpha \leqslant 1$$

$$0 \leqslant A \leqslant 200$$

$$0 \leqslant t\_d \leqslant 100$$

where f_1 and f_2 represent the total power consumption and gear shifting times respectively, and $Gear_{num}$ is a counter for gear shifting. The bounds of the variable are set below certain values because with larger values, the weight of shifting stabilizer will be too strong so that there are no gear changes anymore.

Since $f_2 \ll f_1$, the fitness value should be normalized by dividing its values by the average value of all children in the generation. For example, if f_{1i} is the fitness value for i^{th} generation, and $\overline{f_1}$ is the average value of all children in this generation, the normalized fitness f'_{1i} is expressed as:

$$f'_{1i} = \frac{f_{1i}}{\bar{f}_1} \quad (41)$$

Similarly, for the second objective, the normalized value is expressed as

$$f'_{2i} = \frac{f_{2i}}{\bar{f}_2} \quad (42)$$

As for the multi-objective optimization, the most important part during the iteration process is the population evolution. In the multi-objective optimization problem, if an individual X has at least one feature better than Y while the rest features are not worse than that of the individual Y, individual X is non-inferior to Y and the rank value of Y is set lower than that of X. In the condition where X, Y is non-inferior to each other, X and Y are set to have the same rank value. The rank system is showed as Fig. 6-4. The ranking value depends on the numbers of the individual within the rectangle formed by the fitness value [f_1,f_2] and the axes. The individuals within this rectangle indicate that their fitness values are inferior to the current individual. For example, there is only 1 individual falls in the rectangle formed by the fitness value of individual i [f_{1i}, f_{2i}], then its rank is set to 2.

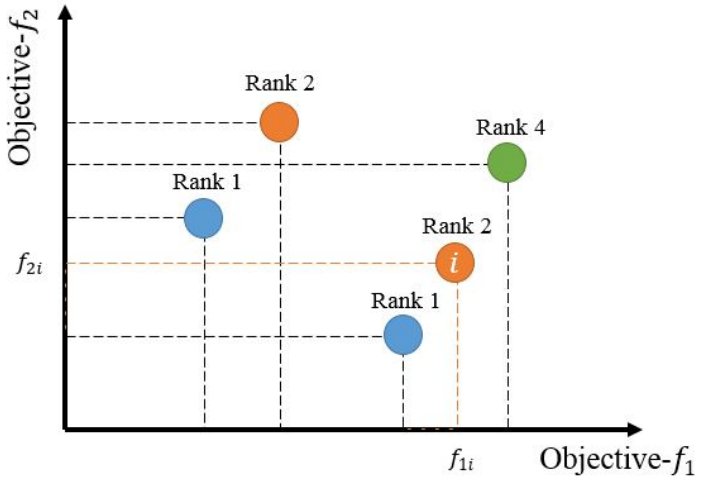

Figure. 6-4 The principle of fitness ranking.

Besides the rank value, population diversity is also important because the selection and replacement of individuals are based on rank value and diversity. When the rank values are different, the individuals with the smaller rank value will be selected, regardless of their diversity. When the rank value is the same, individuals with better diversity will be selected so that those elite individuals are automatically retained in the selection and replacement process.

Since gear shifting is based on minimum energy consumption, reducing gear events will definitely increase energy consumption. The goal is to reduce the undesired gear shifting while ensuring that there is not much increase in energy consumption. Hence, the weight of energy consumption should be higher than reducing gear shifting. In order to alleviate the penalty against individuals concentrating around an attractor, individuals are divided into subpopulations. Based on a combination of uniform distribution and

Gaussians probabilistic distribution, the individuals $\mathrm{I}(X)$ is expressed by π and θ respectively.

$$\mathrm{I}(X) = w_0 U(X|\pi) + \sum_{i=1}^{c} w_i \, I(X|\theta_i) \quad (43)$$

where c denote the number of Gaussians, $\{w_i\}$ denote the weights, subject to $\sum_{i=0}^{c} w_i = 1$.

Then entropy is introduced as a measure of population diversity. For a population$\mathrm{X} = \{f_i | i = 1,2\}$, the entropy is defined as the following

$$\mathrm{H(X)} = \frac{1}{2}\sum_{i=1}^{2} p(f_i) \log p(f_i) \quad (44)$$

As $p(f_i) \log p(f_i)$ is higher at the distribution margin, individuals will not be punished for being congested until most of the population converges.

Besides the population, to describe the distribution of objective function, the Gaussians is introduced as the following:

$$p(f_i) = \mathrm{N}(\mu, \sigma) = \frac{1}{\sqrt{2\pi}\sigma} \exp\left(-\frac{1}{2}\frac{(f-\mu)^2}{\sigma^2}\right) \quad (45)$$

where

$$\mu = \frac{1}{2}\sum_{i=1}^{2} f \quad (46)$$

$$\sigma^2 = \sum_{i=1}^{2} (f - \mu)^2 \quad (47)$$

The differential entropy of $\mathrm{N}(\mu, \sigma)$ is calculated as the following

$$\mathrm{H}(\mathrm{N}) = \int \mathrm{N}(\mu, \sigma) \log \mathrm{N}(\mu, \sigma)\, df \quad (48)$$

Then, through crossover and mutation, the non-inferior solution will converge to the Pareto front. In order to include all driving conditions as much as possible, some typical parts of different driving cycles are chosen as a hybrid driving condition, where the energy consumption before optimization is 2.3698 $kw \cdot h$, and the total shifting time is 352. After optimization, the Pareto solutions, are selected as shown in Fig. 6-5.

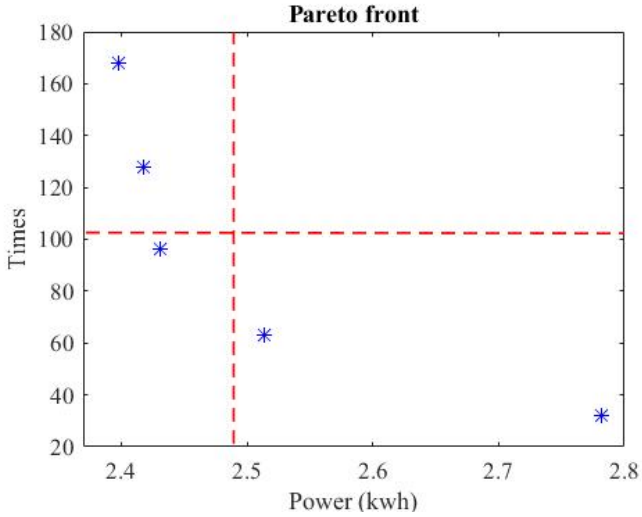

Figure. 6-5 The optimization results of the Pareto front.

Fig. 6-5 shows that there are five sets of feasible solutions. However, for specific situation about the balance between energy consumption and gear shifting times, limitations of less than 5% extra energy consumption (the vertical dotted line) and more

than 70% gear shifting reduction (the horizontal dotted line) are used as index to decide the final optimization results, which is within the lower left corner. The corresponding coefficients are listed in Table 6-1.

Table 6-1 Optimization results

α	A	t_d
0.0818	157.8525	48.9767

6.4 Driving cycle results analysis

In this section, the proposed shifting stability control strategy is verified by using two typical driving cycles, LA92 and HWFET. The LA-92 driving cycle is used to validate the effectiveness of these strategies in low-speed conditions, while HWFET driving cycle is used to validate the vehicle performance in medium to high-speed cruising conditions. These two driving cycles cover most situations for light-duty vehicles from daily use to traveling.

6.4.1 LA-92 driving cycle

The LA-92 driving cycle is a light-duty chassis dynamometer schedule and a representation of urban driving patterns. This cycle has a distance of 15.8km and an average speed of 39.6km/h in1435s.

Fig. 6-6 (a) shows gear shifting events and corresponding angular speed of both motors, directed by the proposed PSC without shifting stabilizer. It shows that the minimum

power consumption oriented PSC often leads to excessive gear shifting. Fig. 6-6 (b) shows the results directed by PSC with shifting stabilizer, in which the undesired and unnecessary gear shifting are reduced heavily. Besides, both figures show that motor 1 and motor 2 work in a complementary way to provide power. The motor speed figure demonstrates that the motor 1 mainly works when vehicle speed is below 40km/h while the motor speed is high to achieve high efficiency. In low speed conditions, the motor 1 works together with AMT to achieve high economic efficiency, because AMT provides high starting torque without compromising the efficiency at high operating speed.

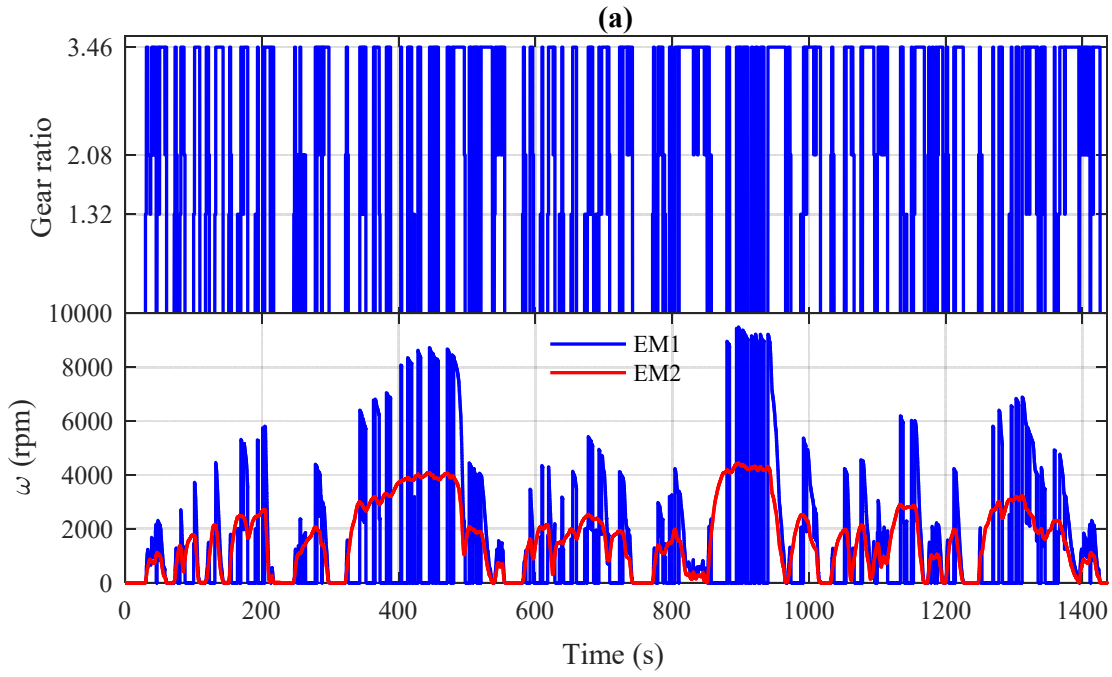

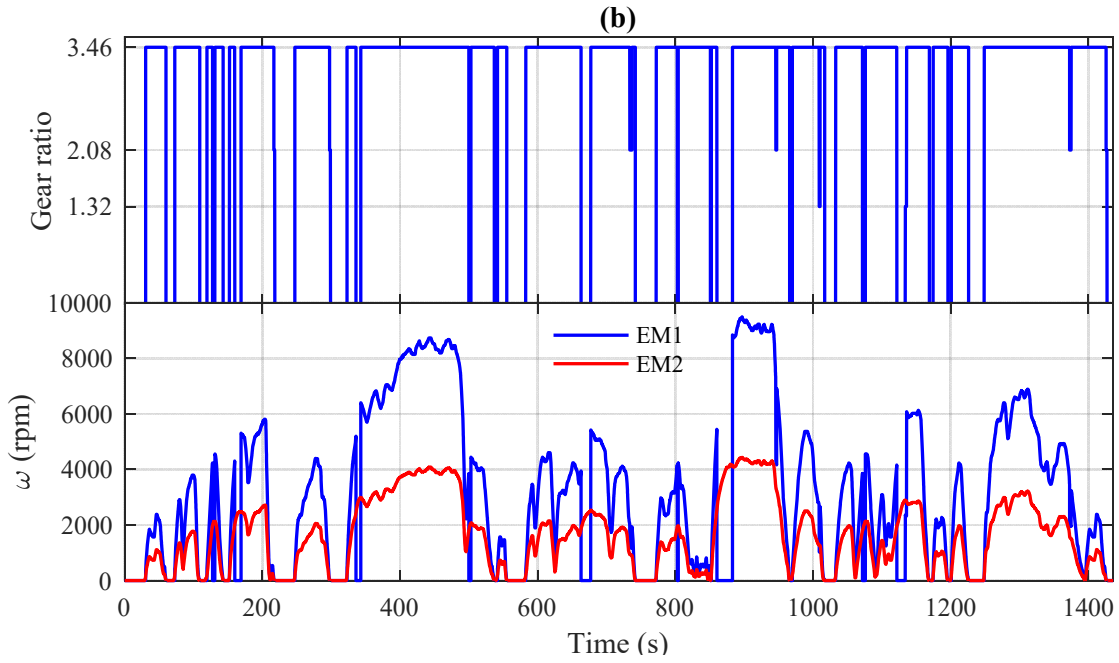

Figure. 6-6 Gear shifting with and without shifting stabilizer.

When the vehicle speed is above 40km/h, motor 2 will take over to provide power due to the design of fixed gear ratio for motor 2. Moreover, the performance of motor 1 in Fig. 6-6 (a) appears more aggressive with discontinuous working and frequent starting and stopping. With the designed shifting stabilizer, not only the excessive gear shifting is significantly reduced, the working pressure of electric motor is also lessened. As shown in Fig. 6-6 (b), the performance of motor 1 works in a steady and continuous way with less frequent launching and stopping.

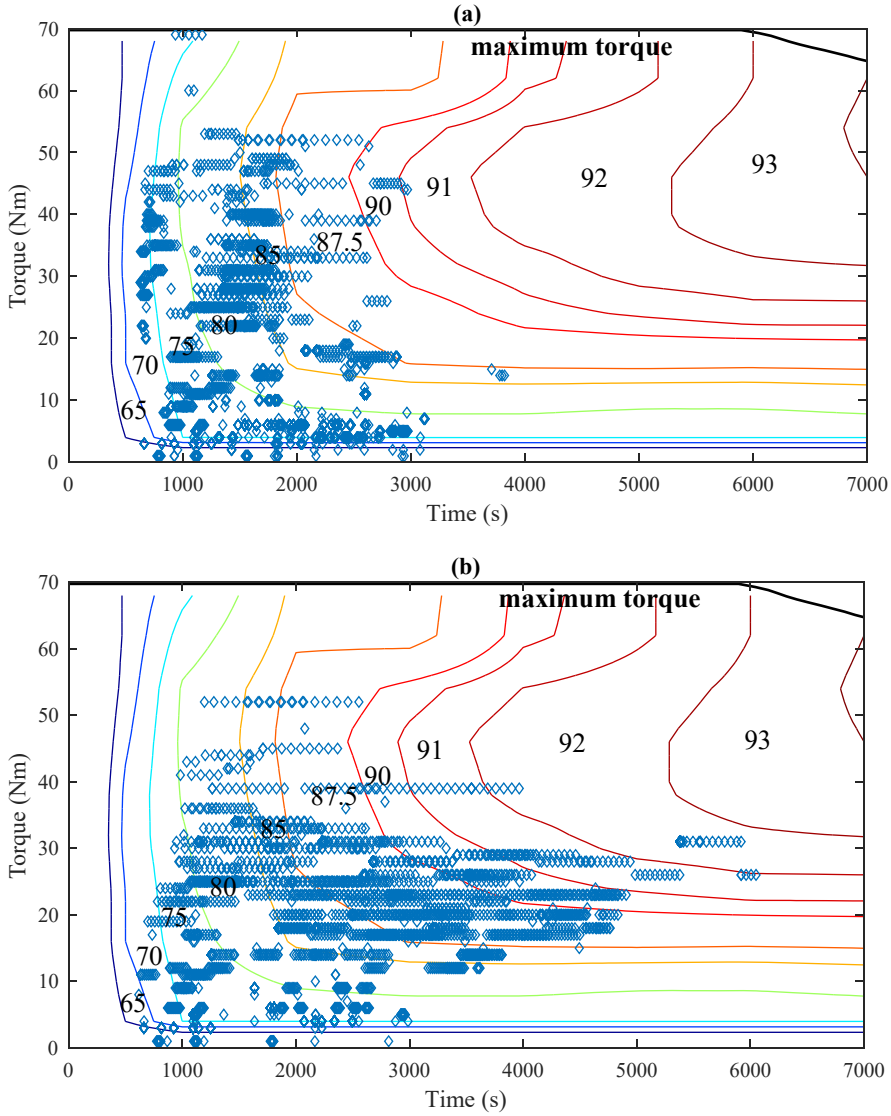

Figure. 6-7 Motor 1 efficiency map with and without shifting stabilizer.

Fig. 6-7 (a) shows the efficiency map of motor 1 without shifting stabilize, in which most working points concentrate around (1500 rpm, 35Nm). This is because the power distribution strategy directed by PSC keeps the motor working in an efficient area as much as possible, but this also leads to excessive gear shifting. In comparison, Fig. 6-7 (b) shows the efficiency map of motor 1 with shifting stabilizer, where the working points are more scattered. This is because many working points remain the same gear

ratio instead of changing gear. Accordingly, the working points with low speeds and high torques will move towards high speed and low torque area driven by the shifting stabilizer. These results show that the shifting stabilizer not only reduces the number of gear shifting but also improves the usable speed range. Moreover, it is worth noting that the overall efficiency with and without the shifting stabilizer is quite similar.

Fig. 6-8 (a) shows the actual power consumption of each gear at every instant. The solid lines refer to power consumption oriented PSC without shifting stabilizer, while the dotted lines refer to PSC with shifting stabilizer. Since the power distribution strategy is still working when the gear ratio is fixed, the power consumption in each gear state is quite close, which verifies the effectiveness of the proposed PSC.

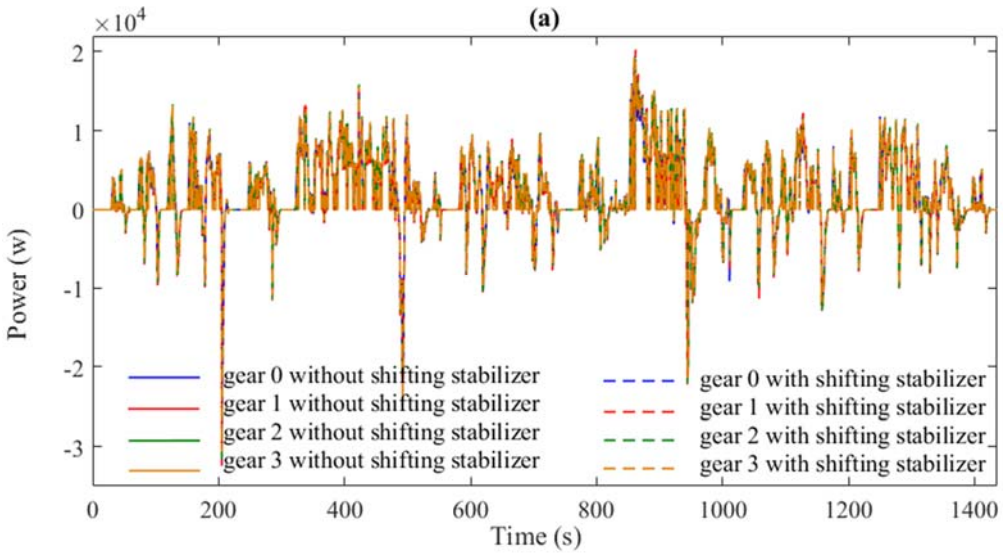

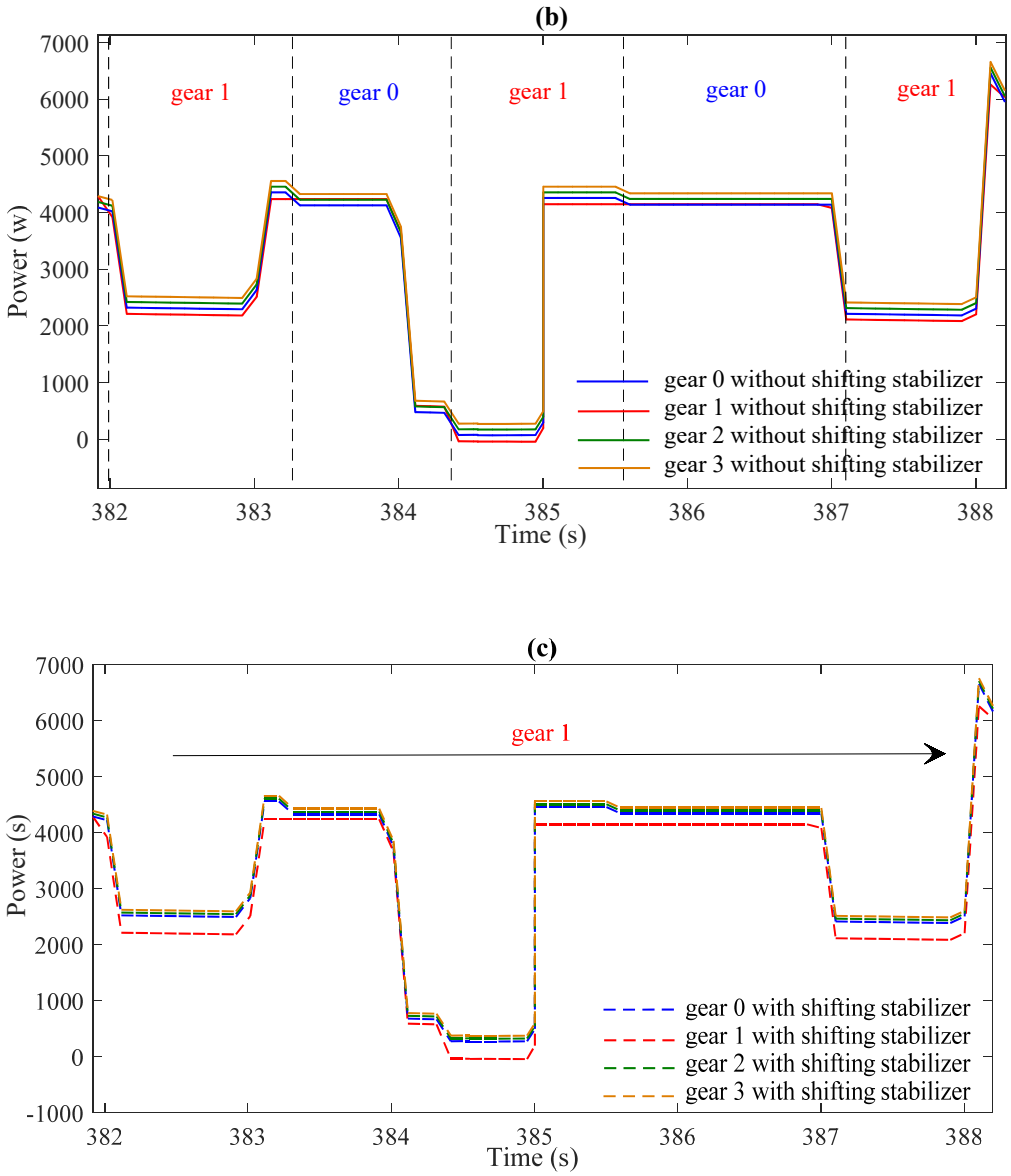

Figure. 6-8 Power distribution with and without shifting stabilizer.

According to the PSC, the gear state with lowest power consumption will be set as the working gear. As shown in Fig. 6-8 (b), gear 0 and gear 1 alternate to have the lowest power consumption, so that the corresponding working gear switches between them frequently. However, the shifting stabilizer will keep the power consumption of the working gear unchanged while imposing a penalty to the non-working gears. This is

showed in Fig. 6-8 (c), having the lowest power consumption makes gear 1 the working gear in early state. Therefore, the power consumption of the non-working gears is modified to a higher level by the shifting stabilizer. As a result, the gear 1will remain to have the lowest power consumption, and gear states will be stable during this period.

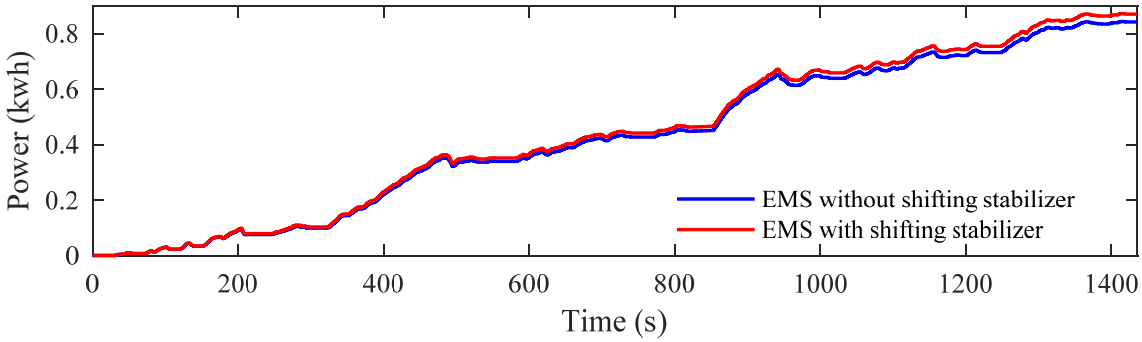

Figure. 6-9 Power consumption with and without shifting stabilizer in LA-92.

Fig. 6-9 compares the power consumption with and without shifting stabilizer in LA-92 driving cycle. The goals of saving-power consumption and reducing-gear shifting are contradictory, which means the reduction in gear shifting causes the increase of power consumption. As a result, while the gear changes are reduced significantly, the extra power consumption caused by shifting stabiliser is relatively small. However, it should be noted that the shifting process also consumes energy. Considering the cumulative energy consumption caused by gear events, the reduction in excessive gear shifting saves energy as well.

In the whole LA-92 driving cycle, the number of gear events reduces from 392 times to 60 times (84.693% down), while the energy consumption rises by 3.387%. Considering the shifting process, the hydraulic cost and motor loss are about 120w and 180w

respectively, and the shifting duration is set to be 1.2s. Thus, the shifting cost is about $0.0001kw \cdot h$. Adding the cost, from all gear shifting, the total energy consumption is saved by 0.532% instead.

6.4.2 HWFET driving cycle

HWFET driving cycle is a representation of high speed cruising with a distance of 16.45 km and an average speed of 77.7km/h in 765s.

Fig. 6-10 (a) shows the gear shifting events and corresponding angular speed of both motors directed by the proposed PSC without shifting stabilizer. Compared to LA-92, as the driving condition is simple, the overall gear shifting is much less. However, excessive gear shifting still exists when speed changes. Fig. 6-10 (b) shows the results directed by PSC with shifting stabilizer, in which the excessive gear shifting is further reduced. The motor speed figure demonstrates that the motor 1 only helps provide power during acceleration and deceleration. But the angular speed of motor 1 is high to guarantee high efficiency. At the same time, motor 2 works as the main power source because the designed fixed gear can not only satisfy the dynamic performance but also guarantee high efficiency of motor 2 in high speed cruising. In comparison, the number of gear shifting is reduced significantly, while the performance of motor 1 becomes steadier without on and off interruptions.

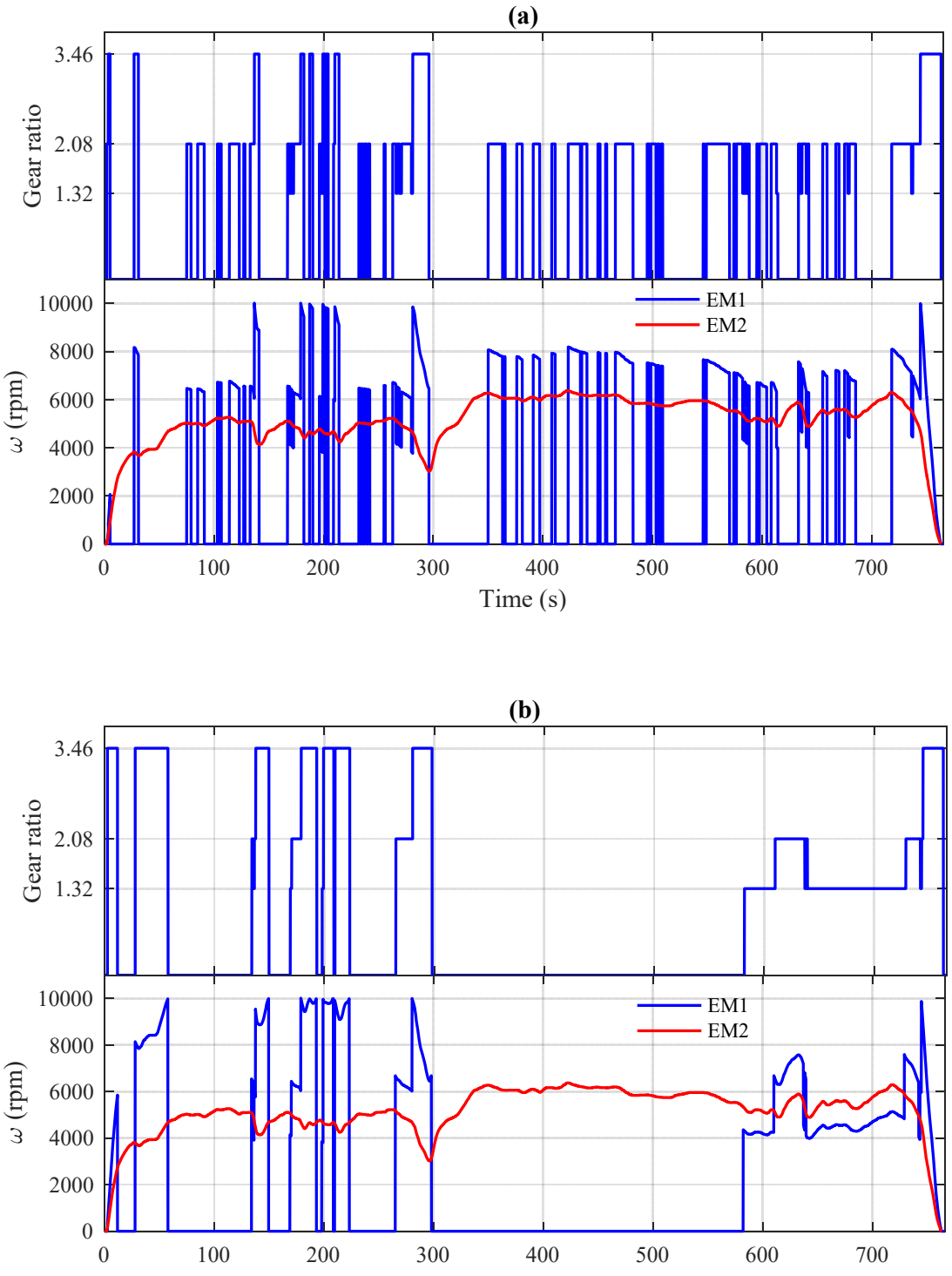

Figure. 6-10 Gear shifting reduction with and without shifting stabilizer.

Fig. 6-11 (a) shows the actual power consumption of each gear at every instant.The solid lines refer to energy consumption oriented PSC without shifting stabilizer, while the dotted lines refer to PSC with shifting stabilizer.

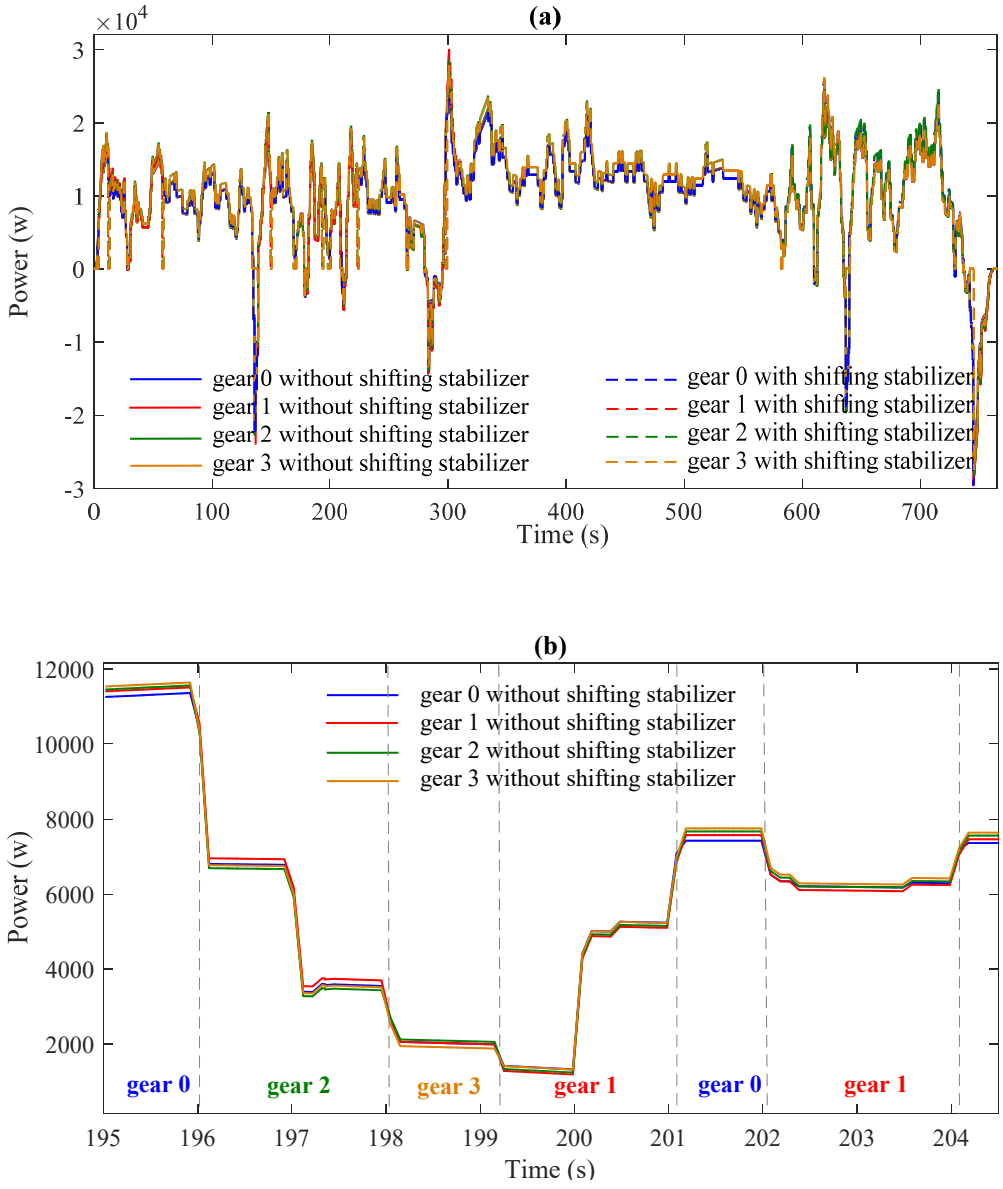

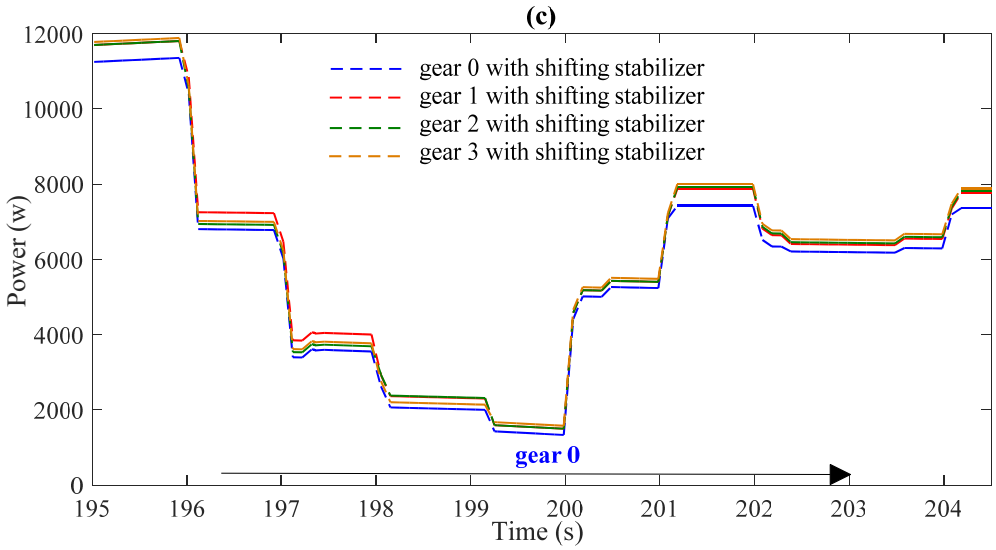

Figure. 6-11 Power distribution with and without shifting stabilizer.

Since the power distribution strategy is still working when the gear ratio is fixed, the power consumption in each gear state is quite close, which verifies the effectiveness of the proposed PSC. According to the PSC, the gear state with lowest power consumption will be set as the working gear. As shown in Fig. 6-11 (b), the working gear change frequently in a short period from gear 0, gear 2, gear 3, gear 1, gear 0 and to gear 1. With the shifting stabilizer, the strategy will keep the instant power consumption of the working gear unchanged while imposing a penalty to all the non-working gear states, which is showed in Fig. 6-11 (c). Having the lowest power consumption makes gear 0 the working gear in the early state. With the shifting stabilizer, the power consumption of the non-working gears is modified to a higher level by the shifting stabilizer. As a result, the gear 0 will remain to have the lowest power consumption so that short shifting intervals are avoid.

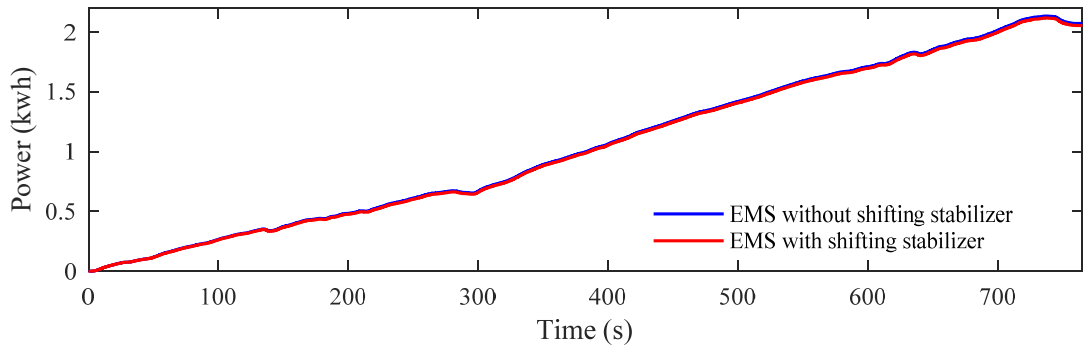

Figure. 6-12 Power consumption with and without shifting stabilizer in HWFET.

Fig. 6-12 compares the power consumption with and without shifting stabilizer in the HWFET driving cycle. Since the basic overall efficiency of the HWFET driving cycle is higher than that of the LA-92, the power consumption with and without shifting stabilizer is closer. In the whole HWFET driving cycle, the gear events reduce from 122 times to 31 times (75.590% down), while the energy consumption rise by 0.811%. Since the driving condition is simpler than that of LA-92, the shifting times and the shifting reduction is less. At the same time, as the average speed is much higher than that of LA-92, both motors are easy to work in their high efficiency area so that the extra energy consumption caused by gear shifting reduction is much less. The extra energy consumption will be further minimized when taking shifting cost for each gear change into account. After this, the total extra energy consumption is saved by 0.111%.

6.5 Conclusions

Since the energy management strategy is based on minimizing the energy consumption of the two motors at every instant, excessive gear shifting will be a problem. To avoid undesired gear shifting, a shifting stabilizer is proposed to improve shifting stability. To reach a balance between gear shifting and energy consumption, a multi-objective optimization algorithm is adopted to determine the optimal coefficient of proposed shifting stabilizer. Two driving cycles covering from urban driving conditions to mid-high cruising driving conditions are used to demonstrate the improvement of the shifting stability. With the designed shifting stabilizer, the excessive gear shifting is reduced significantly by improving the shifting margin and interval. The results show that the reduction of unnecessary gear shifting makes motor 1 operate in a more stable and continuous way. Moreover, considering the shifting cost from actuator, it also save energy by reducing the number of shifts.

CHAPTER 7 : A novel uninterrupted multi-speed transmission for hybrid electric mining trucks

7.1 Introduction

As the working conditions and specification requirements of mining trucks are different from commercial passenger vehicles [76], and the improvement of mining truck fuel efficiency could lead to more significant economic benefits, the investigation of hybrid transmission system becomes significantly important. Considering the energy consumption and specific performance requirements of mining trucks, a novel uninterrupted multi-speed transmission is proposed in this chapter, which is composed of a power-split device, and a 3-speed lay-shaft transmission with a traction motor. The power-split device is adopted to enhance the efficiency of the engine by adjusting the gear ratio continuously. The combination of the power-split device and 3-speed lay-shaft transmission can realise uninterrupted gear shifting with the proposed shift strategy, which benefits from the proposed adjunct function by adequately compensating the torque hole. The detailed dynamic models of the system are built to verify the effectiveness of the proposed shift strategy. To evaluate the maximum fuel efficiency that the proposed UMST could achieve, dynamic programming is implemented as the baseline. Due to the “dimension curse” of DP, a real-time control strategy is designed, which can significantly improve the computing efficiency. The simulation results demonstrate that the proposed UMST with DP and RTCS can

improve fuel efficiency by 11.63% and 8.51% compared with conventional automated manual transmission system, respectively.

7.2 System description

. The configuration of the proposed UMST is illustrated in Fig. 7-1.

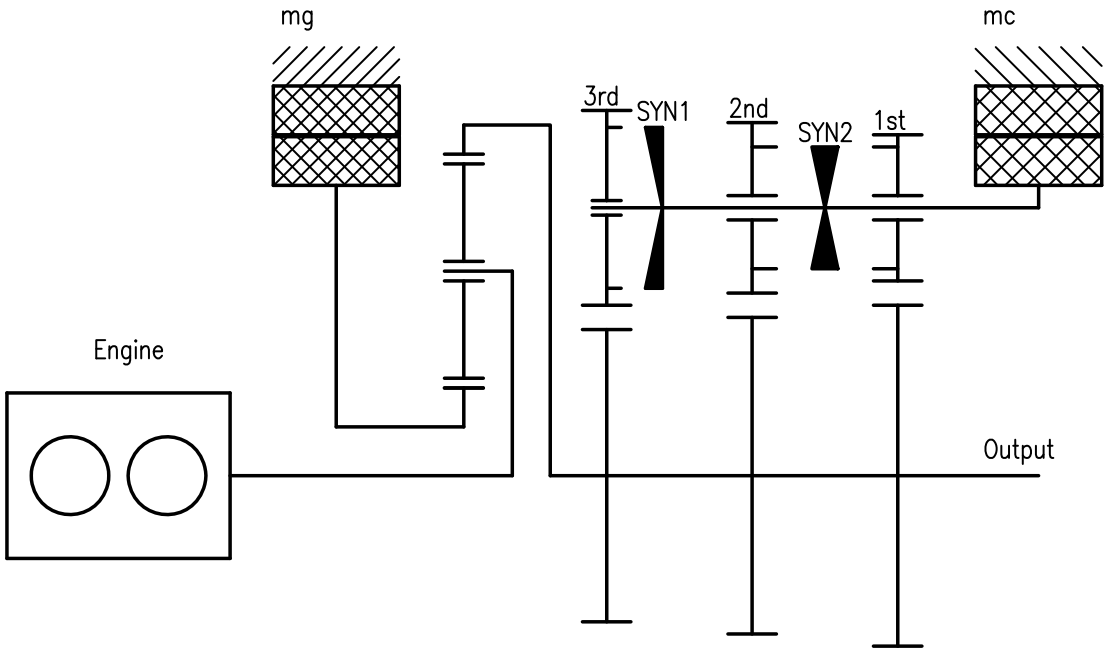

Figure. 7-1 Structure of the proposed UMST for mining truck.

The planetary gear set is treated as a power-split device between the engine and the generator (mg). The engine and generator are connected to the carrier and sun gear, respectively. The ring gear can directly drive the truck, and the traction motor (mc) is connected to the input shaft of 3-AMT. The purpose of generator is to adjust the engine speed to improve the engine efficiency according to the various external conditions, which is not completely the same as the traction motor. Meantime, the output torque of the ring gear can also improve the shift quality by offsetting or alleviating the torque

hole, which is unavoidable during shifting process of traditional AMT. The traction motor is designed to drive the truck in low-speed and high-torque conditions. Meanwhile, the traction motor can also adjust the speed of synchronizer to achieve quickly shifting. According to the authors' previous research, the parameters of the various components are calculated to meet the performance indicators proposed by the enterprises, the technical specifications are shown in Table 7-1.

Table 7-1 Technical specifications of the hybrid electric mining truck

Component	Parameter	Value
Engine	Rated power	243kW
	Max torque	1282Nm
	Speed range	0-2200r/min
Generator/mg	Rated/Peak power	100kW@1800r/min
	Speed range	0-3500r/min
Traction motor/mc	Rated power	150kW@800r/min
	Speed range	0-3500r/min
Battery	Capacity	65Ah
	Voltage	460v
Planetary gear	Ratio	3.6
3-speed AMT	Ratio	1.32/2.08/3.46

7.2.1 Dynamic Modeling

Fig. 7-2 shows the dynamic model of the planetary gear in detail, where, J, ω, T represent the inertia, the angular speed, and the torque, respectively.

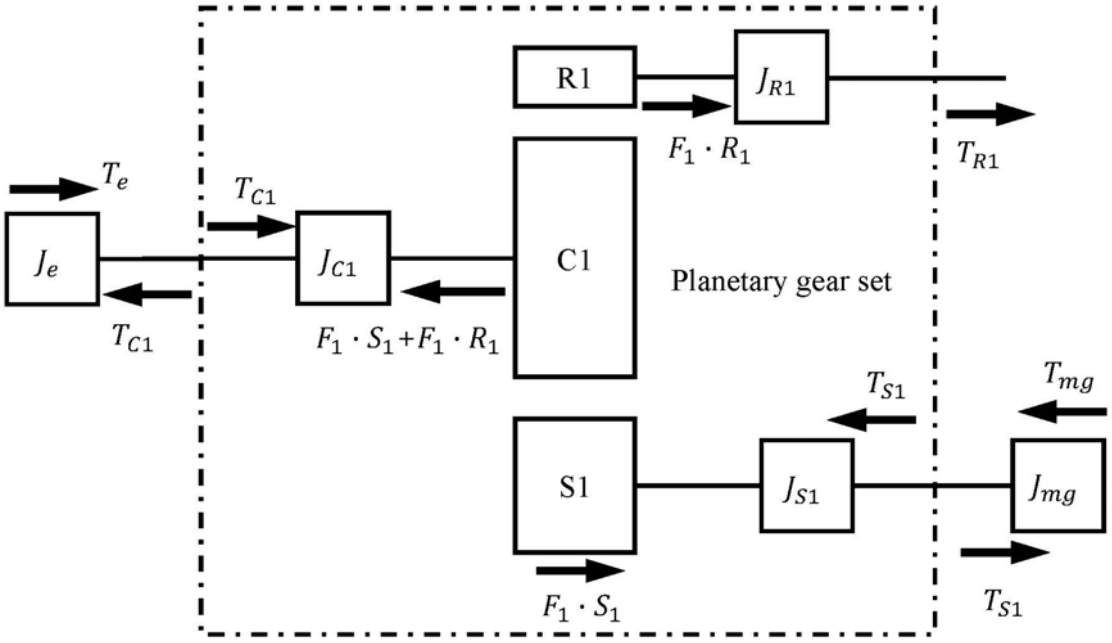

Figure. 7-2 The planetary gear model.

Assuming that both the sun gear, the ring gear, the carrier and the planet gears are properly intermeshing, and there is no slip between each other. Considering the moment of inertia, the output torques and the speeds of the engine and the generator, the expressions can be as:

$$
\begin{aligned}
&J_e \dot{\omega}_e = T_e - T_{C1} \\
&J_{mg} \dot{\omega}_{mg} = -T_{mg} + T_{S1} \\
&\omega_e = \omega_{C1} \\
&\omega_{mg} = \omega_{S1}
\end{aligned}
\qquad (49)
$$

where subscripts $e, mg, C1, S1$ are the engine, the generator, the carrier and the sun gear respectively.

Euler's formula is applied to demonstrate the relationship of the three components for the single planetary gear set. The dynamic equations are expressed as follows:

$$\begin{aligned} J_{R1}\dot{\omega}_{R1} &= F_1 R_1 - T_{R1} \\ J_{C1}\dot{\omega}_{C1} &= -F_1 R_1 - F_1 S_1 + T_{C1} \\ J_{S1}\dot{\omega}_{S1} &= F_1 S_1 - T_{S1} \end{aligned} \tag{50}$$

where, subscripts $R1$ is the ring gear, the carrier, and the sun gear, $F1$ is the internal force of planetary gear set, R_1, S_1 are the radius of the ring gear and the sun gear, respectively.

According to Eq. (49) and Eq. (50), the dynamic equation of the torque and speed for the engine, the generator, and the planetary gear set can be obtained as follows:

$$\begin{aligned} (J_e + J_{C1})\dot{\omega}_e &= -F_1 R_1 - F_1 S_1 + T_e \\ (J_{mg} + J_{S1})\dot{\omega}_{mg} &= F_1 S_1 - T_{mg} \end{aligned} \tag{51}$$

Due to the intermeshing linear velocity between the sun gear and planet gear is equal to the linear velocity between planet gear and carrier, the equations can be as

$$\omega_{mg} + k\omega_{R1} - (1+k)\omega_e = 0 \tag{52}$$

where k is the ratio between the ring gear and sun gear.

There are still two input variables in 3-AMT including the ring gear output and the traction motor output. The free-body diagram of 3-AMT is demonstrated in Fig. 7-3,

where K, C represent the stiffness and the damping coefficient of the coupling shaft, respectively, θ represent the angular displacement, J, ω, T represent the inertia, the angular speed, and the torque, respectively.

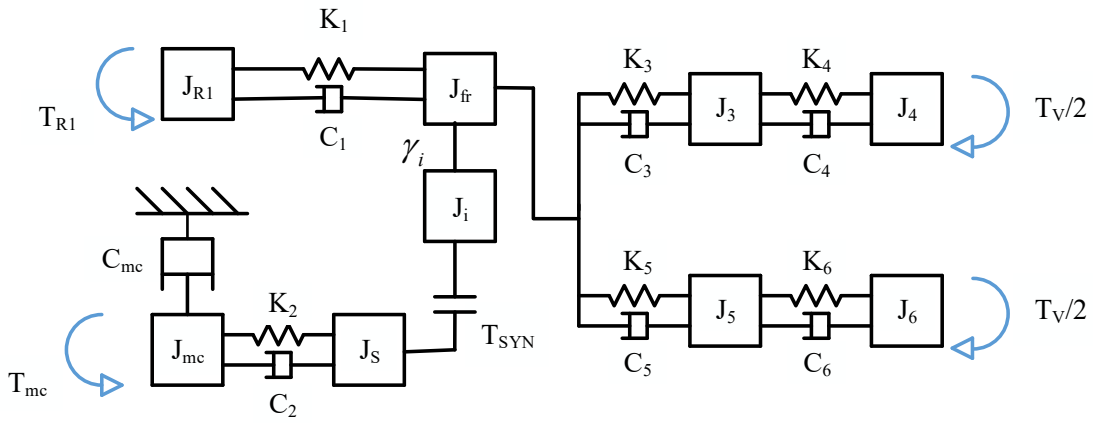

Figure. 7-3 The layout gear model.

Similarly, the input of them can be described as follows:

$$J_{R1}\dot{\omega}_{R1} = T_{R1} - K_1(\theta_{R1} - \theta_{fr}) - C_1(\omega_{R1} - \omega_{fr}) \quad (53)$$
$$J_{mc}\dot{\omega}_{mc} = T_{mc} - C_{mc}\omega_{mc} - K_2(\theta_{mc} - \theta_S) - C_2(\omega_{mc} - \omega_S)$$

where, subscripts $1, 2, fr, mc, S$ are for the connecting shaft, the spur gear, the final drive, the traction motor, and the synchronizer, respectively.

The variation of gear ratio depends on the engagement or disengagement of the synchronizers, which affects the vehicle jerk. Therefore, the torque calculation is essential. Assume S_c is the state of synchronizer, S_c=0 means the synchronizer is completely disengaged. On the contrary, S_c=1 means the synchronizer is engaged.

When $S_c \in (0,1)$, more especially, the synchronizer is in disengaging or engaging process, the transfer functions are:

$$J_S \omega_S = K_2(\theta_{mc} - \theta_S) + C_2(\omega_{mc} - \omega_S) - T_{SYN} \quad (54)$$

$$\begin{aligned}(J_{fr} + J_i \gamma_i^2)\dot{\omega}_{fr} &= \gamma_i T_{SYN} + K_1(\theta_{R1} - \theta_{fr}) + C_1(\omega_{R1} - \omega_{fr}) \\ &- K_3(\theta_{fr} - \theta_3) - C_3(\omega_{fr} - \omega_3) \\ &- K_5(\theta_{fr} - \theta_5) - C_5(\omega_{fr} - \omega_5)\end{aligned} \quad (55)$$

where subscripts $i, 3, 5$ are the gear ratio, the left haft axle, and the right haft axle, respectively, T_{SYN} is the cone clutch's torque.

When S_c=1, namely, the synchronizer is completely engaged, the transfer function is as:

$$\begin{aligned}(J_{fr} + \gamma_i^2 J_S + \gamma_i^2 J_i)\dot{\omega}_{fr} &= \gamma_i K_2(\theta_{mc} - \gamma_i \theta_{fr}) + \gamma_i C_2(\omega_{mc} - \gamma_i \omega_{fr}) \\ &+ K_1(\theta_{R1} - \theta_{fr}) + C_1(\omega_{R1} - \omega_{fr}) \\ &- K_3(\theta_{fr} - \theta_3) - C_3(\omega_{fr} - \omega_3) \\ &- K_5(\theta_{fr} - \theta_5) - C_5(\omega_{fr} - \omega_5)\end{aligned} \quad (56)$$

Considering the symmetry of the half shafts and the tires, only the equations of one side are given, as follows:

$$
\begin{aligned}
&J_3\dot{\omega}_3 = K_3(\theta_{fr}-\theta_3)-C_3(\omega_{fr}-\omega_3)\\
&-K_4(\theta_3-\theta_4)-C_4(\omega_3-\omega_4)\\
&J_4\dot{\omega}_4 = K_4(\theta_3-\theta_4)+C_4(\omega_3-\omega_4)-T_V/2
\end{aligned}
\tag{57}
$$

where subscript 4 is the left tire, T_V is the resistance torque.

7.2.2 Vehicle model

According to the longitudinal dynamic performance, the resistance force of the rear axle can be analysed. Here, the damping and compliance are ignored to simplify the analysis. Due to the truck speed is relatively low, the aerodynamic resistance is also ignored. The expressions are as follows:

$$
T_V/\mathrm{R}_V = \mu(m+M)\,\mathrm{gcos}(\varphi)+(m+M)\,\mathrm{gsin}(\varphi)+\delta(\mathrm{m}+M)\frac{dV}{dt} \tag{58}
$$

where R_V is the effective radius of the tire, μ is the rolling resistance coefficient, m is the truck curb mass, M is the truckload mass, g is the acceleration constant of gravity, φ is the road slope, V is the vehicle speed and δ is the rotation component coefficient.

7.2.3 Battery model

According to previous study, the battery module is simplified to the first order approximated internal resistance model, and the impact of temperature and battery life are ignored [151], as shown in Fig. 7-4.

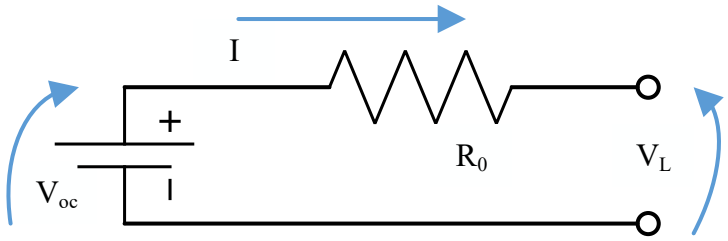

Figure. 7-4 The first order approximated internal resistance model.

Hence, the battery power is derived where a positive value represents discharging process and a negative value represents charging.

According to the battery equivalent circuit, state of charge (SOC) is calculated as:

$$\dot{SOC}(\mathrm{t}) = -\frac{1}{Q_{\max}} \frac{V_{oc} - \sqrt{V_{oc}^2 - 4R_0 P_{batt}(t)}}{2\mathrm{R}_0} \quad (59)$$

where $P_{batt}(t)$ is the battery power varying with SOC, V_{OC} is the open-loop voltage, V_L is the output voltage, R_0 is the internal resistance, $Q_{\max}$ is the maximum electrical charge.

7.2.4 Power model

Because the engine is a time-varying nonlinear system, the complicated internal dynamic process of the engine is not considered. The throttle, speed, and torque of the engine are used to calculate instantaneous fuel consumption with the fuel consumption contour map, as shown in Fig. 7-5.

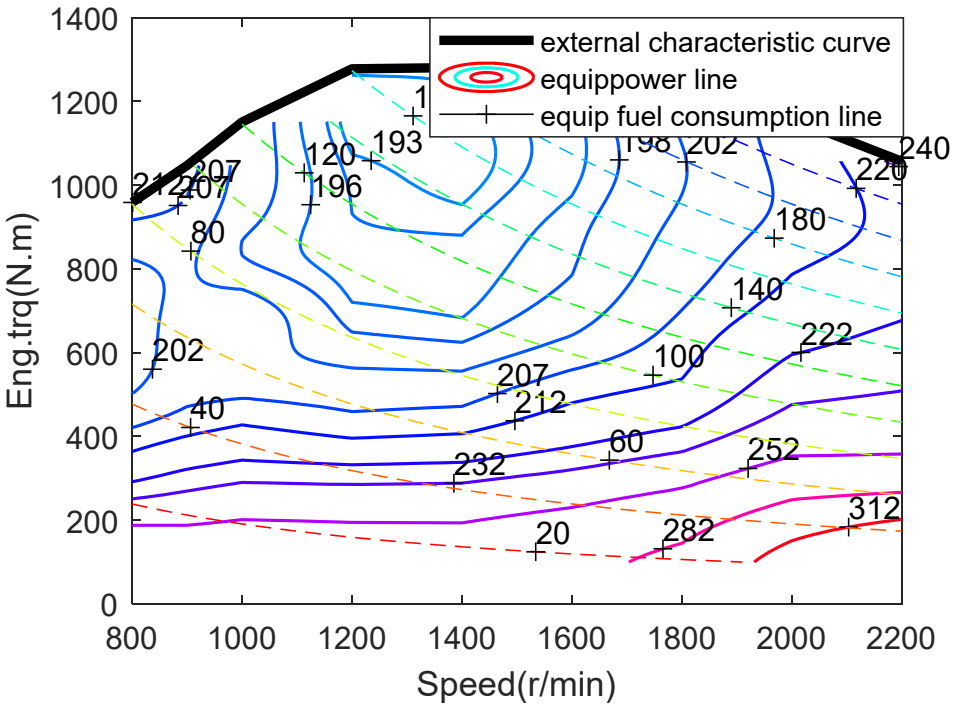

Figure. 7-5 The fuel consumption contour map of the engine.

The equation can be expressed as follows.

$$m_e = f(w_e, T_e) \tag{60}$$

As the motor cannot only drive the truck but also recover the braking energy, the motor power can be calculated with the following expression.

$$P_{mc} = \begin{cases} \dfrac{T_{mc}\omega_{mc}}{\eta_m} & T_{mc} \geq 0 \\ T_{mc}\omega_{mc}\eta_r & T_{mc} < 0 \end{cases} \tag{61}$$

where T_{mc} is the motor output torque, ω_{mc} is the motor output speed, η_m, η_r are the discharging and charging efficiency, respectively.

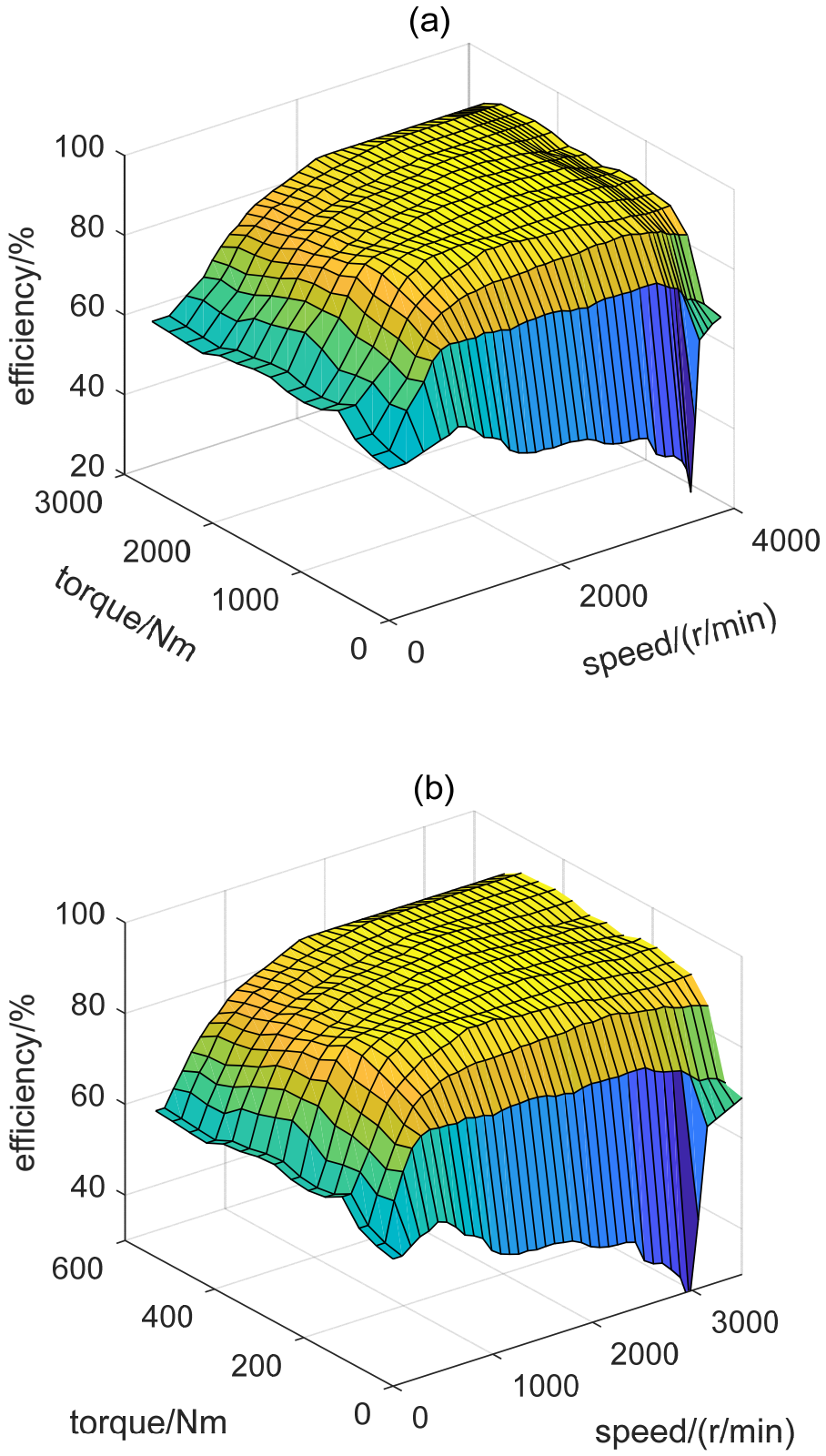

Figure. 7-6 The efficiency map of motor (a) and generator (b).

The efficiency of motor varied from 0.6 to 0.96, so it can largely affect the battery consumption. Here, the efficiency is determined by using a two-dimensional map whose data are obtained by the measurement during discharging and charging process, as shown in Fig. 7-6.

7.3 Implementation of shifting control

7.3.1 Shift process

The coordinated control of shifting process is illustrated in Fig. 7-7.

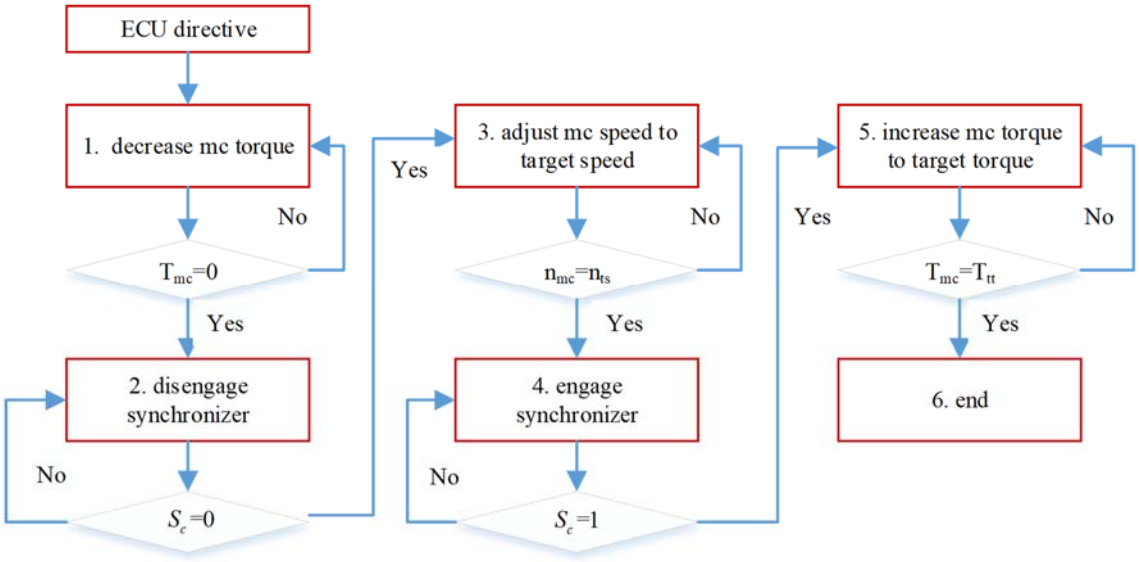

Figure. 7-7 The coordinated control of the shift progress.

After receiving the command from electronic control unit (ECU), the shifting process will be implemented. In the first step, the traction motor torque reduces to 0 step by step, and the motor operates in the torque mode at this moment. At the same time, the ring

gear output torque increases with opposite variation of the traction motor output torque to counteract the torque hole by controlling the generator, which can improve the shift quality. However, due to the limitation of engine output torque, the ring gear output torque cannot exceed the maximum value. In the second step, when the motor torque is 0, and the operating mode turns into the free mode, the synchronizer of current gear ratio can smoothly disengage in no-load condition. The output torque of ring gear remains unchanged. In the third step, the motor turn to operate in the speed mode, which can adjust the motor speed to target speed to reduce the speed gap. The ring gear output torque stays the same. In the fourth step, when the motor speed is close to the target speed, the motor turns to operate in the free mode again, the synchronizer of the target gear ratio can accomplish non-shock engagement. The output torque of ring gear remains the same. In the fifth step, when the synchronizer is completely engaged, the motor turn to operate in torque mode, and gradually increases the output torque to the target value. Meanwhile, the ring gear output torque reduces according the demand torque.

According to the foresaid shifting process, the output torque of the traction motor and the ring gear must be properly controlled to improve driving comfort during shifting process. Therefore, an adjunct function is proposed to control the variation of torque during the five stages of shifting progress, as shown in Fig. 7-8.

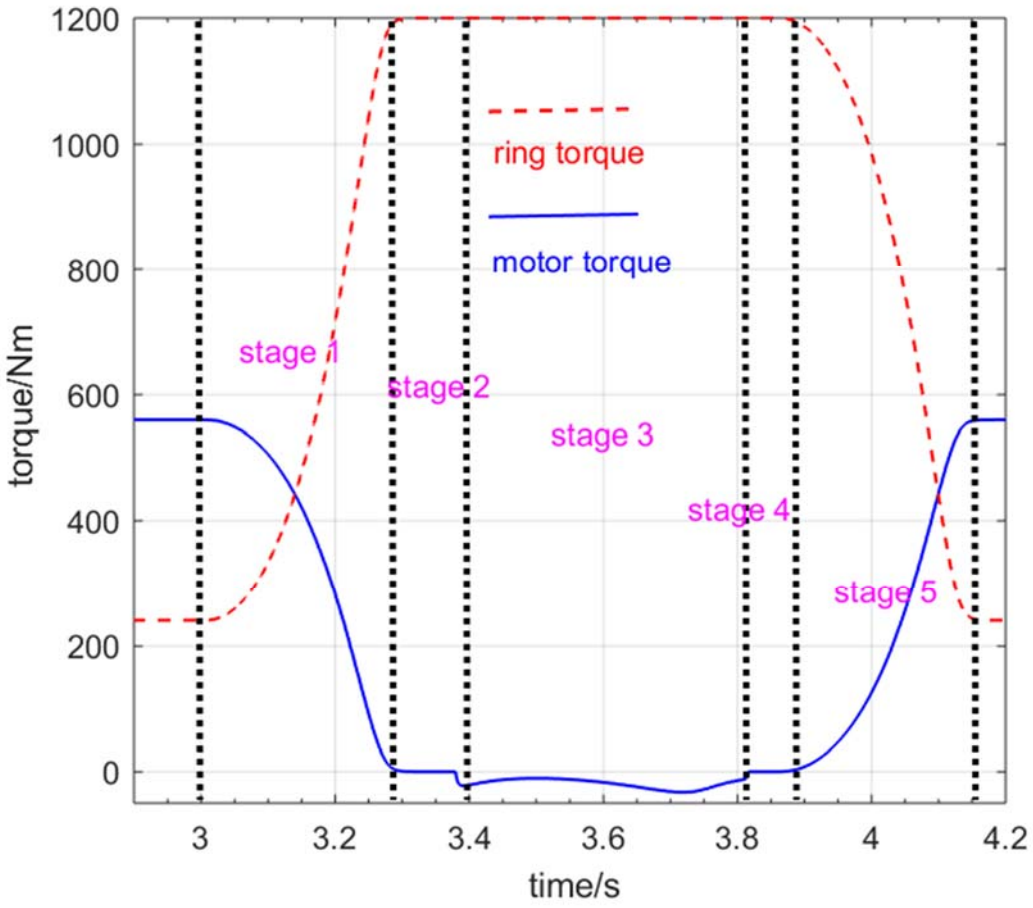

Figure. 7-8 Torque variation during the shifting progress.

Stage 1 represents that the motor torque decreases and the ring gear output torque increases at the same time. Stage 2 indicates that the synchronization disengages within 0.1s. Then the process of speed synchronization is implemented in the stage 3. The negative motor torque can make the synchronization time shorter. When the slip is close to zero, the synchronization will be engaged in the stage 4. The ring gear supplies the demand torque in the stage 2 to 4, but the maximum torque is limited to 1200Nm. At last, the ring gear torque decreases and the motor torque increases to demand value in the stage 5. The expressions are given as follows.

$$T_{mc} = \begin{cases} T_{mc}^{\ 0} & t < t_0 \\ T_{mc}^{\ 0}(1+(\dfrac{t_0 - t}{t_d})^3) & t_0 < t < t_0 + t_d \\ 0 & t_0 + t_d < t < t_1 \\ T_{mc}^{\ 0}(\dfrac{t - t_1}{t_e})^3 & t_1 < t < t_1 + t_e \\ T_{mc}^{\ 0} & t > t_1 + t_e \end{cases} \quad (62)$$

$$T_r = \begin{cases} T_r^{\ 0} & t < t_0 \\ T_{mc}^{\ 0}\gamma_i(\dfrac{t - t_0}{t_d})^3 + T_r^{\ 0} & t_0 < t < t_0 + t_d \\ T_{mc}^{\ 0}\gamma_i + T_r^{\ 0} & t_0 + t_d < t < t_1 \\ T_r^{\ 0} + T_{mc}^{\ 0}\gamma_i(1+(\dfrac{t_1 - t}{t_e})^3) & t_1 < t < t_1 + t_e \\ T_r^{\ 0} & t > t_1 + t_e \end{cases} \quad (63)$$

$$0 \le T_r \le 1200$$

where $T_{mc}^{\ 0}, T_r^{\ 0}$ are the initial input torque of traction motor and the ring gear, respectively, t_0 is the starting time of the synchronizer disengagement, t_d is the duration time of the synchronizer disengagement, t_1 is the starting time of the synchronizer engagement, t_e is the duration of the synchronizer engagement.

7.3.2 Drivability performance analysis

To verify the feasibility of proposed shift control strategy and the adjunct function, an acceleration process is designed, as shown in Fig. 7-9 (a). According to the actual working conditions, if the traction motor output torque is 560Nm and ring gear output torque is 240Nm, then the transmission output torque should be 2177.6Nm, 1404.8Nm, and 979.2Nm, in the first gear, second gear, and third gear, respectively.

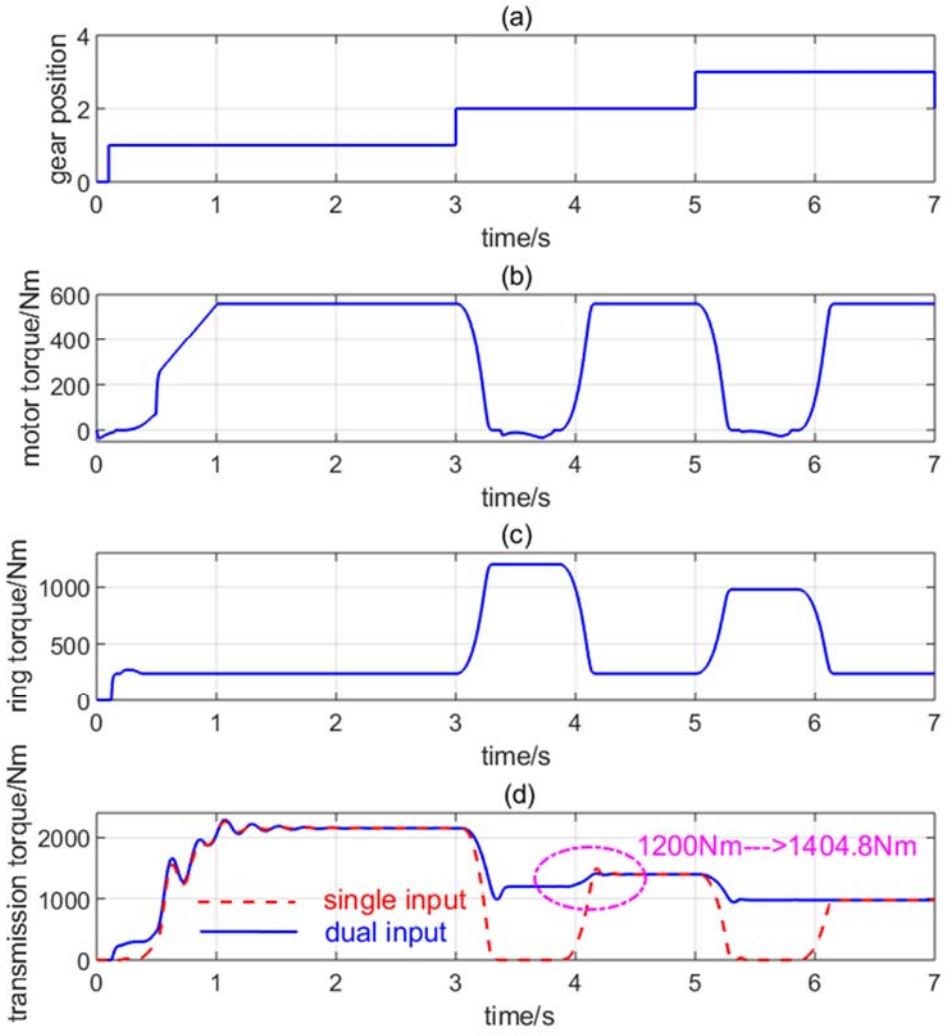

Figure. 7-9 Torque variation during upshifting process.

Fig. 7-9 (b) shows that the traction motor output torque varies with the gear position, the torque is close to 0 during the shift process, that is what caused the power interruption of traditional AMT. It can be seen that the ring gear output torque smoothly increases to compensate the torque hole within the limitation in Fig. 7-9 (c). Fig. 7-9 (d) shows the comparison of the proposed dual input control configuration and single input control configuration. It can be obviously seen that the output torque of single input transmission is zero during shifting process, the dual input transmission can adequately compensate the torque hole. For instance, the ring torque is limited to 1200Nm when gear ratio upshifts from the first to the second, which should be 1404.8Nm. At this moment, the torque hole can be partially offset. When gear ratio upshifts from the second ratio third, the demand torque is 979.2Nm, and it is less than the maximum torque that the ring gear can output where there is no torque interruption. Therefore, compared to the single input transmission, the proposed dual input UMST can improve the drivability significantly.

The shift jerks of two configurations are shown in Fig. 7-10. It can be seen that the jerk of proposed dual input UMST is obviously smaller than the single input configuration. The jerk occurs in three aspects: 1). Synchronizer disengages, 2) synchronizer engages, 3) demand torque recovers. The torque absence during shifting process cause large jerk for single input configuration, because the torque varies between 0 and the demand value. However, proposed UMST can supply partial or the entire demand torque.

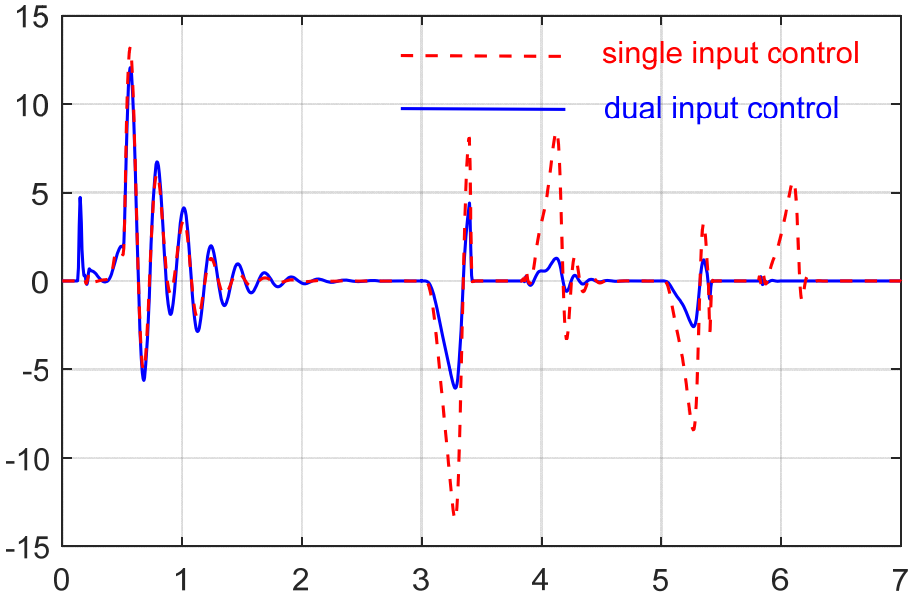

Figure. 7-10 Comparison of vehicle jerk.

For instance, when gear ratio changes from the first ratio to second, although the limitation of ring gear output torque causes that the torque hole cannot be completely offset, the jerk is still small because the torque varies between the limitation value and the demand value. In particularly, the jerk causing by the demand torque reconversion can be eliminated for the proposed dual input UMST, because the ring gear output torque can meet the demand torque, as shown in shifting process from the second gear to the third.

7.4 A real-time control strategy

According to the operation datum of mining trucks given by the enterprise, a speed cycle is established, as shown in Fig. 7-11.

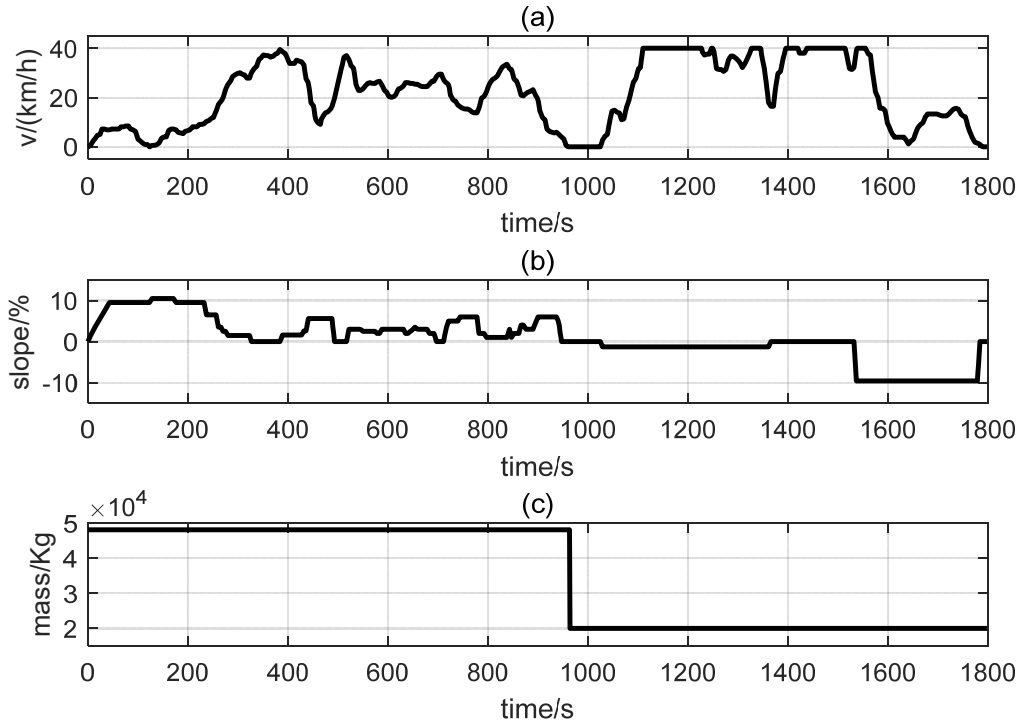

Figure. 7-11 The working cycle of a mining truck, (a) truck speed varying with time, (b) road slope changing with time, (c) truckload varying with time.

Dynamic programming is a numerical algorithm to solve multi-stage decision issues, which is based on Berman optimization principle. The basic idea is to obtain the performance index of each state and each control variable in the reverse process, and then the control variables corresponding to the optimal performance index in the forward process can be found. Therefore, DP is usually applied to get the global optimal solution for evaluating the novel design, which is regarded as a benchmark. According to the reference 6, the state variables and control variables are selected based on the different kind of vehicles with DP. Assuming that the fuel consumption is zero if the demand power is less than 0, the fuel consumption of proposed UMST and AMT is

7.0341kg and 6.2164kg, respectively. It should be noted that the engine (Commins QSL9) and the transmission (MRT-11710B) are equipped with the traditional mechanical truck.

However, it is well-known that DP easily causes “dimension curse” and requires much time of calculation, so it is hard to be applied in real time. To overcome the drawbacks of DP, a real-time control strategy based on equivalent consumption minimization strategy (ECMS) is proposed. The RTCS aims at minimizing the sum of engine fuel consumption and electricity consumption at every moment. Therefore, the cost function can be expressed as follows.

$$Je(t) = \min(m_{eng}(t) + m_{bat}(t)) \tag{64}$$

where, $m_{eng}(t), m_{bat}(t)$ are the engine fuel consumption and equivalent fuel consumption of battery at some point, respectively.

Due to the traditional ECMS cannot guarantee the balance of SOC, PI controllers are applied to balance the wave range [152]. The expressions are as follows.

$$m_{bat}(t) = \begin{cases} \lambda_{eq} P(SOC(t)) I(SOC(t)) \dfrac{P_b(t)}{\eta_{dis}(t) Q_{lhv}} & P_b(t) > 0 \\ \lambda_{eq} P(SOC(t)) I(SOC(t)) \cdot \dfrac{\eta_{chg}(t) P_b(t)}{Q_{lhv}} & P_b(t) < 0 \end{cases} \tag{65}$$

$$P(SOC(t)) = 1 - 8\left(\frac{SOC(t) - SOC_0}{SOC_{\max} - SOC_{\min}}\right)^3$$

$$I(SOC(t)) = \begin{cases} 1 - a(SOC(t) - SOC_0)^3 \\ 1 - b(SOC(t) - SOC_0)^3 + c(SOC(t) - SOC_0)^4 \end{cases}$$

where, λ_{eq} is equivalent fuel coefficient, $P_b(t)$ is battery power, $\eta_{dis}(t)$ is discharge efficiency, $\eta_{chg}(t)$ is charge efficiency, SOC_0 is initial value of SOC, a, b, c are all fit coefficients.

According to the proposed RTCS, the simulation results are shown in Fig. 7-12.

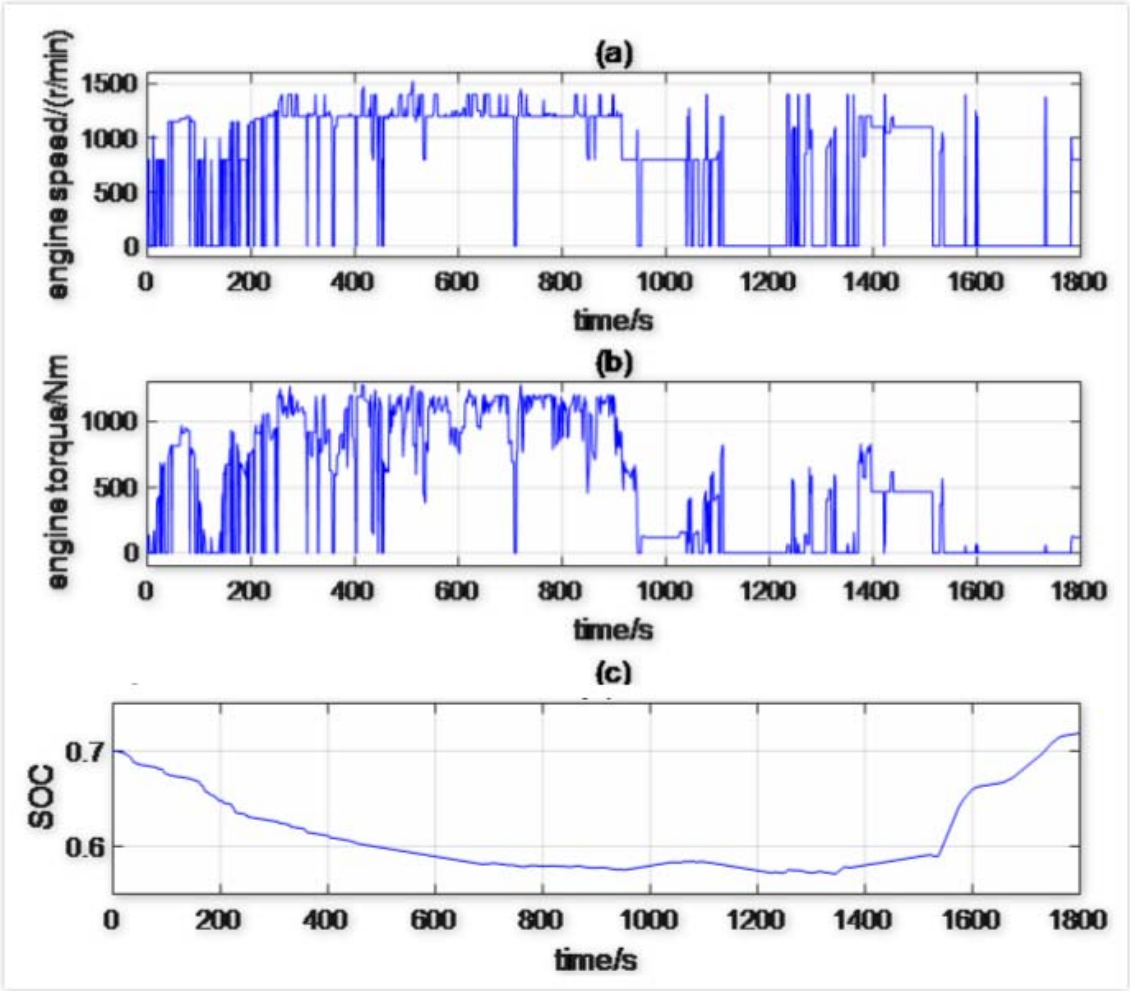

Figure. 7-12 The simulation results with RTCS, (a) engine speed, (b) engine torque, (c) SOC variation.

Fig. 7-12 (a) and Fig. 7-12 (b) illustrate that the engine speed and torque vary in the whole cycle, respectively. The engine drives the generator to generate the electric power

for supplying the motor or charging the battery. Fig. 7-12 (c) shows that SOC varies with time. Because the truck is driving uphill before 900s, the battery is discharging in this time and SOC drops from 0.7 to 0.58. During the loading point, SOC is lightly increased. When the truck drives downhill, the motor can recover the braking energy and store the electricity in the battery.

According to the aforementioned simulation results, the fuel economy of proposed UMST is evaluated during the given cycle with DP and RTCS, which is shown in Table 7-2.

Table 7-2 Comparison of fuel economy

Configuration	Fuel consumption	Improve economy
AMT with DP	7.0341	-
UMST with DP	6.2164	11.63%
UMST with RTCS	6.4357	8.51%

Compared to the AMT system, the proposed UMST with DP and RTCS can enhance fuel economy by 11.63% and 8.51, respectively. The reason why the proposed UMST can reduce the fuel consumption is because of the improvement of energy efficiency. As the above description, the proposed UMST can make the engine work in high-efficiency region by adjusting the generator speed, the gear ratio, and the motor torque.

7.5 Conclusions

A novel non-interrupted multi-speed transmission with power and shift control strategy is proposed for hybrid mining trucks. The purpose is to improve fuel economy and shift

quality. The proposed UMST consists of a planetary gear set integrated with 3-AMT, which can save manufacturing cost, achieve non-interruption, and enhance system efficiency. Compared to traditional mechanical mining truck, the proposed UMST with DP and RTCS can improve fuel efficiency by 11.63% and 8.51%, respectively.

To reduce vehicle jerk, the shift control strategy with an adjunct function is proposed, which can adequately compensate the torque hole during shifting process. Sometimes only partial torque is compensated in shifting process, but the simulation results indicate the proposed shifting strategy still can meet the jerk demand and be superior to the single input control.

CHAPTER 8 : Thesis conclusions

The development of electric and hybrid electric vehicles has attracted the attention both from the academic and industry world. In order to develop a complete powertrain solution to achieve high overall efficiency and desirable drivability performance, improve the driving comfort and the powertrain robustness, novel and advanced methods have been investigated and designed in this thesis.

Considering the efficiency of the fundamental structure of the transmission system, automated manual transmission is adopted as it has higher efficiency, lower manufacturing cost, more compact and less weight compared with other multispeed transmission systems. Based on the automated manual transmission system, a novel dual input clutchless transmission configuration is proposed with many variations. The removal of the friction clutch will further improve the overall efficiency by avoid the corresponding hydraulic loss. In order to overcome the drawback of automated manual transmission which is the torque hole during gear shifting, a novel modified bump function based gear shifting control strategy is designed. With the proposed gear shifting control strategy, the torque hole can be eliminated, improving both the drivability and driving comfort. As there are two motors in the proposed system, a suitable power sharing control strategy is in need. The designed real-time power sharing control strategy could properly distribute the power demand between the two motors and achieve a sub-optimal efficiency performance. However, the proposed power sharing control strategy suffers from excessive gear shifting problem just like other solutions. To solve this problem, a shift stabilizer is designed and embedded into the

system. With the proposed stabilizer, frequent gear shifting has been avoided without compromising the overall efficiency. Moreover, a powertrain configuration for mining trucks is also proposed as the requirements of mining trucks are very different from those of passenger vehicles.

Further Research

Although the related emerging problems such as motor efficiency, energy management strategies and the associated control systems have been significantly alleviated, the long-lasting problem of low battery energy and power density still prevent the battery based electric vehicles from dominating the market. As a result, together with the limited battery life, high initial cost, relatively long charging time and limited driving range per charge, the large-scale commercialization of battery based electric vehicles is still hindered.

In general, about 42% of energy is consumed in rolling, 25% wasted in the form of heat during deceleration, 23% by air drag and 10% in other forms. As the consumed energy in rolling cannot be notably reduced and the energy wasted by air drag depends on the shape of vehicles, the kinetic energy during braking becomes very important. If the kinetic energy could be recaptured and transformed into electrical energy stored in the battery again during braking, the driving range per charge and the overall efficiency would be significantly improved.

As a result, in order to further improve the overall efficiency of the transmission system, un-interrupted gear shifting control strategy during regenerative braking will be focus of the investigations.

Bibliography

[1] A.G. Boulanger, A.C. Chu, S. Maxx, D.L. Waltz, Vehicle electrification: Status and issues, Proc. IEEE. 99 (2011) 1116–1138.

[2] B. Egardt, N. Murgovski, M. Pourabdollah, L.J. Mardh, Electromobility studies based on convex optimization: Design and control issues regarding vehicle electrification, IEEE Control Syst. 34 (2014) 32–49.

[3] R. Wang, C. Hu, Z. Wang, F. Yan, N. Chen, Integrated optimal dynamics control of 4WD4WS electric ground vehicle with tire-road frictional coefficient estimation, Mech. Syst. Signal Process. 60 (2015) 727–741.

[4] N. Denis, M.R. Dubois, A. Desrochers, Fuzzy-based blended control for the energy management of a parallel plug-in hybrid electric vehicle, IET Intell. Transp. Syst. 9 (2014) 30–37.

[5] J.L. Torres, R. Gonzalez, A. Gimenez, J. Lopez, Energy management strategy for plug-in hybrid electric vehicles. A comparative study, Appl. Energy. 113 (2014) 816–824.

[6] T. Miro-Padovani, G. Colin, A. Ketfi-Chérif, Y. Chamaillard, Implementation of an energy management strategy for hybrid electric vehicles including drivability constraints, IEEE Trans. Veh. Technol. 65 (2016) 5918–5929.

[7] C.-C. Chan, A. Bouscayrol, K. Chen, Electric, hybrid, and fuel-cell vehicles: Architectures and modeling, Veh. Technol. IEEE Trans. 59 (2010) 589–598.

[8] H. He, Z. Liu, L. Zhu, X. Liu, Dynamic coordinated shifting control of automated mechanical transmissions without a clutch in a plug-in hybrid electric vehicle, Energies. 5 (2012) 3094–3109.

[9] D.F. Opila, X. Wang, R. McGee, R.B. Gillespie, J.A. Cook, J.W. Grizzle, Real-world robustness for hybrid vehicle optimal energy management strategies incorporating drivability metrics, J. Dyn. Syst. Meas. Control. 136 (2014) 61011.

[10] B. Powell, K. Bailey, S.C.-I.C. Systems, undefined 1998, Dynamic modeling and control of hybrid electric vehicle powertrain systems, Ieeexplore.Ieee.Org. (n.d.). https://ieeexplore.ieee.org/abstract/document/722250/ (accessed July 9, 2018).

[11] L. Qiu, L. Qian, H. Zomorodi, P. Pisu, Global optimal energy management control strategies for connected four-wheel-drive hybrid electric vehicles, IET Intell. Transp. Syst. 11 (2017) 264–272.

[12] Y. Sato, S. Ishikawa, T. Okubo, M. Abe, K. Tamai, Development of high response motor and inverter system for the Nissan LEAF electric vehicle, 2011.

[13] J.G. Hayes, K. Davis, Simplified electric vehicle powertrain model for range and energy consumption based on EPA coast-down parameters and test validation by Argonne National Lab data on the Nissan Leaf, in: Transp. Electrif. Conf. Expo (ITEC), 2014 IEEE, 2014: pp. 1–6.

[14] S.J. Andreasen, L. Ashworth, S. Sahlin, H.-C.B. Jensen, S.K. Kær, Test of hybrid power system for electrical vehicles using a lithium-ion battery pack and a reformed methanol fuel cell range extender, Int. J. Hydrogen Energy. 39 (2014) 1856–1863.

[15] S. Greaves, H. Backman, A.B. Ellison, An empirical assessment of the feasibility of battery electric vehicles for day-to-day driving, Transp. Res. Part A Policy Pract. 66 (2014) 226–237.

[16] J. Huh, W. Lee, G.-H. Cho, B. Lee, C.-T. Rim, Characterization of novel inductive power transfer systems for on-line electric vehicles, in: Appl. Power Electron. Conf. Expo. (APEC), 2011 Twenty-Sixth Annu. IEEE, 2011: pp. 1975–1979.

[17] J. Larminie, J. Lowry, Electric vehicle technology explained, John Wiley & Sons, 2012.

[18] M. Ehsani, Y. Gao, S. Longo, K. Ebrahimi, Modern electric, hybrid electric, and fuel cell vehicles, CRC press, 2018.

[19] J.O. Estima, A.J.M. Cardoso, Efficiency analysis of drive train topologies applied to electric/hybrid vehicles, IEEE Trans. Veh. Technol. 61 (2012) 1021–1031.

[20] L. Li, X. Li, X. Wang, J. Song, K. He, C. Li, Analysis of downshift's improvement to energy efficiency of an electric vehicle during regenerative braking, Appl. Energy. 176 (2016) 125–137.

[21] F. Bottiglione, S. De Pinto, G. Mantriota, A. Sorniotti, Energy consumption of a battery electric vehicle with infinitely variable transmission, Energies. 7 (2014) 8317–8337.

[22] A.H. Heap, B. Wu, W. Brunssen, J.J. McConnell, K.Y. Kim, B.R. Medema, Method for operating an internal combustion engine to transmit power to a driveline, (2012).

[23] K.Ç. Bayindir, M.A. Gözüküçük, A. Teke, A comprehensive overview of hybrid electric vehicle: Powertrain configurations, powertrain control techniques and electronic control units, Energy Convers. Manag. 52 (2011) 1305–1313.

[24] N. Rotering, M. Ilic, Optimal charge control of plug-in hybrid electric vehicles in deregulated electricity markets, IEEE Trans. Power Syst. 26 (2011) 1021–1029.

[25] X. Zhu, H. Zhang, J. Xi, J. Wang, Z. Fang, Robust speed synchronization control for clutchless automated manual transmission systems in electric vehicles, Proc. Inst. Mech. Eng. Part D J. Automob. Eng. 229 (2015) 424–436.

[26] A. Greco, K. Mistry, V. Sista, O. Eryilmaz, A. Erdemir, Friction and wear behaviour of boron based surface treatment and nano-particle lubricant additives for wind turbine gearbox applications, Wear. 271 (2011) 1754–1760.

[27] K. Holmberg, P. Andersson, A. Erdemir, Global energy consumption due to friction in passenger cars, Tribol. Int. 47 (2012) 221–234.

[28] M. Andersson, Churning losses and efficiency in gearboxes, KTH Royal Institute of Technology, 2014.

[29] X. Zhou, P. Walker, N. Zhang, B. Zhu, J. Ruan, Numerical and experimental investigation of drag torque in a two-speed dual clutch transmission, Mech. Mach. Theory. 79 (2014) 46–63.

[30] C. Changenet, X. Oviedo-Marlot, P. Velex, Power loss predictions in geared transmissions using thermal networks-applications to a six-speed manual gearbox, J. Mech. Des. 128 (2006) 618–625.

[31] E. Galvagno, M. Velardocchia, A. Vigliani, Analysis and simulation of a torque assist automated manual transmission, Mech. Syst. Signal Process. 25 (2011) 1877–1886.

[32] B. Gao, Q. Liang, Y. Xiang, L. Guo, H. Chen, Gear ratio optimization and shift control of 2-speed I-AMT in electric vehicle, Mech. Syst. Signal Process. 50 (2015) 615–631.

[33] S.-I. Kim, J. Cho, S. Park, T. Park, S. Lim, Characteristics comparison of a conventional and modified spoke-type ferrite magnet motor for traction drives of low-speed electric vehicles, IEEE Trans. Ind. Appl. 49 (2013) 2516–2523.

[34] A. Hughes, W. Drury, Electric motors and drives: fundamentals, types and applications, Newnes, 2013.

[35] R. Wang, Y. Chen, D. Feng, X. Huang, J. Wang, Development and performance characterization of an electric ground vehicle with independently actuated in-wheel motors, J. Power Sources. 196 (2011) 3962–3971.

[36] C.-Y. Tseng, C.-H. Yu, Advanced shifting control of synchronizer mechanisms for clutchless automatic manual transmission in an electric vehicle, Mech. Mach. Theory. 84 (2015) 37–56.

[37] P.D. Walker, N. Zhang, Engagement and control of synchroniser mechanisms in dual clutch transmissions, Mech. Syst. Signal Process. 26 (2012) 320–332.

[38] C. Sankavaram, B. Pattipati, K.R. Pattipati, Y. Zhang, M. Howell, Fault diagnosis in hybrid electric vehicle regenerative braking system, IEEE Access. 2 (2014) 1225–1239.

[39] R. Mura, V. Utkin, S. Onori, Energy management design in hybrid electric vehicles: A novel optimality and stability framework, IEEE Trans. Control Syst. Technol. 23 (2015) 1307–1322.

[40] S.G. Wirasingha, A. Emadi, Classification and review of control strategies for plug-in hybrid electric vehicles, Veh. Technol. IEEE Trans. 60 (2011) 111–122.

[41] B. Mashadi, S.A.M. Emadi, Dual-mode power-split transmission for hybrid electric vehicles, IEEE Trans. Veh. Technol. 59 (2010) 3223–3232.

[42] B.M. Baumann, G. Washington, B.C. Glenn, G. Rizzoni, Mechatronic design and control of hybrid electric vehicles, IEEE/ASME Trans. Mechatronics. 5 (2000) 58–72.

[43] Z. Chen, R. Xiong, J. Cao, Particle swarm optimization-based optimal power management of plug-in hybrid electric vehicles considering uncertain driving conditions, Energy. 96 (2016) 197–208.

[44] S. Kelouwani, K. Agbossou, Y. Dubé, L. Boulon, Fuel cell plug-in hybrid electric vehicle anticipatory and real-time blended-mode energy management for battery life preservation, J. Power Sources. 221 (2013) 406–418.

[45] Y.-P. Yang, Y.-C. Shih, J.-M. Chen, Real-time torque-distribution strategy for a pure electric vehicle with multiple traction motors by particle swarm optimisation, IET Electr. Syst. Transp. 6 (2016) 76–87.

[46] F.R. Salmasi, Control strategies for hybrid electric vehicles: Evolution, classification, comparison, and future trends, IEEE Trans. Veh. Technol. 56 (2007) 2393–2404.

[47] W. Yang, J. Liang, J. Yang, N. Zhang, Investigation of a novel coaxial power-split hybrid powertrain for mining trucks, Energies. 11 (2018). doi:10.3390/en11010172.

[48] H. Hemi, J. Ghouili, A. Cheriti, An optimal control solved by Pontryagin's Minimum Principle approach for a fuel cell/supercapacitor vehicle, in: Electr. Power Energy Conf. (EPEC), 2014 IEEE, 2014: pp. 87–92.

[49] X. Hu, C.M. Martinez, Y. Yang, Charging, power management, and battery degradation mitigation in plug-in hybrid electric vehicles: A unified cost-optimal approach, Mech. Syst. Signal Process. 87 (2017) 4–16.

[50] N. Kim, S. Cha, H. Peng, Optimal control of hybrid electric vehicles based on Pontryagin's minimum principle, IEEE Trans. Control Syst. Technol. 19 (2011) 1279–1287.

[51] K. Chen, Y. Deng, F. Zhou, G. Sun, Y. Yuan, Control strategy optimization for hybrid electric vehicle based on particle swarm and simulated annealing algorithm, in: Electr. Inf. Control Eng. (ICEICE), 2011 Int. Conf., 2011: pp. 2054–2057.

[52] X. Wu, X. Hu, S. Moura, X. Yin, V. Pickert, Stochastic control of smart home energy management with plug-in electric vehicle battery energy storage and photovoltaic array, J. Power Sources. 333 (2016) 203–212.

[53] S.G. Li, S.M. Sharkh, F.C. Walsh, C.-N. Zhang, Energy and battery management of a plug-in series hybrid electric vehicle using fuzzy logic, IEEE Trans. Veh. Technol. 60 (2011) 3571–3585.

[54] M. Zandi, A. Payman, J.-P. Martin, S. Pierfederici, B. Davat, F. Meibody-Tabar, Energy management of a fuel cell/supercapacitor/battery power source for electric vehicular applications, IEEE Trans. Veh. Technol. 60 (2011) 433–443.

[55] N. Sulaiman, M.A. Hannan, A. Mohamed, E.H. Majlan, W.R.W. Daud, A review on energy management system for fuel cell hybrid electric vehicle: Issues and challenges, Renew. Sustain. Energy Rev. 52 (2015) 802–814.

[56] Z. Chen, C.C. Mi, J. Xu, X. Gong, C. You, Energy management for a power-split plug-in hybrid electric vehicle based on dynamic programming and neural networks, IEEE Trans. Veh. Technol. 63 (2014) 1567–1580.

[57] D.F. Opila, X. Wang, R. McGee, R.B. Gillespie, J.A. Cook, J.W. Grizzle, An energy management controller to optimally trade off fuel economy and

drivability for hybrid vehicles, IEEE Trans. Control Syst. Technol. 20 (2012) 1490.

[58] P. Pisu, K. Koprubasi, G. Rizzoni, Energy management and drivability control problems for hybrid electric vehicles, in: IEEE Conf. Decis. Control, 2005: p. 1824.

[59] M. Debert, T. Miro Padovani, G. Colin, Y. Chamaillard, L. Guzzella, Implementation of comfort constraints in dynamic programming for hybrid vehicle energy management, Int. J. Veh. Des. 58 (2012) 367–386.

[60] H. Rakha, M. Snare, F. Dion, Vehicle dynamics model for estimating maximum light-duty vehicle acceleration levels, Transp. Res. Rec. J. Transp. Res. Board. (2004) 40–49.

[61] J. Andreasson, Enhancing active safety by extending controllability-How much can be gained?, in: Intell. Veh. Symp. 2009 IEEE, 2009: pp. 658–662.

[62] R.A. Blanchard, A.M. Myers, Examination of driving comfort and self-regulatory practices in older adults using in-vehicle devices to assess natural driving patterns, Accid. Anal. Prev. 42 (2010) 1213–1219.

[63] A. Tapani, Vehicle trajectory effects of adaptive cruise control, J. Intell. Transp. Syst. 16 (2012) 36–44.

[64] T. Nüesch, P. Elbert, M. Flankl, C. Onder, L. Guzzella, Convex optimization for the energy management of hybrid electric vehicles considering engine start and gearshift costs, Energies. 7 (2014) 834–856.

[65] J.Y. Wong, Theory of ground vehicles, John Wiley & Sons, 2008.

[66] D. Kum, H. Peng, N.K. Bucknor, Control of engine-starts for optimal drivability of parallel hybrid electric vehicles, J. Dyn. Syst. Meas. Control. 135 (2013) 21020.

[67] D.F. Opila, D. Aswani, R. McGee, J.A. Cook, J.W. Grizzle, Incorporating drivability metrics into optimal energy management strategies for hybrid vehicles, in: Decis. Control. 2008. CDC 2008. 47th IEEE Conf., 2008: pp. 4382–4389.

[68] E. Galvagno, D. Morina, A. Sorniotti, M. Velardocchia, Drivability analysis of through-the-road-parallel hybrid vehicles, Meccanica. 48 (2013) 351–366.

[69] E.J. Schacht, B. Bezaire, B. Cooley, K. Bayar, J.W. Kruckenberg, Addressing drivability in an extended range electric vehicle running an equivalent consumption minimization strategy (ECMS), 2011.

[70] J.-L. Zhang, C.L. Yin, J.W. Zhang, Improvement of drivability and fuel economy with a hybrid antiskid braking system in hybrid electric vehicles, Int. J. Automot. Technol. 11 (2010) 205–213.

[71] K. Deb, Multi-objective optimization, in: Search Methodol., Springer, 2014: pp. 403–449.

[72] Q. Kang, S. Feng, M. Zhou, A.C. Ammari, K. Sedraoui, Optimal load scheduling of plug-in hybrid electric vehicles via weight-aggregation multi-objective evolutionary algorithms, IEEE Trans. Intell. Transp. Syst. 18 (2017) 2557–2568.

[73] S. Buerger, B. Lohmann, M. Merz, B. Vogel-Heuser, M. Hallmannsegger, Multi-objective optimization of hybrid electric vehicles considering fuel consumption and dynamic performance, in: Veh. Power Propuls. Conf. (VPPC), 2010 IEEE, 2010: pp. 1–6.

[74] M. Khorshidi, M. Soheilypour, M. Peyro, A. Atai, M.S. Panahi, Optimal design of four-bar mechanisms using a hybrid multi-objective GA with adaptive local search, Mech. Mach. Theory. 46 (2011) 1453–1465.

[75] G.M. Brown, B.J. Elbacher, W.G. Koellner, Increased productivity with AC drives for mining excavators and haul trucks, in: Ind. Appl. Conf. 2000. Conf. Rec. 2000 IEEE, 2000: pp. P28--P37.

[76] Y. Shao, J. Liu, C.K. Mechefske, Drive axle housing failure analysis of a mining dump truck based on the load spectrum, Eng. Fail. Anal. 18 (2011) 1049–1057.

[77] L.K. Sahoo, S. Bandyopadhyay, R. Banerjee, Energy performance of dump trucks in opencast mine, Proc. ECOS. (2010) 1899–1906.

[78] I.P. on Climate Change, Climate change 2014: Mitigation of climate change, Cambridge University Press, 2015.

[79] S. Mirzaei, A. Fernandez, Retard system solution on electric mining trucks, in: Sensorless Control Electr. Drives (SLED), 2012 IEEE Symp., 2012: pp. 1–5.

[80] D. Gao, W. Zhang, A. Shen, Y. Wang, Parameter Design and Energy Control of the Power Train in a Hybrid Electric Boat, Energies. 10 (2017) 1028.

[81] F. Bender, M. Kaszynski, O. Sawodny, others, Drive cycle prediction and energy management optimization for hybrid hydraulic vehicles, Veh. Technol. IEEE Trans. 62 (2013) 3581–3592.

[82] M. Cipek, D. Pavković, J. Petrić, A control-oriented simulation model of a power-split hybrid electric vehicle, Appl. Energy. 101 (2013) 121–133.

[83] J.P. Trovao, M.-A. Roux, E. Menard, M. Dubois, Energy-and Power-Split Management of Dual Energy Storage System for a Three-Wheel Electric Vehicle, IEEE Trans. Veh. Technol. (2016).

[84] J. Wu, J. Liang, J. Ruan, N. Zhang, P.D. Walker, A robust energy management strategy for EVs with dual input power-split transmission, Mech. Syst. Signal Process. 111 (2018) 442–455. doi:10.1016/j.ymssp.2018.04.007.

[85] X. Zhang, C.-T. Li, D. Kum, H. Peng, Prius+ and Volt−: Configuration Analysis of Power-Split Hybrid Vehicles With a Single Planetary Gear, IEEE Trans. Veh. Technol. 61 (2012) 3544–3552.

[86] M. Ehsani, Y. Gao, A. Emadi, Modern electric, hybrid electric, and fuel cell vehicles: fundamentals, theory, and design, CRC press, 2009.

[87] R.H. Staunton, C.W. Ayers, L.D. Marlino, J.N. Chiasson, B.A. Burress, Evaluation of 2004 Toyota Prius hybrid electric drive system, 2006.

[88] T.A. Burress, S.L. Campbell, C. Coomer, C.W. Ayers, A.A. Wereszczak, J.P. Cunningham, L.D. Marlino, L.E. Seiber, H.-T. Lin, Evaluation of the 2010 Toyota Prius hybrid synergy drive system, 2011.

[89] J. Liu, H. Peng, Modeling and control of a power-split hybrid vehicle, Control Syst. Technol. IEEE Trans. 16 (2008) 1242–1251.

[90] J.M. Miller, Hybrid electric vehicle propulsion system architectures of the e-CVT type, Power Electron. IEEE Trans. 21 (2006) 756–767.

[91] J.D. Wishart, Z. Dong, Modeling and Simulation of Two-Mode Hybrid Vehicle Architecture, in: 19th Int. Conf. Des. Theory Methodol. USA 2009, 2009.

[92] C.-T. Li, X. Zhang, H. Peng, Design of power-split hybrid vehicles with a single planetary gear, in: ASME 2012 5th Annu. Dyn. Syst. Control Conf. Jt. with JSME 2012 11th Motion Vib. Conf., 2012: pp. 857–865.

[93] J.D. Wishart, Y. Zhou, Z. Dong, Review, modelling and simulation of two-mode hybrid vehicle architecture, in: ASME 2007 Int. Des. Eng. Tech. Conf. Comput. Inf. Eng. Conf., 2007: pp. 1091–1112.

[94] K. Ahn, S. Cho, W. Lim, Y. Park, J.M. Lee, Performance analysis and parametric design of the dual-mode planetary gear hybrid powertrain, Proc. Inst. Mech. Eng. Part D J. Automob. Eng. 220 (2006) 1601–1614.

[95] K. Qin, E. Wang, H. Zhao, G. Shi, R. Wang, Z. Kong, W. Wang, Development and experimental validation of a novel hybrid powertrain with dual planetary gear sets for transit bus applications, Sci. China Technol. Sci. 58 (2015) 2085–2096.

[96] A. Villeneuve, Dual mode electric infinitely variable transmission, 2004.

[97] F.U. Syed, M.L. Kuang, J. Czubay, H. Ying, Derivation and experimental validation of a power-split hybrid electric vehicle model, IEEE Trans. Veh. Technol. 55 (2006) 1731–1747.

[98] Y. Zhang, H. Lin, B. Zhang, C. Mi, Performance modeling and optimization of a novel multi-mode hybrid powertrain, J. Mech. Des. 128 (2006) 79–89.

[99] M.D. Coppola, R.E. Eastman, R.J. Mayville, C.W. Phelan, M.S. Tianello Sr, A.P. Zajac, S.K. Mohan, Single speed transmission for an electric motor vehicle, (1998).

[100] S. Thomas, M. Hammond, Multi-speed transmission and integrated drive transfer mechanism, (2005).

[101] F. Di Nicola, A. Sorniotti, T. Holdstock, F. Viotto, S. Bertolotto, Optimization of a multiple-speed transmission for downsizing the motor of a fully electric vehicle, SAE Int. J. Altern. Powertrains. 1 (2012) 134–143.

[102] A. Sorniotti, T. Holdstock, G.L. Pilone, F. Viotto, S. Bertolotto, M. Everitt, R.J. Barnes, B. Stubbs, M. Westby, Analysis and simulation of the gearshift methodology for a novel two-speed transmission system for electric powertrains with a central motor, Proc. Inst. Mech. Eng. Part D J. Automob. Eng. 226 (2012) 915–929.

[103] M.S.R. Mousavi, A. Pakniyat, B. Boulet, Dynamic modeling and controller design for a seamless two-speed transmission for electric vehicles, in: Control Appl. (CCA), 2014 IEEE Conf., 2014: pp. 635–640.

[104] I. Brajevic, M. Tuba, An upgraded artificial bee colony (ABC) algorithm for constrained optimization problems, J. Intell. Manuf. 24 (2013) 729–740.

[105] N. Marjanovic, B. Isailovic, V. Marjanovic, Z. Milojevic, M. Blagojevic, M. Bojic, A practical approach to the optimization of gear trains with spur gears, Mech. Mach. Theory. 53 (2012) 1–16.

[106] S. Golabi, J.J. Fesharaki, M. Yazdipoor, Gear train optimization based on minimum volume/weight design, Mech. Mach. Theory. 73 (2014) 197–217.

[107] X. Zhu, H. Zhang, D. Cao, Z. Fang, Robust control of integrated motor-transmission powertrain system over controller area network for automotive applications, Mech. Syst. Signal Process. 58 (2015) 15–28.

[108] W. Mo, P. Walker, Y. Fang, J. Wu, … J.R.-M.S. and, undefined 2018, A novel shift control concept for multi-speed electric vehicles, Elsevier. (n.d.). https://www.sciencedirect.com/science/article/pii/S0888327018302073 (accessed July 9, 2018).

[109] X. Fan, P.D. Walker, Q. Wang, Modeling and simulation of longitudinal dynamics coupled with clutch engagement dynamics for ground vehicles, Multibody Syst. Dyn. (2018) 1–22.

[110] V.D. Ngo, J.A. Colin Navarrete, T. Hofman, M. Steinbuch, A. Serrarens, Optimal gear shift strategies for fuel economy and driveability, Proc. Inst. Mech. Eng. Part D J. Automob. Eng. 227 (2013) 1398–1413.

[111] A. Sciarretta, L. Guzzella, Control of hybrid electric vehicles, IEEE Control Syst. 27 (2007) 60–70.

[112] M. Sorrentino, G. Rizzo, I. Arsie, Analysis of a rule-based control strategy for on-board energy management of series hybrid vehicles, Control Eng. Pract. 19 (2011) 1433–1441.

[113] H. Borhan, A. Vahidi, A.M. Phillips, M.L. Kuang, I. V Kolmanovsky, S. Di Cairano, MPC-based energy management of a power-split hybrid electric vehicle, IEEE Trans. Control Syst. Technol. 20 (2012) 593–603.

[114] J.P. Trovão, P.G. Pereirinha, H.M. Jorge, C.H. Antunes, A multi-level energy management system for multi-source electric vehicles--an integrated rule-based meta-heuristic approach, Appl. Energy. 105 (2013) 304–318.

[115] J. Peng, H. He, R. Xiong, Rule based energy management strategy for a series--parallel plug-in hybrid electric bus optimized by dynamic programming, Appl. Energy. 185 (2017) 1633–1643.

[116] G. Rizzoni, H. Peng, Hybrid and Electrified Vehicles, Mech. Eng. Mag. Sel. Artic. 135 (2013) S10--S17.

[117] X. Hu, N. Murgovski, L. Johannesson, B. Egardt, Energy efficiency analysis of a series plug-in hybrid electric bus with different energy management strategies and battery sizes, Appl. Energy. 111 (2013) 1001–1009.

[118] L. Xu, F. Yang, J. Li, M. Ouyang, J. Hua, Real time optimal energy management strategy targeting at minimizing daily operation cost for a plug-in fuel cell city bus, Int. J. Hydrogen Energy. 37 (2012) 15380–15392.

[119] L. Serrao, S. Onori, A. Sciarretta, Y. Guezennec, G. Rizzoni, Optimal energy management of hybrid electric vehicles including battery aging, in: Am. Control Conf. (ACC), 2011, 2011: pp. 2125–2130.

[120] Z. Yuan, L. Teng, S. Fengchun, H. Peng, Comparative study of dynamic programming and Pontryagin's minimum principle on energy management for a parallel hybrid electric vehicle, Energies. 6 (2013) 2305–2318.

[121] S. Zhang, R. Xiong, Adaptive energy management of a plug-in hybrid electric vehicle based on driving pattern recognition and dynamic programming, Appl. Energy. 155 (2015) 68–78.

[122] F. An, R. Earley, L. Green-Weiskel, Global overview on fuel efficiency and motor vehicle emission standards: policy options and perspectives for international cooperation, United Nations Backgr. Pap. 3 (2011).

[123] V. Franco, M. Kousoulidou, M. Muntean, L. Ntziachristos, S. Hausberger, P. Dilara, Road vehicle emission factors development: A review, Atmos. Environ. 70 (2013) 84–97.

[124] J. Liang, J. Wu, N. Zhang, Z. Luo, S. Zhu, Interval uncertain analysis of active hydraulically interconnected suspension system, Adv. Mech. Eng. 8 (2016). doi:10.1177/1687814016646331.

[125] H. Naunheimer, B. Bertsche, J. Ryborz, W. Novak, Automotive transmissions: fundamentals, selection, design and application, Springer Science & Business Media, 2010.

[126] M.A. Kluger, D.M. Long, An overview of current automatic, manual and continuously variable transmission efficiencies and their projected future improvements, 1999.

[127] M.S.R. Mousavi, B. Boulet, Modeling, simulation and control of a seamless two-speed automated transmission for electric vehicles, in: 2014 Am. Control Conf., 2014: pp. 3826–3831.

[128] P. Walker, B. Zhu, N. Zhang, Powertrain dynamics and control of a two speed dual clutch transmission for electric vehicles, Mech. Syst. Signal Process. 85 (2017) 1–15.

[129] S. Fang, J. Song, H. Song, Y. Tai, F. Li, T.S. Nguyen, Design and control of a novel two-speed Uninterrupted Mechanical Transmission for electric vehicles, Mech. Syst. Signal Process. 75 (2016) 473–493.

[130] S. De Pinto, P. Camocardi, A. Sorniotti, P. Gruber, P. Perlo, F. Viotto, Torque-Fill Control and Energy Management for a Four-Wheel-Drive Electric Vehicle Layout With Two-Speed Transmissions, IEEE Trans. Ind. Appl. 53 (2017) 447–458.

[131] L. De Novellis, A. Sorniotti, P. Gruber, Driving modes for designing the cornering response of fully electric vehicles with multiple motors, Mech. Syst. Signal Process. 64 (2015) 1–15.

[132] F. Bottiglione, A. Sorniotti, L. Shead, The effect of half-shaft torsion dynamics on the performance of a traction control system for electric vehicles, Proc. Inst. Mech. Eng. Part D J. Automob. Eng. (2012) 0954407012440526.

[133] S. Murata, Innovation by in-wheel-motor drive unit, Veh. Syst. Dyn. 50 (2012) 807–830.

[134] Z. Zhong, G. Kong, Z. Yu, X. Chen, X. Chen, X. Xin, Concept evaluation of a novel gear selector for automated manual transmissions, Mech. Syst. Signal Process. 31 (2012) 316–331.

[135] G. Lucente, M. Montanari, C. Rossi, Modelling of an automated manual transmission system, Mechatronics. 17 (2007) 73–91.

[136] J. Greiner, M. Grumbach, Automatic Transmission Systems Beyond 2020-Challenges and Competition, in: SAE Techinical Pap. Ser., 2013.

[137] X. Jun-Qiang, X. Guang-Ming, Z. Yan, Application of automatic manual transmission technology in pure electric bus, in: 2008 IEEE Veh. Power Propuls. Conf., 2008: pp. 1–4.

[138] Y. Hori, Future vehicle driven by electricity and control-research on four-wheel-motored" UOT Electric March II", IEEE Trans. Ind. Electron. 51 (2004) 954–962.

[139] R.P.G. Heath, A.J. Child, Zeroshift. A seamless Automated Manual Transmission (AMT) with no torque interrupt, in: SAE Techinical Pap. Ser., 2007.

[140] K. Zhao, Y. Liu, X. Huang, R. Yang, J. Wei, Uninterrupted shift transmission and its shift characteristics, Mechatronics, IEEE/ASME Trans. 19 (2014) 374–383.

[141] H. Liu, Y. Lei, Z. Li, J. Zhang, Y. Li, Gear-shift strategy for a clutchless automated manual transmission in battery electric vehicles, SAE Int. J. Commer. Veh. 5 (2012) 57–62.

[142] M. Zeraouila, M.E.H. Benbouzid, D. Diallo, Electric motor drive selection issues for HEV propulsion systems: A comparative study, in: Veh. Power Propulsion, 2005 IEEE Conf., 2005: p. 8--pp.

[143] Y. Zhang, H. Yang, Model predictive torque control of induction motor drives with optimal duty cycle control, IEEE Trans. Power Electron. 29 (2014) 6593–6603.

[144] Y. Zhang, H. Yang, Model-predictive flux control of induction motor drives with switching instant optimization, IEEE Trans. Energy Convers. 30 (2015) 1113–1122.

[145] R.C. Baraszu, S.R. Cikanek, Torque fill-in for an automated shift manual transmission in a parallel hybrid electric vehicle, in: Proc. 2002 Am. Control Conf. (IEEE Cat. No. CH37301), 2002: pp. 1431–1436.

[146] J. Cao, A. Emadi, A new battery/ultracapacitor hybrid energy storage system for electric, hybrid, and plug-in hybrid electric vehicles, IEEE Trans. Power Electron. 27 (2012) 122–132.

[147] M.-J. Kim, H. Peng, Power management and design optimization of fuel cell/battery hybrid vehicles, J. Power Sources. 165 (2007) 819–832.

[148] S.F. Tie, C.W. Tan, A review of energy sources and energy management system in electric vehicles, Renew. Sustain. Energy Rev. 20 (2013) 82–102.

[149] K. Maalej, S. Kelouwani, K. Agbossou, Y. Dubé, Enhanced fuel cell hybrid electric vehicle power sharing method based on fuel cost and mass estimation, J. Power Sources. 248 (2014) 668–678.

[150] L. Wang, E.G. Collins, H. Li, Optimal design and real-time control for energy management in electric vehicles, IEEE Trans. Veh. Technol. 60 (2011) 1419–1429.

[151] C. Zhang, A. Vahidi, Route preview in energy management of plug-in hybrid vehicles, IEEE Trans. Control Syst. Technol. 20 (2012) 546–553.

[152] Y. Cai, M. Ouyang, F. Yang, Energy management and design optimization for a series-parallel PHEV city bus, Int. J. Automot. Technol. 18 (2017) 473–487.